AN INNOVATIVE INFLATABLE MORPHING BODY STRUCTURE FOR CRASHWORTHINESS OF MILITARY AND COMMERCIAL VEHICLES

by

Dong Wook Lee

A dissertation submitted in partial fulfillment
of the requirements for the degree of
Doctor of Philosophy
(Mechanical Engineering)
in The University of Michigan
2008

Doctoral Committee

Professor Noboru Kikuchi, Co-Chairman
Research Scientist Zheng-Dong Ma, Co-Chairman
Professor Gregory M. Hulbert
Professor Nickolas Vlahopoulos

To my adorable wife, So Young

“나의 힘이 되신 여호와여 내가
주를 사랑하나이다” (시편 18:1)

ACKNOWLEDGEMENTS

I would like to express the deepest appreciation to my committee co-chairs Professor Noboru Kikuchi and Doctor Zheng-Dong Ma for accepting me as their student when I had no background on automotive crashworthiness, guiding me in the ways of professional engineers, and helping me finish my graduate work in this innovative field. Their enthusiasm and unwavering support gave me the inspiration to undertake and complete this doctoral research. Professor Kikuchi has also offered helpful suggestions and advice for my doctoral work. I greatly appreciate Professor Kikuchi's personal support, technical guidance and encouragement. I will keep the openhearted and indispensable advice he gave me in my mind for the rest of my life. Dr. Ma's personal aid, considerate and enthusiastic advice, profound expertise and recommendations on this research have been critical prime movers for me to finish this research. I am greatly indebted to Dr. Ma for providing me with meticulous ongoing support in every step of my research. Professor Kikuchi and Doctor Ma were not only my academic advisors, but also teachers who showed me the direction I should follow.

I would like to thank Professors Gregory Hulbert and Nickolas Vlahopoulos for their support and assistance in the preparation of this thesis and completion of my graduate work. Their insightful observations and insightful ideas were responsible for some of the key developments of this work. I am deeply indebted to both of them for their help and encouragement.

I would like to sincerely acknowledge the help I received from Dr. Farzad Rostam-Abadi and Dr. Basvaraju Raju of US Army REDCOM, Dr. Bing C. Chen of Rockwell Scientific Company LLC, and Dr. Ciro A. Soto of Ford Scientific Research Lab for their help with this research.

Finally, I am very thankful to my devoted wife, So Young, for providing me the unconditional support all through my life. There are no words to adequately express how thankful I am to her. Thanks also to God for everything you have given me in my life.

TABLE OF CONTENTS

DEDICATION……...…..……..ii

ACKNOWLEDGEMENTS...……..iii

LIST OF FIGURES...…..……..x

LIST OF TABLES...……..…….……xvi

LIST OF APPENDICES.……..xvii

ABSTRACT..……...……...…..xviii

CHAPTER

I INTRODUCTION.....……..1

1.1 Motivations and scope of this research…….....……...1

1.2 Vehicle structure design for vehicle safety…….…….…....……...3

1.3 Restraint system and occupant protection devices for occupant safety ……..……..……...……...7

1.4 Inflatable bumper design for vehicle safety.....8

1.5 Deployable systems..…….…….……...……...11

1.6 Intermediate material filled tube for vehicle safety ……....15

1.7 Organization of this dissertation…….…….…..…….18

II PROPOSED DESIGN CONCEPT AND FINITE ELEMENT ANALYSIS MODEL……22

2.1 Proposed design concept.....……22

2.2 Preliminary analysis of active inflatable bumper with only spring and mass ……..……...……...25

2.3 Preliminary analysis of active inflatable bumper with proposed design concept …….…...31

2.3.1 Overview…….…….……..31

2.3.2 Design and analysis……...32

2.3.3 Validation of the C-2500 truck and dummy model……...35

III FIRST-ORDER ANALYSIS (FOA) MODEL OF AN EXPLOSIVE AIRBAG ……..…….…..……..39

3.1 Introduction…….……...……..39

3.2 FOA (First-order-analysis) model for an external explosive airbag model…….....……..40

3.3 FOA model of a conventional airbag…….42

3.3.1 Spring coefficients of airbag ……...…….42

3.3.2 Damping coefficient of airbag …….…….……44

3.3.3 Wang and Nefske state variables …….45

3.3.4 Analytic solution for c_β and $\Delta\dot{V}$ ……...…….……..47

3.3.5 Effective area (A_e) ……..…….……...50

3.3.6 Prediction of airbag failure ……..…...…….52

3.4 Explosive model in an airbag for the system with an initial velocity...…...…53

3.4.1 Airbag bumper equipped with an explosive charge and Gurney's model……..……....…….…….53

3.4.2 Modified Gurney's model with initial velocity (for velocity and

pressure during detonation)……..……..54

3.4.3 Volume calculation during detonation using the effective explosive mass……..59

3.4.4 Collision time issue……..……...…....61

3.4.5 Issues of explosive design ……..……..…….63

3.5 Integrated airbag-vehicle model and its solution……..…63

3.6 Validation of the integrated airbag and vehicle model…….65

3.7 Design variables for the explosive airbag…….…69

3.8 Closure…….……..…….....70

IV DESIGN OF LATTICE STRUCTURE …….71

4.1 Introduction…….……..…….....71

4.2 Absorbed energy in the pre-buckling region based on the strain energy..…73

4.2.1 Strain energy of lattice structure in pre-elastic buckling……...…73

4.2.2 Strain energy of lattice structure in pre-plastic buckling…….…….76

4.3 Absorbed energy in the pre-buckling region based on the stiffness approach…….……..……...79

4.3.1 Stiffness of a single plate in the lattice structure…….……79

4.3.2 Stiffness of lattice structure……..……..……..……83

4.3.3 Absorbed energy in lattice structure……..……..……...84

4.4 Absorbed energy in the post buckling region……..86

4.5 Maximum force (ultimate compressive load) of lattice structure……...90

4.6 Optimization of lattice structure's shape and size……..……..91

4.7 Validation of the analytic model of a crash energy absorption structure using LS-DYNA…….……...……...…...92

4.8 Closure…….……...……..95

V APPLICATION OF TUBES FILLED WITH GRANULES FOR CRASHWORTHY DESIGN OF AUTOMOBILES…….…….97

5.1 Introduction……..…….....97

5.2 Effective thickness of a tube filled with granules…….….98

5.3 Stress on granular material (Walton, 1978 and 1987)…….....104

5.4 Validation of effective thickness approach for tubes filled with granules using LS-DYNA……...…….108

5.5 Comparisons of crashworthiness of typical sections of motor compartment rails with empty tubes and tubes filled with granules…….……...113

5.5.1 Motor compartment side rails – front crash load……...…..…113

5.5.2 Under-floor longitudinal rails – reaction crash loads ……..……114

5.6 Closure…….……..…….....117

VI INTEGRATION, VALIDATION, DEVELOPED SOFTWARE, AND APPLICATION OF I-BUMPER TO HIGH-SPEED CRASH …….....118

6.1 Integration of I-bumper and vehicle…….……..….....118

6.1.1 FOA model for a system with an explosive airbag, lattice structure, and mechanical spring (I-bumper at active state).....118

6.1.2 FOA model for a system with a front-post filled with granules (I-bumper at passive state)…….....……....120

6.1.3 The integrated I-bumper and vehicle model……...……120

6.2 Validation of the FOA model of the I-bumper…….……..….....125

6.3 Software developed using MATLAB…..…….…….…..……129

6.4 Application of the I-bumper to a high-speed crash…….……138

VII CONCLUSIONS AND FUTURE WORK…….……..……143

7.1 Conclusions...…….……..……..…..……...…143
7.2 Contributions ……..……..……..……145
7.3 Future work..…….…….……....….……...…146

APPENDICES…...……..…….150

BIBLIOGRAPHY……...…….171

LIST OF FIGURES

FIGURE

1.1 Research categories for vehicle safety design……..…….4

1.2 Fixed front end structure of current automobile (Ford and Toyota)..…….5

1.3 Frontal airbag bumper with Kevlar cover sheet on a 1989 Oldsmobile Cutlass Ciera (Clark and Young, 1995)……...…….9

1.4 Rotorcraft external airbag protection system (REAPS)…..…….……...…10

1.5 External airbag system developed by Autoliv……..11

1.6 Patents on inflatable external airbags…..……...…….……12

1.7 Examples of deployable systems..……....14

1.8 Granular materials (http://www.phy.duke.edu/research/ltb).....……...…16

1.9 Fatal crash distributions (from Traffic Safety Facts 2004, NHTSA)……17

2.1 Concept of the inflatable body……..…….…...23

2.2 Split and mitigation of the crash energy by inflatable body…….24

2.3 FEM model of inflatable bumper with only spring and mass…….……..25

2.4 Crash force curve for a collision between two cars (speed: 30 mph)…….…..…26

2.5 Kinetic energy curves for a collision between two cars (speed: 30 mph)…..……...26

2.6 Response surface of reduced kinetic energy of each mass and spring coefficient (speed: 30 mph)……....27

2.7 FEM model of inflatable bumper car with normal shape and flat shape……..28

2.8 Kinetic energy curves for offset collision and non-offset collision…….……..…29

2.9 FEM model for offset collision and non-offset collision…….…..29

2.10 Crash peaks for various collisions……30

2.11 FEM models for various collisions……....30

2.12 I-Bumper……...31

2.13 Components of active inflatable bumper……...……...32

2.14 HIC number for various masses and spring coefficients……...……...32
2.15 Truck with an innovative inflatable body before deployment……..……..…..…..33
2.16 Truck body shape after deployment (side view)……..……..….33
2.17 Truck body shape after deployment (bottom view)……..34
2.18 Lattice structure for locking……..……34
2.19 Comparison of the accelerations at the right seat for a frontal crash into a rigid wall Left figure: GWU's results. Right figure: UM's result……..…….....35
2.20 Comparison of the velocities for the frontal crash into a rigid wall Left figure: GWU's results. Right figure: UM's result……36
2.21 Comparison of accelerations of the head and pelvis between the simplified dummy model and hybrid III: 1) head acceleration of Hybrid III, 2) pelvis acceleration of Hybrid III, 3) head acceleration of the simplified model, 4) pelvis acceleration of the simplified model …...……..……...37
2.22 Simplified FEA dummy model……38
3.1 Simplified FOA model (3 DOF) for a head-on collision between cars ……..……40
3.2 Simplified FOA model (2 DOF) for head-on car collision using e_r, the coefficient of restitution (COR)……..…40
3.3 FEA model for external airbag using LS-DYNA……..…42
3.4 Simple airbag FOA model……42
3.5 Airbag properties and geometry for the Bernoulli equation……..……...44
3.6 Cross section of spherical airbag……...…49
3.7(a) Force vs. bag (gauge) pressure by Nefske (1972) ……..……51
3.7(b) Effective area vs. displacement by Nefske (1972)……..51
3.8 Estimated shape of airbag during compression……52
3.9 Examples of Gurney's equation……53
3.10 Asymmetric sandwich configuration with initial velocity v_0 for modified Gurney's model……55

3.11 Effective explosive mass in driving the plate……...59
3.12 Effective explosive mass in driving the plate and residual explosive mass in lateral inflation……60
3.13 Comparison between original Gurney's equation and modified Gurney's equation……61
3.14 Deployment velocity and distance of bumper from an LS-DYNA simulation……62
3.15 Explosive model and FOA model of airbag……..64
3.16 Process flow of the complete airbag model including explosive……..64
3.17 Analytic FOA model and FEA model for the complete airbag model…….65
3.18 Velocity of Mass1……..…66
3.19 Velocity of Mass 3……67
3.20 Velocity of Mass 2 (bumper)……68
3.21 Design variable sensitivity……...…….69
4.1 Prototype of expandable lattice structure for crashworthiness…….71
4.2 Pre-buckling region and post-buckling region in plate crush behavior……...72
4.3 Lattice structure with the U shape of a thin-walled member (a) and rectangular jagged member (b)…….……...73
4.4 Stress and strain curve for elastic buckling……...74
4.5 Element to be repeated in lattice structure and plate edge condition for buckling coefficient k…….……75
4.6 Stress and strain curve for plastic buckling……..77
4.7 Modified stress and strain curve using reduced modulus for plastic buckling…….78
4.8 Elastic region and plastic region in plate crush behavior……..…80
4.9 Load path of a single plate in lattice structure…….…….80
4.10 Plate under longitudinal force and declined by θ ……81
4.11 Stiffness of a single plate (90 degree simply supported)...……...…83
4.12 F-D curve of lattice structure……83
4.13 Serial and parallel combination of lattice structure…….….84

4.14 Deformation of a plate……..86
4.15 The cross section shape of plates before and after buckling……....88
4.16 The shape of the deformation of a plate (one loop and four hinges)……..……88
4.17 Deformation angle of some polygons..……....89
4.18 Given volume for lattice structure and size of element……92
4.19 FEM model for verification of analytic solution…….…….93
4.20 Absorbed energy of analytic model and LS-DYNA simulation (X axis: mass of lattice structure (kg), Y axis: energy (KNm))…….…….……94
4.21 Maximum force of analytic solution and LS-DYNA simulation (X axis: mass of lattice structure (kg), Y axis: force (KN))…….……...……95
5.1 Example of granular material: sand…….…….98
5.2 Tubes filled with granules……...100
5.3 Non-square thin-walled section for plastic bending…….……..101
5.4 Random packing of granular spheres……..105
5.5 The initial deformation……...105
5.6 Tubes filled with granules and the effective tube……...108
5.7 Axial deformation (a) and global bending deformation (b) of tubes with filled with granules……..109
5.8 Force and deformation curve for an effective tube and a tube filled with granules (axial deformation)…….……109
5.9 Energy absorbed by an effective tube and a tube filled with granules and obtained by analytic model (axial deformation)……...…110
5.10 Force and deformation curve for an effective tube and a tube filled with granules (global bending)……..……110
5.11 Energy absorbed by an effective tube and a tube filled with granules and obtained by analytic model (global bending)……111
5.12 Comparison of energy absorbed by a tube filled with granules and empty tube for axial and global bending deformation……..……..112

5.13 Deformation model of under-floor longitudinal rails with small deflection (from the course pack of an automotive body class at the University of Michigan)……..…115
6.1 Simplified First-Order-Analysis model (3 DOF) for car head-on collision in active state……...…118
6.2 Simplified First-Order-Analysis model (2-DOF) for a car head-on collision using e_r, the coefficient of restitution (COR), in active state…….……..……119
6.3 Simplified First-Order-Analysis model (2-DOF) for a car head-on collision in the passive state……..…….……120
6.4 Explosive model and FOA model of I-bumper……..…121
6.5 Process flow of a complete collision model for a car with an I-bumper……..….124
6.6 FOA model and FEA model for a complete I-bumper model……...…….....125
6.7 Velocity of Mass1……...126
6.8 Velocity of Mass 3……..127
6.9 Velocity of Mass 2 (bumper)……..128
6.10 Accelerations of the center of the compartment……..……...…129
6.11 Snapshot of initial screen of analysis software……...…130
6.12 Optimization tool for lattice structure…….130
6.13 Jagged member element……..132
6.14 Snapshot of analysis software for the I-bumper…….133
6.15 Snapshot of graphs shown by analysis software for the I-bumper……134
6.16 High speed crash and incompatibility problem (H. Nishigaki, Toyota Central R&D Lab.)……..…….……...……138
6.17 FEA model for a high speed crash……..139
6.18 Accelerations of the center of the compartment (V_0=30mph, TNT:100g)…….…140
6.19 Accelerations of the center of the compartment (V_0=50mph, TNT:100g)…….140
6.20 Accelerations of the center of the compartment (V_0=50mph, TNT:500g)…….…141
7.1 Human body models……...…...……...147
7.2 IABS….……..…….149

A1.1 Two schemes for collision model between inflated bumper and oncoming car's body……151
A1.2 Collision between two masses……153
A1.3 Deformation period and restoration period……154
A1.4 Experimental tests for COR with various closing velocities (Antonetti, 1998)....155
A1.5 Velocity curve of mass for COC and COR……156
A1.6 Momentum curve for COC and COR……157
A1.7 Deformation and restoration period for COC and COR……157
A1.8 Typical bounce of tennis ball on a hard surface……160
A1.9 Stacking of 1000 non-convex rings (Guendelman et al., 2003)……160
A1.10 Relationship between COC and COR……161
A1.11 Example of COC and COR……162
A1.12 Test velocity curve for a car (Zaouk, et al., 1996)……162
A1.13 Repeat of Fig. A1.12 with COC and COR……163
A2.1 Blast deflection system (RKT Constructors Inc.)……166
A2.2 Face-on loading and side-on loading of explosive wave……167
A2.3 General considerations and criteria for blast-worthiness design……169
A2.4 Design strategies and criteria……170

LIST OF TABLES

TABLE

1.1 Comparison between inflatable space structure and inflatable body for crashworthiness…….....…….15

2.1 Reduced kinetic energy for each material of bumper (speed: 30 mph)…….…...28

2.2 Reduced kinetic energy for each shape of bumper (speed: 30 mph)…….…...28

2.3 Stiffness and frequency test results……...……..……..35

2.4 Physical dimension and weight comparison for simplified dummy model and Hybrid III…….....……...……...…….36

3.1 Total reduced kinetic energy according to the deployment distance……62

5.1 Effective thickness of tubes filled with granules……...…102

5.2 Numerical structural values for an empty-tube body and a granule-filled tube body …...……..116

6.1 Spring coefficients and damping coefficient for I-body components……...…..121

6.2 Input parameters for lattice structure ……...…..131

6.3 Output values for lattice structure …….…...…..132

6.4 Input parameters for I-bumper ……..…...…..135

6.5 Output values and graphs for I-bumper ……...…..136

6.6 Input parameters for granules and front post……....…….…...…..137

6.7 Output values for front-post filled with granules ……..……...…..137

LIST OF APPENDICES

APPENDIX

I COEFFICIENT OF RESTITUTION (COR) AND COEFFICIENT OF CRASH (COC)....……..…151

A1.1 Coefficient of Restitution (COR) [Meriam and Kraige, 1993; Greenwood, 1988]…….....……..151

A1.2 Coefficient of Crash (COC) – Minus COR …….…....…….156

A1.3 Application of Coefficient of Crash (COC) in tennis balls (Cross, 2002) and rigid bodies with stacking (Geundelman et al., 2003)…….…….159

A1.4 Application of Coefficient of Restitution (COR) and Coefficient of Crash (COC) in automotive collision.....161

II CONSIDERATIONS OF BLAST-WORTHINESS OF VEHICLES …...……165

A2.1 Absorption of energy…….…….....……...166

A2.2 Deflection of blast away from the hull ….……..……...……...166

A2.3 Prevention of entrapment of the blast wave…….....167

A2.4 Distance from the detonation point…….....168

A2.5 Protection against the fragmentation (penetration) effect of mines….....168

A2.6 Blast-worthiness design strategies and criteria.…….....169

ABASTRACT

AN INNOVATIVE INFLATABLE MORPHING BODY STRUCTURE FOR CRASHWORTHINESS OF MILITARY AND COMMERCIAL VEHICLES

by

Dong Wook Lee

Co-Chairs: Noboru Kikuchi and Zheng-Dong Ma

The greatest demand facing the automotive industry has been to provide safer vehicles with high fuel efficiency at minimum cost. Current automotive vehicle structures have one fundamental handicap: a short crumple zone for crash energy absorption. This leaves limited room for further safety improvements, especially for high-speed crashes. Breakthrough technologies are needed. One potential breakthrough is to use active devices instead of conventional passive devices.

An innovative inflatable bumper concept, called the "I-bumper," is developed in this research for improved crashworthiness and safety of military and commercial vehicles. The developed I-bumper has several active structural components, including a morphing mechanism, a movable bumper, two explosive airbags, and a morphing lattice structure with a locking mechanism that provides desired rigidity and energy absorption capability during a vehicular crash. Another additional innovative means for improving crashworthiness is the use of tubes filled with a granular material to absorb energy during the process of a crash.

An analytical design model is also developed in this research for the optimal design of the I-bumper system, with a focus on up-front design. Major design variables include those of the explosive airbag, the morphing lattice structure, and the granular material used in the front posts. The morphing lattice structure is designed to maximize energy absorption during the crash impact. The granular material in the front posts is used for further crash energy management in the passive stage. The new design methodology has been implemented in MATLAB and validation has been conducted at a full vehicle level in order to demonstrate the effectiveness of the I-bumper for improved suitability in a high-speed crash.

In future research, this I-bumper can be extended to address other types of crashes (for example, side impacts, rear impacts, roll over, and collision with pedestrian) and to innovative blast-worthiness applications for military vehicles.

The main achievement of this work has been an introduction of the I-bumper and the development of an analytical model of the I-bumper for absorbed energy during a crash.

CHAPTER I

INTRODUCTION

1.1 Motivations and scope of this research

An automobile (from Greek *auto*, self and Latin *mobilis*, moving) is a vehicle that moves itself with its own motor rather than being moved by another vehicle or animal. There were 590 million passenger cars worldwide as of 2002. Today, automobiles are one of the most important transportation devices in our lives.

The automotive body is one of the critical subsystems of an automobile, and it carries out multiple functions. It should hold the parts of the vehicle together and serve to filter noise and vibration. Additionally, it should be able to protect its occupants when accidents happen. To do this, the automotive body designer should create a structure with significant levels of strength, stiffness, and energy absorption. The body stiffness is closely related to the noise and vibration performance of automobiles. Out of the many functions of the automobile body, this research focuses on the crashworthiness of automobiles.

Worldwide, an estimated 1.2 million people are killed in road crashes annually. This translates into more than 3,287 men, women, and children dying every day (according to the World Health Organization). More than six million car accidents happen on the roads of the United States annually, and more than three million people are injured due to car accidents annually, with more than two million of these injuries being permanent injuries (according to the National Highway Transportation Safety Administration). Traffic accidents occur every day. We can't be sure who the victim will be, when the accident will happen or where it occur; the best we can do is to make

automobiles safer. The importance of automotive crashworthiness cannot be emphasized enough.

From an engineering perspective, crashworthiness is the ability of a vehicle to protect its occupants during an impact. Crashworthiness is a rapidly growing field in automotive engineering and it plays a major part in the practical design of automobiles.

In recent years, the greatest demand facing the automotive industry from customers and regulators has been to provide safer vehicles that weigh less, in order to improve the safety and fuel efficiency of these vehicles. The conventional design order, Durability → NVH (Noise, Vibration, and Harshness) → Crashworthiness, has been reversed to Crashworthiness → NVH → Durability, where crashworthiness has become the most important factor in the vehicle design process. For developers of military vehicles, at the forefront of vehicle technology, safety has always been a central concern for the purpose of mission efficiency and survivability.

Conventional safety equipments, such as air bags, seat belts, and various crash avoidance devices, have been developed as standards in many commercial and military vehicles. However, breakthrough technology is still a key requirement for meeting future demands for vehicle safety design for high speed crash.

In this research, a new vehicle concept is developed, one that is able to reconfigure itself during a crash to protect the occupants, and advanced design methodologies for the concept, called innovative inflatable morphing body structures, are developed. In detail, an innovative design concept of inflatable body structures (I-bumper) is proposed, a First-Order Analysis (FOA) model for inflatable bumper system(I-bumper) is developed, an FOA software using MATLAB is implemented, and the I-bumper FOA model is validated using an LS-DYNA Finite Element Analysis (FEA) model.

In this study, the concept of an “inflatable morphing body” is introduced as an example of innovative body designs for crashworthiness and improved safety of military and commercial vehicles. The proposed inflatable body has several components, including an active bumper, airbags, springs, and an energy absorbing lattice structure with a locking capability to increase stiffness during a vehicular crash. These are attached to the main body of a vehicle. A simple dummy model of Livermore Software Technology Corporation (LSTC) is also implemented in the vehicle Computer Aided

Engineering (CAE) model for evaluating the Head Injury Criterion (HIC) of the occupant during the crash process. Extensive CAE model validations are conducted for the truck and dummy models to ensure the suitability for use in the present design study. Major design variables and design guidelines and procedures are introduced based on an analytical design model for airbags, including an explosive that is described by a First-Order-Analysis (FOA) model. The active bumper with an explosive airbag is developed for the inflatable body concept to achieve significant improvement in vehicle crashworthiness. An advanced design method is developed to design lattice-spring structures by using structural optimization to maximize energy absorption. Furthermore, another new design concept using granular material is examined during the passive stage of crash management.

1.2 Vehicle structure design for vehicle safety

Engineering research on crash safety began in 1958 at Ford Motor Company. Initially, safety research focused on increasing the reliability of brake systems and decreasing the flammability of fuel systems. Subsequently, most research has focused on crash energy absorption with crushable components. The addition of safety belts and airbags has notably reduced death and injury of occupants. Today, most of the car companies are putting a significant portion of their development cost and human resources toward crashworthiness of automotive structures. Fig. 1.1 shows the research categories for vehicle safety design.

Previous research on automotive crashworthiness design has typically focused on the passive structure design, which includes cross section and shape, honeycomb or sandwich structures, and alternative materials. Usually, passive safety refers to built-in features of the automobile, like structures that work passively to prevent human injury but which do not change the shape of the vehicle in response to crash. In this dissertation, the term “passive” means that the automotive body is fixed, regardless of the situation it encounters. Thus, absorption of crash energy in the passive state is completely reliant on the stiffness of the car’s structure. Unfortunately, current cars have some fundamental handicaps, including fixed front end structures and limited crumple zones (see Fig. 1.2).

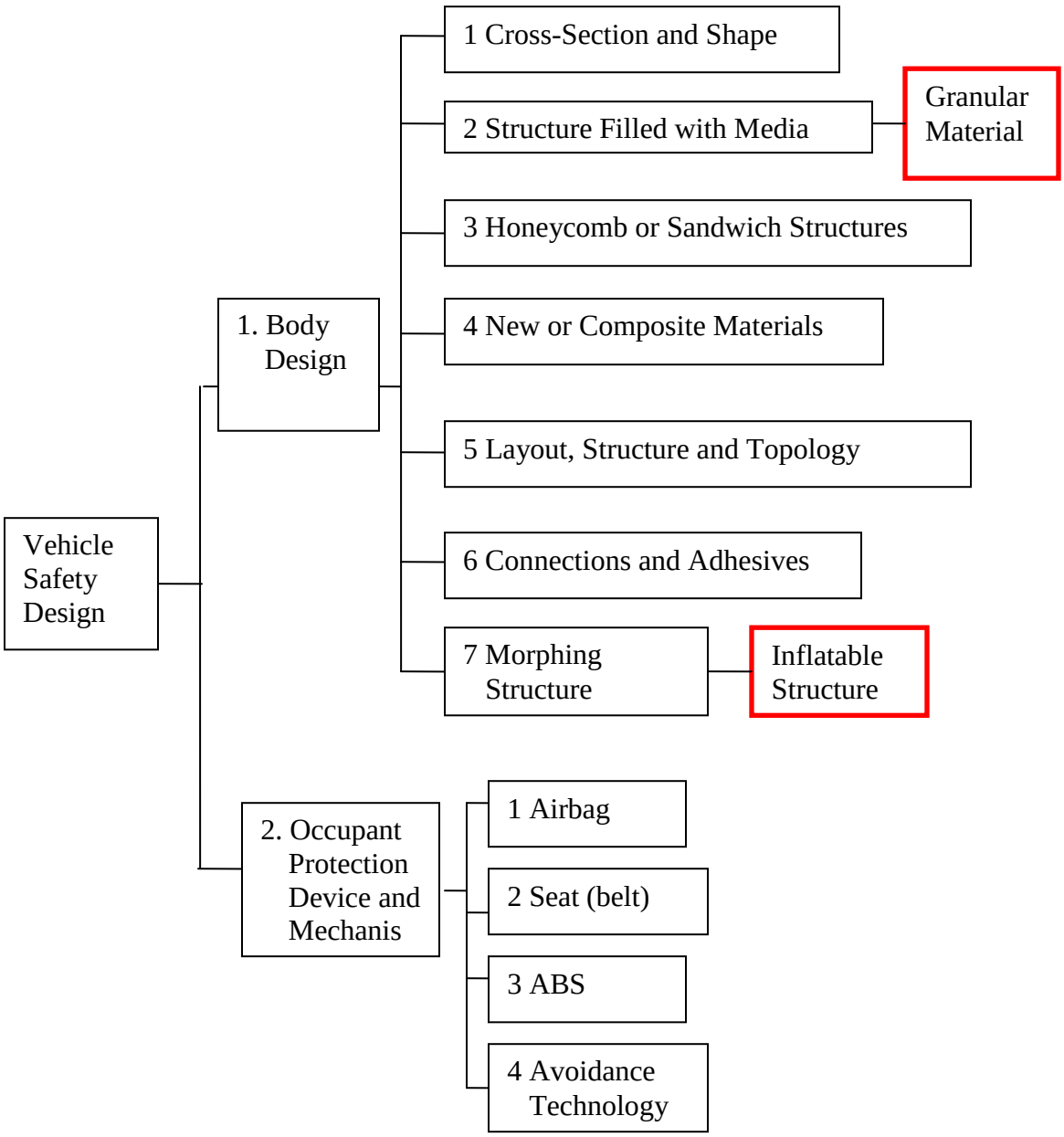

Figure 1.1 Research categories for vehicle safety design

Because of these limitations, the fatality rate increases dramatically in high speed impacts. In order to design a successful lightweight vehicle and significantly improve the crash performance of current cars, technological development is still needed. If the automotive body could extend its front end during or right before a crash, the mechanism of absorbing the crash energy would be totally different from that of the passive structure.

This concept has been implemented with an external airbag fitted with an explosive charge in this research. During a crash, the kinetic energy of moving or inflating parts (i.e. the bumper) activated by the explosive charge can absorb the kinetic energy of the other cars, and intermediate structures like airbags and lattice structure can absorb the remaining kinetic energy before the main body-to-body crash takes place.

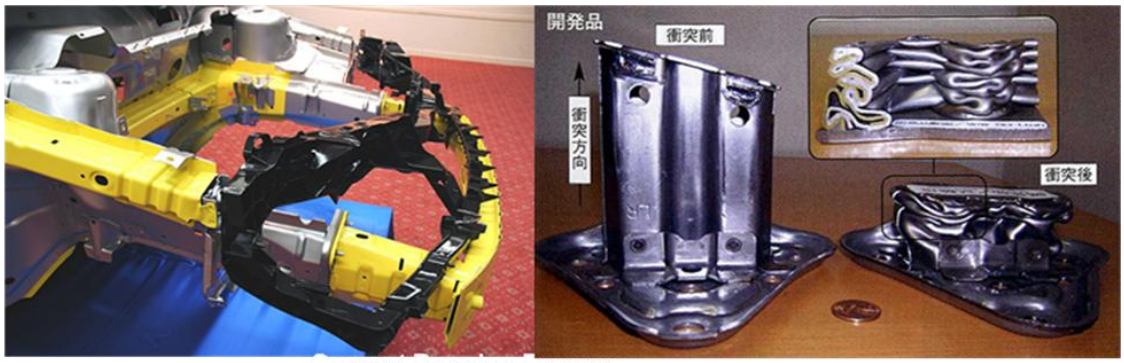

Figure 1.2 Fixed front end structure of current automobile (Ford and Toyota)

During a frontal crash, the front side member is expected to fold progressively, so as to absorb more energy and to ensure enough passenger space. To do so, various cross sections and shapes of tubes or beams have been investigated (Kim and Wierzbicke, 2001(a); Kim and Wierzbicke, 2001(b); Han and Yamazaki, 2003; Alghamdi, 2001). Kim and Wierzbicke (2001(a), 2001(b)) addressed a design for the front rail of the automotive body to maximize crashworthiness and weight efficiency; their design included reinforcing the cross-section. Han and Yamazaki (2003) discussed the axial impact crushing behavior of the S-shape square tube, the effectiveness of stiffening at the curved parts, and shape perturbation at the two straight parts of the tubes. Alghamdi (2001) reviewed several shapes (tubes, frusta, multi corner columns, struts, sandwich plates, honeycomb cells, and other shapes) of collapsible energy absorbers and the different modes (tube inversion, tube splitting, lateral indentation of tubes, and lateral flattening of tubes) of deformation of the most common ones in his paper.

Collapse mode, or the collapse behavior of tubes, has been studied (Andrews, England, and Ghani, 1983; Singace, 1999; White and Jones, 1999; Kim and Wierzbicki 2001 (c)). Andrews et al. (1983) investigated the axial crushing modes of cylindrical

tubes experimentally and formulated the chart of collapse mode of cylindrical tubes which enables a designer to predict the energy-absorbing properties of a given tube and its crush mode. Singace (1999) examined the collapse of tubes in the multi-lobe in order to evaluate the crushing load and developed an analytical model for the mean crushing load, one that is in reasonable agreement with those obtained from experiments. White and Jones (1999) presented the approximate theoretical analysis for the mean crushing forces generated during the dynamic axial loading of top-hat and double-hat sections. Kim and Wierzbicki (2001) studied the crushing behavior of thin-walled prismatic columns under the combined loading of bending and compression.

Sandwich or honeycomb structures (Yasui, 2000; Aktay, Johnson, and Holzapfel, 2005) are extensively employed in the aerospace and automobile industries. Their behavior under impact conditions has been studied. Yasui (2000) examined the dynamic impact crushing behavior of multi-layer honeycomb sandwich panels and the impact tensile loading behavior of their material members, and found that multi-layer honeycomb panels of the built-up pyramid type, accompanied by the uniform built-up type, can be expected to provide high performance. Aktay et al. (2005) addressed the damage behavior of composite sandwich panels with polyetherimide (PEI) foam cores and aramid paper honeycomb (NOMEX) under transverse impacts at high velocities.

Some papers have examined the design of a new material such as aluminum or plastic (Deb et al., 2004; Chen et al., 2004). Deb et al. (2004) investigated the design of an aluminum-intensive small car platform for desirable crashworthiness in the front end. They demonstrated that the aluminum-bodied vehicle design holds promise in terms of crashworthiness. Chen et al. (2004) reviewed various subframe concepts and showed the development process of an aluminum subframe. Their results demonstrated that the aluminum subframe could be designed to meet various load-carrying and energy-absorption targets.

Many researchers have been trying to devise a method by which vehicles can absorb more crash energy through the layout and structure optimization of a car body (Soto, 2001; Fredricson, 2000; Pedersen, 2004; Kim, Mijar, and Arora, 2001; Suh, Lee, and Cho, 2002; Avalle, Chiandussi, and Belingardi, 2002). Soto (2001) reviewed the improvement of the subject of topology optimization of continuum for maximizing

energy absorption. Fredricson (2000) surveyed the literature on structural topology optimization in the vehicle industry, focusing on specific applications. Pedersen (2004) discussed the topology optimization to obtain a crashworthiness design using the plastic zone formulation to model the plasticity. Kim et al. (2001) developed simplified models for design and optimization of automotive structures for crashworthiness, which were particularly useful for the up-front design of automotive structures where formulation was based on the system identification approach. Suh et al. (2002) developed two methods for the optimal design of vehicle body structure, the section property method and the section shape method. Avalle et al. (2002) found the optimal design for automotive components using response surface methodology to improve the mechanical behavior in impact loading.

Structural adhesive or connection improvements (Schulenburg and Kramer, 2004; Yang, Rui, Mohammed, and Singh, 1996) in vehicle crash performance have been made. Schulenburg and Kramer (2004) investigated special flexible polymers for car's structural adhesives, which provided improved stiffness and crash resistance as well.

1.3 Restraint system and occupant protection devices for occupant safety

Conventional safety equipment, such as air bags, seat belts, and Anti-lock Braking System (ABS), has been investigated in the automotive industry for many years.

An airbag is one of the most commonly used devices to protect occupants in the case of an automotive collision. Invented by Patrick W. Hetrick in 1951, the airbag has saved many lives through the years. Shout and Mallon (2000) studied airbag technology from the past, and made projections about the airbag's future in their paper. Glass et al. (2000) investigated whether a child should be restrained, and where the child should be seated, to minimize the risk of fatality, and estimated the effectiveness of passenger-side airbags and rear seating for children. Aside from the airbag mechanism or operation, many studies have focused on airbag-associated injury. Huelke et al. (1992) discussed the cases of air bag-associated injuries, primarily erythema, abrasions, and contusions of the lower face, anterior throat, and upper chest, these injuries being the ones most often observed in automotive crashes. Sefrin et al. (2004) analyzed 394 accidents in which the

airbag was deployed and concluded that occult injuries of the body cavities have to be expected after the release of the airbag. Manche et al. (1997) studied airbag-related ocular injuries and Marshall et al. (1998) discussed airbag-related deaths and serious injuries in children.

Seat belts, invented by George Cayley in the 1800s, are designed to reduce injuries by stopping the occupants from the second impact (hitting hard interior elements of the vehicle or other passengers). Huston (2001) presented a review, analysis, and discussion of the effectiveness and limitations of seat belt systems and discussed expected findings in post-accident inspections of seat belt systems.

There are additional active safety systems for automobiles. Usually, an active safety system in a vehicle uses information about the crash situation to adjust the response of the automobile and enhance the safety of the vehicle, before or during the crash. These include Adaptive Cruise Control, innovative brake systems like Anti-lock Braking Systems (ABS), and pre-crash systems. Adaptive Cruise Control systems use either a radar or laser to reduce the vehicle velocity when approaching another automobile. An anti-lock braking system (ABS) is a system on automobiles that prevents the wheels from locking while braking. Delaney and Newstead (2004) found that ABS can reduce the risk of multiple vehicle crashes by 18 percent and the risk of run-off-the-road crashes by 35 percent. Pre-crash systems also use radar sensors to detect an impending crash. Skutek et al. (2003) described a pre-crash system for vehicles with four short-range radars and the associated signal processing, a system that provides information relevant to the crash situation. I-bumper (Lee et al., 2008) could be added to the category of active safety systems, since I-bumper changes the structure of the automobile using information about the car's external environment.

1.4 Inflatable bumper design for vehicle safety

For several decades, bumper design has focused on material and structure. Andersson et al. (2002) investigated the applicability of stainless steel for crash-absorbing bumpers to increase crash performance in automotive vehicles. Butler (2002) studied the design of efficient epoxy structural foam reinforcements to increase the

energy absorbed in front and rear automotive bumper beams. Carley (2004) introduced Expanded Polypropylene (EPP) foam technologies and techniques for bumper systems. Cheon et al. (1995) developed a new composite bumper that has two pads at each end of the bumper. Evans and Morgan (1999) studied thermoplastic energy absorbers for bumpers.

The concept of safety design using external airbag bumpers was introduced two decades ago. Even though this idea has not yet been implemented in commercial industry or the military, the introduction of the concept alone has had a significant impact.

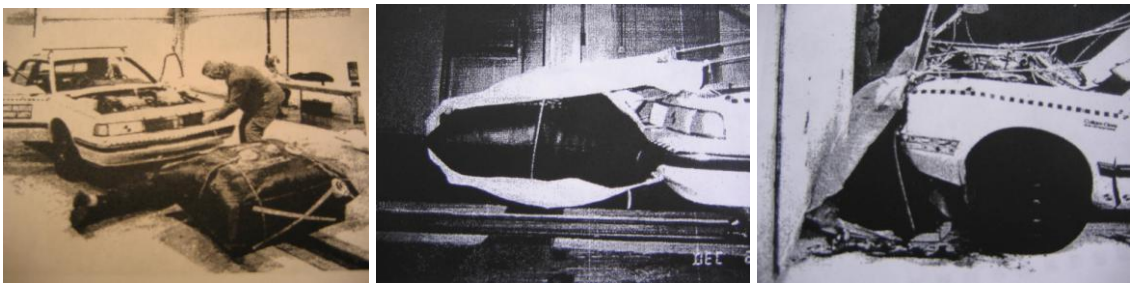

Figure 1.3 Frontal airbag bumper with Kevlar cover sheet on a 1989 Oldsmobile Cutlass Ciera (Clark and Young, 1995)

Fig 1.3 shows an early style of inflatable bumper using an airbag on a 1989 GM Oldsmobile (Clark and Young, 1994 and 1995). The frontal airbag bumper had a high pressure airbag, at 221 kPa and 23 cm thick, embedded on the outboard side of a low pressure airbag, at 20 kPa, whose inboard side was against the original car bumper, with a thickness of an additional 61 cm at the center line, for a combined thickness of 84 cm. The low pressure airbag ruptured as expected in the frontal crash, with this airbag bumper system absorbing about 19 percent of the energy of the crash.

Recently, RAFAEL has made some progress in developing an external airbag (see Fig. 1.4). They developed the Rotorcraft External Airbag Protection System (REAPS) which has an external airbag array attached under the fuselage of passenger rotorcrafts. The system deploys the external airbag array right before an impending crash, thereby reducing passenger injuries and airframe damage. Autoliv has developed two new external airbag systems (a front edge airbag and a bumper airbag) for SUVs (see Fig. 1.5).

The front edge airbag is designed to alleviate the effects of an SUV colliding with a pedestrian, and the bumper airbag handles the compatibility problem of high-hood vehicles like SUVs colliding with lower vehicles like passenger cars. Pipkorn et al. (2007) investigated an external airbag for sport utility vehicle to passenger vehicle compatibility in side impact. In this research, they found that an external bumper airbag reduced the intrusion velocity of the side door structure of a passenger car colliding with an SUV with a bumper airbag, and it also reduced the injury measures for the lower extremity of a pedestrian upon collision with a SUV with an external airbag. Many patents have been granted for inflatable bumper systems; some examples are shown in Fig. 1.6.

Source: www.defense-update.com

Figure 1.4 Rotorcraft external airbag protection system (REAPS)

Source: www.autoliv.com

Figure 1.5 External airbag system developed by Autoliv

1.5 Deployable systems

A deployable structure (see Fig. 1.7) is a structure that can be transformed from a compact configuration to a pre-designed and expanded form, that can carry loads, and that are stable. Well-known examples from daily life include an umbrella, a convertible car, and a “pop-up” camping tent. Deployable structures have been used in the temporary construction industry and the aerospace industry. In civil engineering, the deployable structure has been used for a long time for emergency and temporary structures. A recent application is the retractable roof of stadiums (Escrig, 1998; Kassabian, 1999). In space, deployable structures have been used in booms, aerials and masts, as well as in deployable solar arrays, because of their compactness. Pellegrino (2006) developed a new deployable reflector for an Earth observation mission. Soykasap et al. (2006) developed a novel concept for a deployable antenna that can measure terrestrial biomass levels from a spacecraft in a low Earth orbit. Thus far, it has not been common to use deployable or inflatable structures in the automotive industry. In this research, the application of deployable structures to an automotive body for crashworthiness design has been investigated.

Figure 1.6 Patents on inflatable external airbags

Extendible Bumper System and Method of Control (US6709035B1)
General Motors Corporation

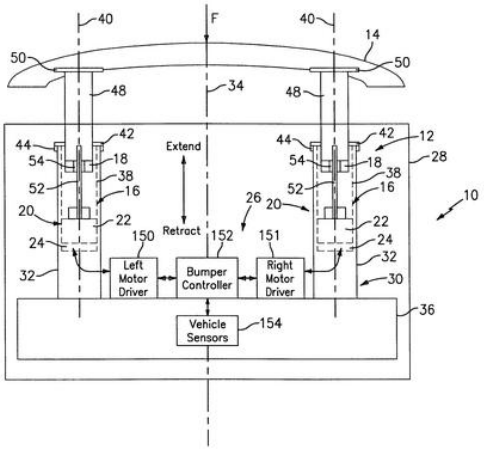

Bumper Airbag and System (WO 02/055343 A1)
Universal Propulsion Company.

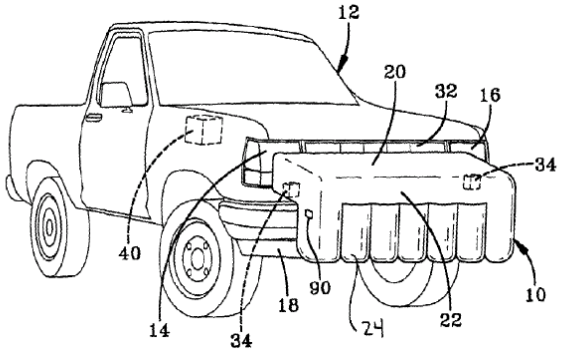

Bumper Airbag with Multiple Chambers (US 2004/0169362 A1)
Ford

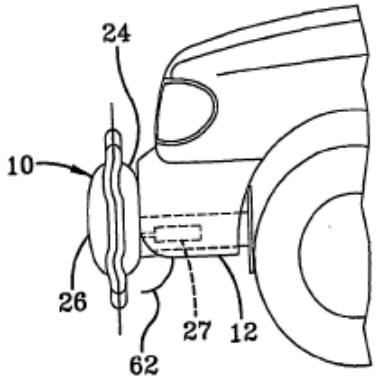

Energy Absorbing Devices (GB1371145)

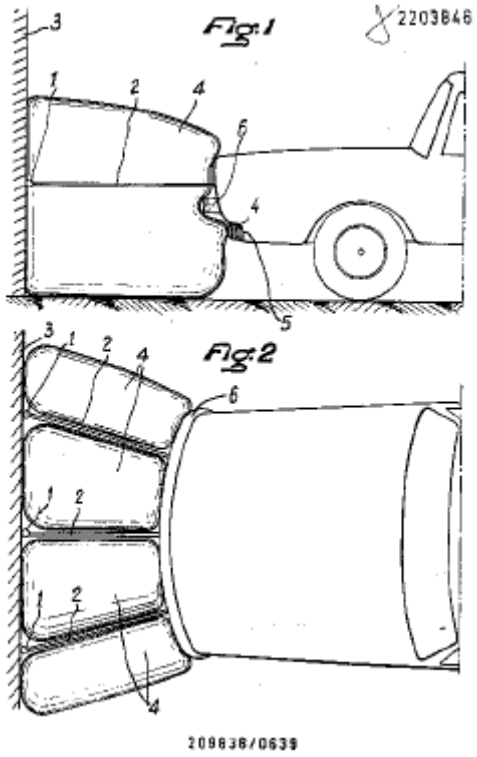

Safety Device for Motor Vehicle (DE 102 39 352 A1)

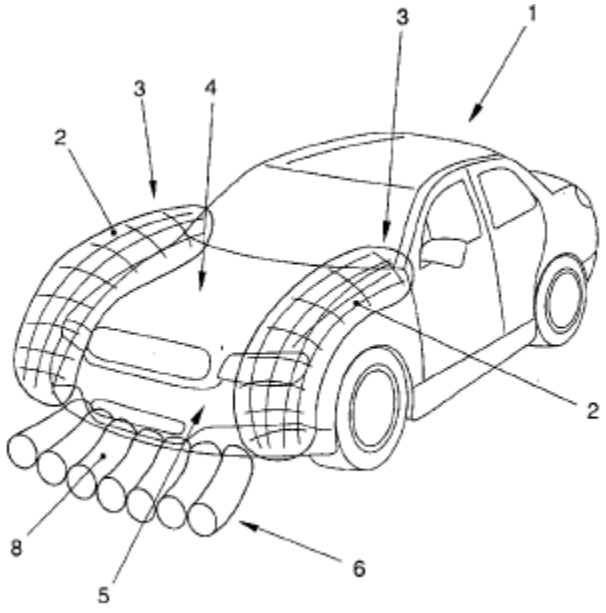

Deployable tent (http://military.eurekatents.com)

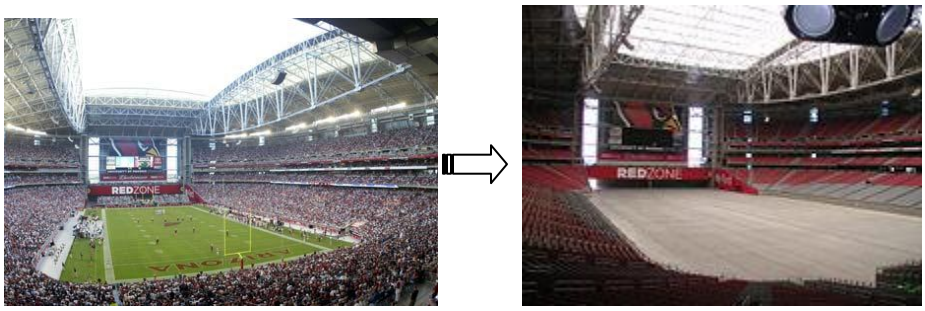

The roof of the University of Phoenix Stadium

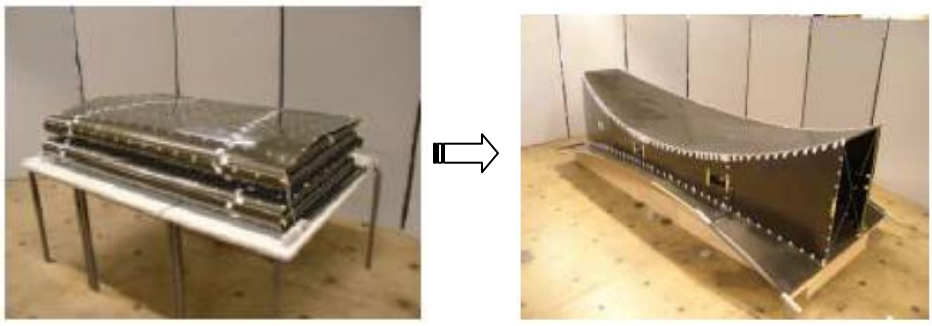

Deployable reflector (Pellegrino (2006))

Figure 1.7 Examples of deployable systems

Table 1.1 shows the comparison between an inflatable space structure and an inflatable body for automotive crashworthiness. The applications of an inflatable structure to the automobile are different from applications to the space structure. Mechanical springs or electromagnetic force can be used as the actuator in automobiles,

whereas space structures use heat, ultraviolet radiation, or shape alloy memory. Inflatable bodies for crashworthiness in automobiles should be able to transform to their desired form much faster than inflatable space structures transform, because vehicle crashes happen so quickly that they are measured in milliseconds. A major requirement of the inflatable space structure is reliability, whereas the major requirement of the inflatable body for automotive crashworthiness is energy absorption. The space deployable system should be easy to disassemble for use; however, for automotive crashworthiness, an inflatable body does not need to be reusable.

Table 1.1 Comparison between inflatable space structure and inflatable body for crashworthiness

	Inflatable Space Structure	Inflatable Body for Crashworthiness
Actuator	Heat, Cold, Ultra-violet Radiation, Shape alloy memory	Mechanical spring or Electromagnetic force
Deployment speed	Slow	Very fast
Major requirement	Reliability	Energy absorption
Reusability	Yes	No

1.6 Intermediate material filled tube for vehicle safety

Regarding the passive state design, an innovative design concept using granular material is introduced in this study. A granular material is a conglomeration of discrete solid, macroscopic particles that absorb energy whenever the particles interact (the most common example would be friction when grains collide). Common materials could be as diverse as sand, rice, ball bearings, or flour (see Fig. 1.8). Granular materials create enormous friction through the interaction of their individual particles, so a tube containing granular material can absorb much more crash energy than an empty tube. The

application of granular material to crashworthiness design will be very challenging and highly effective.

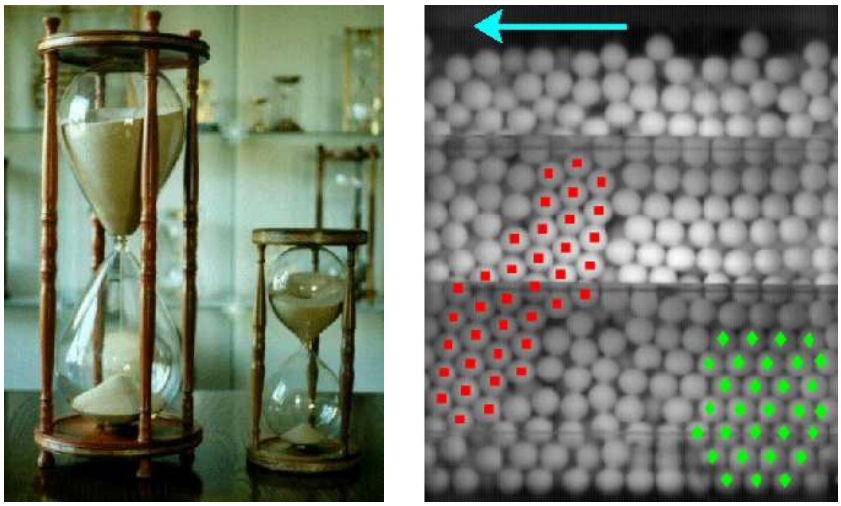

Figure 1.8 Granular materials (http://www.phy.duke.edu/research/ltb)

In previous research, the effects of filling metal tubes with a material such as foam or sawdust (Reid, Reddy, and Gray, 1986; Abramowicz and Wierzbicki, 1988; Santosa and Wierzbicki, 1998; Singace, 2000; Singace, 2003) have been studied with regard to the capabilities of tubes to absorb extra crash energy. Santosa and Wierzbicki (1998) studied the effect of aluminum or foam on the axial crush resistance of square box column. They found that significant energy absorption was obtained by filling the column with moderate or high strength aluminum foam. Singace (2000) investigated the influence of foam-like wood filter on the mode of collapse and energy absorption performance of polyvinylchloride (PVC) tubes. He found that empty PVC tubes normally collapse into a multi-lobe model when axially crushed, but the collapse mode was changed from multi-lobe to the concertina model in the sawdust-filled PVC tubes; therefore the PVC tubes absorbed more energy.

These investigations have been oriented toward a specific material or structure, so the results have been applicable only to that specific material. In addition, the results from these studies cannot be applied directly to an automotive body composed of thin-walled members like empty tubes to determine the bending stiffness or torsion stiffness

of automotive body. To do this, special treatments should be considered for tubes filled with a granular material.

In many fields, granular material is becoming an important subject. Unfortunately, no crashworthiness-related papers about granular material have been published.

In order to design a successful lightweight vehicle and improve the crash performance of current cars, an innovative crashworthiness design called the I-body (I-bumper) is introduced. For an active body, some ideas applicable to the bumper are introduced mainly based on the external airbag systems. They are, however, still in need of development and more theoretical grounding. In this study, some theoretical bases for the external airbag have been given and innovative concepts including explosives are investigated.

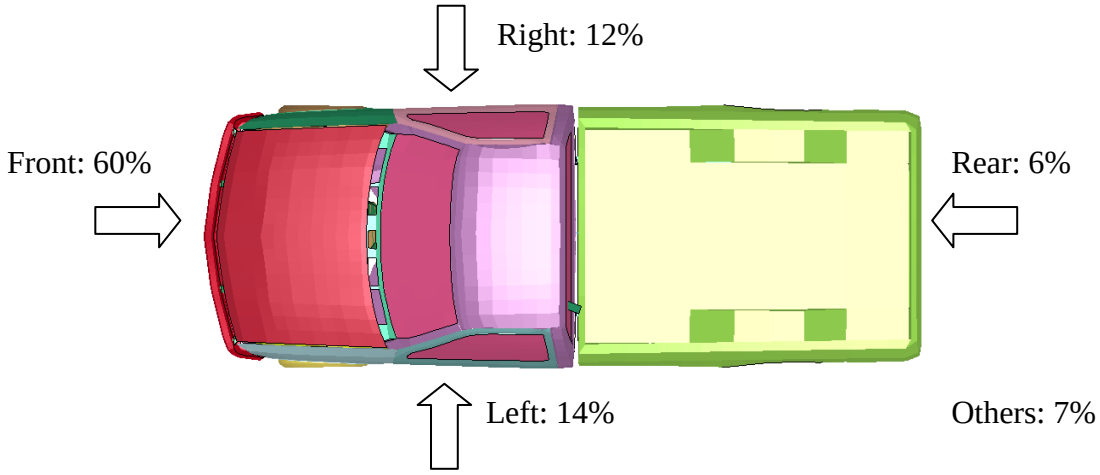

Figure 1.9 Fatal crash distributions (from Traffic Safety Facts 2004, NHTSA)

Frontal crashes have the highest priority in research on crashworthiness design in the automotive industry, because this type of crash accounts for more than half of all serious (injury-producing) and fatal passenger motor vehicle accidents. As seen in Fig. 1.9, the frontal crash is the most common type of fatal car crash, accounting for 60% of all fatal car crashes. Therefore, in this research, innovative I-bumper design is applied to the automotive front structure. In future research, this I-bumper concept can be extended

to side impact, rear impact, and rollover, and will be implemented as an innovative hard-kill means for blast-worthiness of military vehicles.

1.7 Organization of this dissertation

This dissertation discusses an innovative design for automotive crashworthiness focusing on front crashes, called the "I-bumper." This dissertation is organized as follows.

In chapter 2, a new design concept is proposed for the "I-bumper" inflatable bumper for automotive crashworthiness. The preliminary design analysis of a simplified FEA model with only mass and spring is performed. A comparison of crashworthiness or safety between conventional cars and cars with I-bumpers is made. The geometry effects and material effects of inflatable bumpers on energy absorption are examined in this chapter. Validation of the Finite Element Method (FEM) truck model and dummy model used in this research is conducted. To analyze and predict the crash motion of a car with an I-bumper, a simplified First Order Analysis (FOA) model is investigated in this research. For simplicity the three degrees-of-freedom (DOF) model or the two DOF model is used in this research. I-bumper components, and the impact between the bumper and the moving barrier, are modeled by a spring coefficient in a spring matrix and by a damping coefficient in a damping matrix. It is also necessary to know the initial conditions (displacements and velocities) for each mass in the models. The analytic approach for those coefficients of I-bumper components and initial conditions is shown in the next chapters.

In chapter 3, a First-Order Analysis (FOA) model for an external explosive airbag is developed based on lumped mass, spring coefficients, and damping coefficients. Two spring coefficients and one damping coefficient for external explosive airbags are derived in terms of the change in pressure and contact area. For damping coefficient of leakage and vent, the Bernoulli equation is used. The state variables appearing in the spring coefficients are obtained by the Wang and Nefske model. This external explosive airbag is different from a conventional airbag in that it uses an explosive instead of compressed

gas as an inflator. Because of this, the effect of this explosive in the airbag is investigated. Investigation starts with the Gurney's model, and with Jones' model for explosives. The initial velocity of the FOA model is determined by this modified Gurney's and Jones' equation. Validation of the explosive airbag system using LS-DYNA is given in this chapter.

In chapter 4, a crash energy absorbing (CEA) lattice structure is studied. Analytic modeling of an active (foldable and expendable) lattice structure is conducted. This structure is folded while driving, and is expanded and locked during the crash in order to absorb the crash energy. The energy absorbed in the lattice structure should be maximized. To do this, the optimization for structure size and shape is performed. To calculate the spring coefficient of the lattice structure, the deformation region is separated into a pre-buckling region and a post-buckling region. For the pre-buckling region, strain energy is used. For the post-buckling region, the theory of plastic limit analysis is applied to absorbed energy in the lattice structure. Final energy absorption by the lattice structure is obtained by summation of the absorbed energies in the pre-buckling region and the post-buckling region. The equivalent spring coefficient for lattice structure is given based on the derived energy absorption equation.

In chapter 5, one of the innovative means for crashworthiness of an automotive body is introduced: to use tubes filled with granular materials like sand or grain. To do this, a new concept called "effective thickness" is introduced and applied to find an analytical model of a tube filled with granules. An analytical model based on the effective thickness theory of a tube filled with granules is developed. Effective thickness is the thickness of an empty tube that is equivalent to a tube filled with granules. Various effective thicknesses for tubes filled with granules are developed in this chapter. The equation of the energy absorbed by a tube filled with granules is developed based on the effective thickness theory for the axial deformation and global bending deformation. The equivalent spring coefficient for a granule-filled tube is defined according to a predetermined energy absorption equation.

In chapter 6, each component of the I-bumper, including the explosive airbag, lattice structure, and tube filled with granular materials, is integrated into the total system. The incremental differential equation of crash motion for the system is expressed as

$$[m_i][\Delta\ddot{x}_i] + [k_i][\Delta x_i] + [c_i][\Delta\dot{x}_i] = [F_i] \quad (1\text{-}1)$$

I-bumper components, and the impact between the bumper and the moving barrier, are modeled by a spring coefficient and a damping coefficient characterized by nonlinearity in the spring matrix and the damping matrix of equation (1-1). The nonlinear characteristics of the spring and damping coefficients are taken into account in this method by updating these coefficients at the beginning of each time increment. To solve the incremental differential equation that appears in the FOA model, the step-by-step integration method is utilized. In this method, the equation is solved at successive increments Δt (or dt) of time.

A validation of the I-bumper system is presented, and the developed software is introduced in this chapter. The effectiveness and availability of the I-bumper are shown from a comparison of the acceleration of the compartment between a conventional car and an innovative car with an I-bumper. The application of a high-speed crash of a light truck and a heavy tuck using the FEM model is investigated. It is possible to have an indirect experience of high speed crashes and estimate the effectiveness of the I-bumper from this simulation.

In chapter 7, the conclusion of this dissertation is reached and future work is also discussed, including the extension of the I-bumper concept to other impacts (side impact, rear impact, and roll over), as well as to blast-worthiness. The future work including the optimization of I-bumper variables and sensor technology is presented.

In the appendices, the Coefficient of Restitution (COR) and Coefficient of Crash (COC) used for a collision between an inflated bumper and closing car's body are

discussed in Appendix 1, while design considerations and criteria for blast-worthiness are addressed in Appendix 2.

CHAPTER II

PROPOSED DESIGN CONCEPT AND FINITE ELEMENT ANALYSIS MODEL

2.1 Proposed design concept

In this chapter, an idea for morphing vehicle technology is proposed. The body of a conventional car is always fixed, regardless of whether it is driving, parking, or crashing. However, it would be more efficient if the car body could be changed according to the situation, transforming the car into a so-called “morphing” vehicle. Out of the many scenarios that a car might encounter, the crashworthiness during a crash is the focus of this design research.

The concept of a morphing vehicle to enhance crashworthiness is essentially that the volume of the vehicle can be increased very rapidly, much like the “Incredible HULK,” as shown in Fig. 2.1. Through this concept, possibilities such as extending the front end structure, expanding the space available for crumple zones, and increasing the stiffness and strength of the vehicle body can be realized. Finally, the inflated body would be able to mitigate and split the crash energy as depicted in Fig. 2.2.

This morphing concept is called the “Inflatable body,” or simply “I-body.” The substance with which the increased volume can be filled must be considered. The performance of the car in terms of crashworthiness hinges on the material and structure in the increased volume, and the kinetic energy of the colliding vehicle absorbed by the kinetic energy of the inflatable body. In this study, the airbag and lattice structure is filled in the increased volume to expand the crumple zone of the car body and absorb more crash energy. An explosive is used to increase the kinetic energy of the inflatable body.

The “break fall” in martial arts and the behavior of a cat when it falls down are good examples that illustrate crashworthiness in nature. Martial artists can minimize impact force through employment of various break-fall techniques when they hit the ground. The cat reduces its falling velocity and distributes its impact force through positioning its body, thus allowing it to land on the ground safely without hurting itself. Although the cat’s skill and the break-fall techniques of martial arts weren’t implemented in the design of this study, these concepts are worthwhile enough to be researched in the crashworthiness design. The concept of morphing a vehicle body for crashworthiness has something in common with them, in that they all mitigate and split the crash or impact energy.

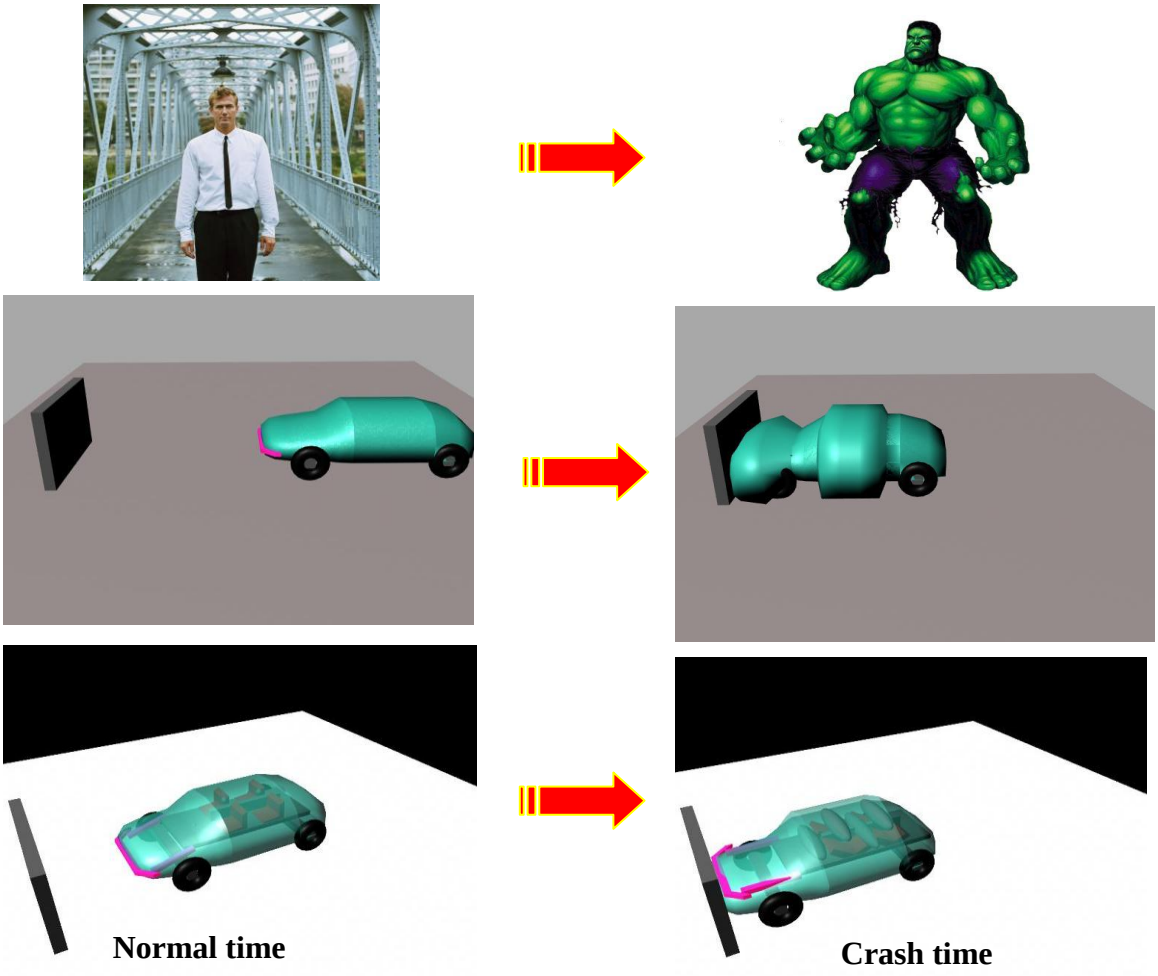

Figure 2.1 Concept of the inflatable body

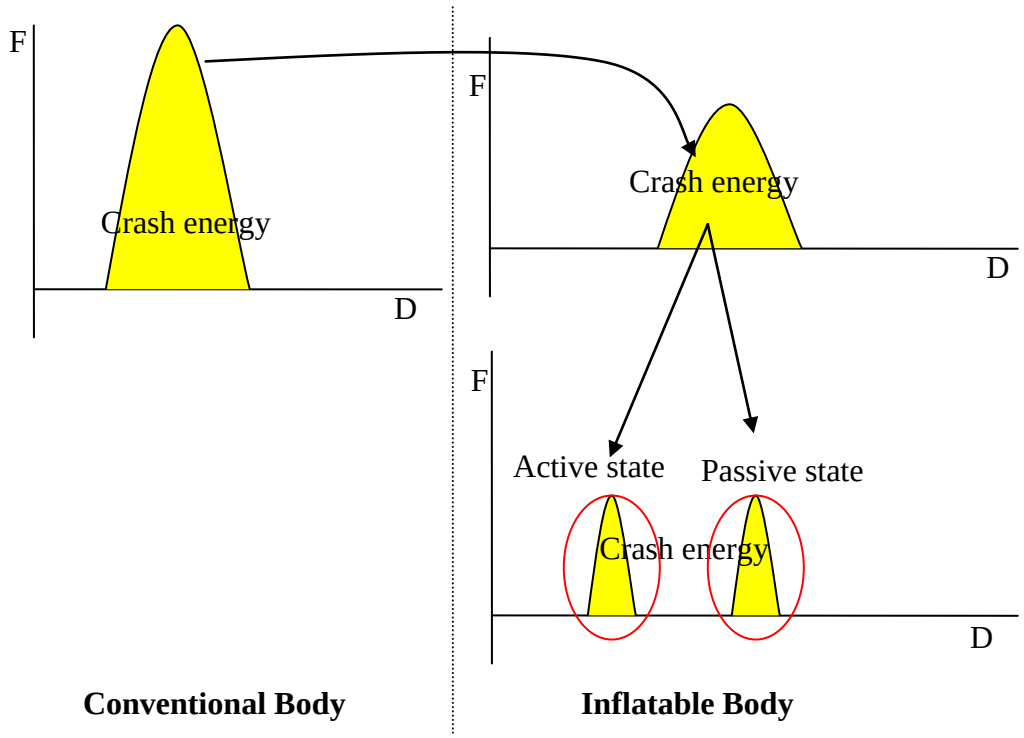

Figure 2.2 Split and mitigation of the crash energy by inflatable body

The inflatable body has two states. The first is the active state, in which the dynamic energy of the inflatable body (bumper) and special structures such as an external explosive airbag and lattice structure, can absorb the energy of cars before body-to-body contact occurs. To do so, an explosive (i.e. TNT) has been considered in this study. Explosives are very efficient at imparting high kinetic energy to projectiles (i.e. a bumper) while using only a small amount of explosive material. In this case, safety is also a very important factor to be considered. The second is the passive state, in which the stiffness of the fixed body will absorb the energy of the crashing cars. To reinforce the crashworthiness of an automotive fixed body, a front-post filled with granular material has been considered in this research. This study will both demonstrate and prove how the crash energy is mitigated and split using the aforementioned techniques.

2.2 Preliminary analysis of active inflatable bumper with only spring and mass

First, an active inflatable bumper employing only springs and mass (without explosive airbag and lattice structure) has been modeled below. Although this is not the ultimate design for the inflatable body, new and interesting facts have been revealed through the design. Fig. 2.3 shows the FEM model of an inflatable bumper with only springs and mass.

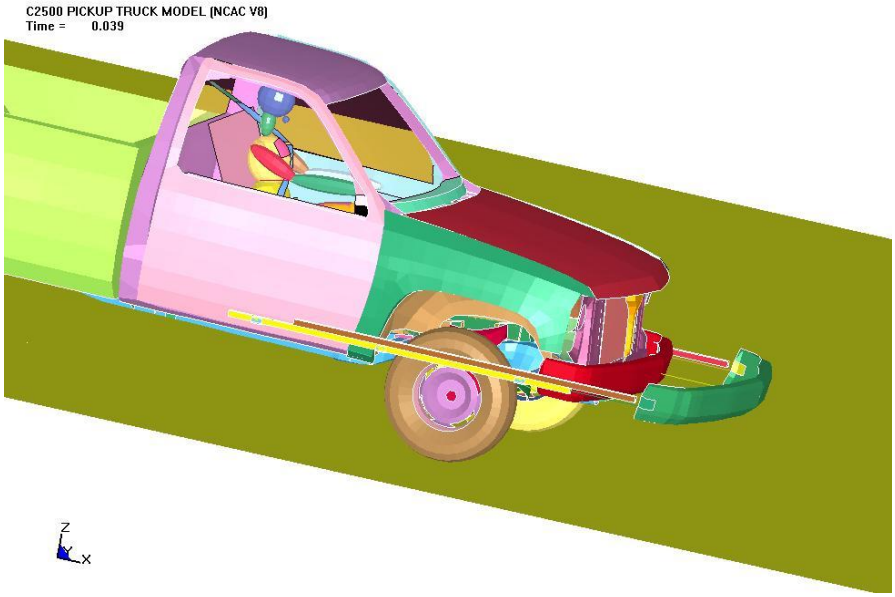

Figure 2.3 FEM model of inflatable bumper with only spring and mass

Fig 2.4 shows a crush force curve for two kinds of collision. Line A represents a collision between two conventional car bodies where neither car has an inflatable bumper, and line B represents a collision of two cars in which both cars have inflatable bumpers. Whereas line A has only one crash peak, line B has multiple discrete peaks as indicated by the arrows. The split and distribution of a crash force during a collision will work positively for energy absorption, which is the same approach used in martial arts as a safe way of falling down. As mentioned in Fig. 2.2, the I-body (or I-bumper) turns out to be able to mitigate and split the crash energy.

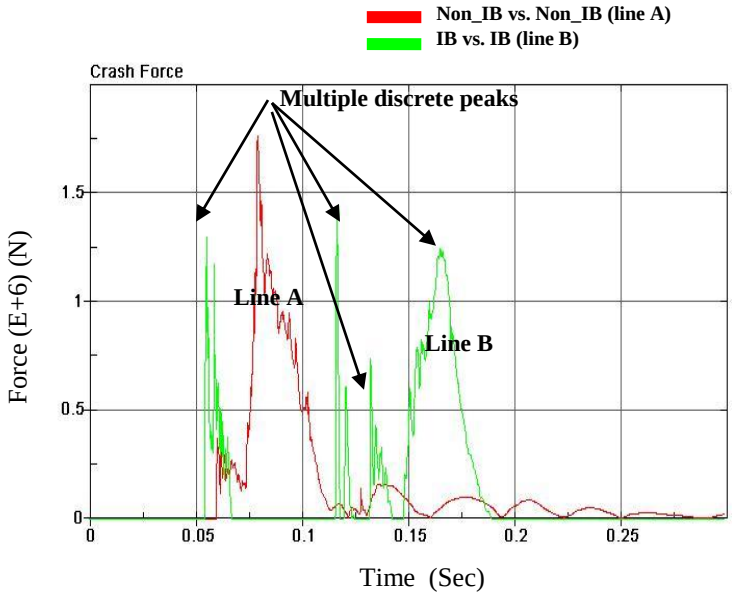

where non_IB means the car without inflatable body

IB means the car with inflatable body

Figure 2.4 Crash force curves for a collision between two cars (speed: 30 mph)

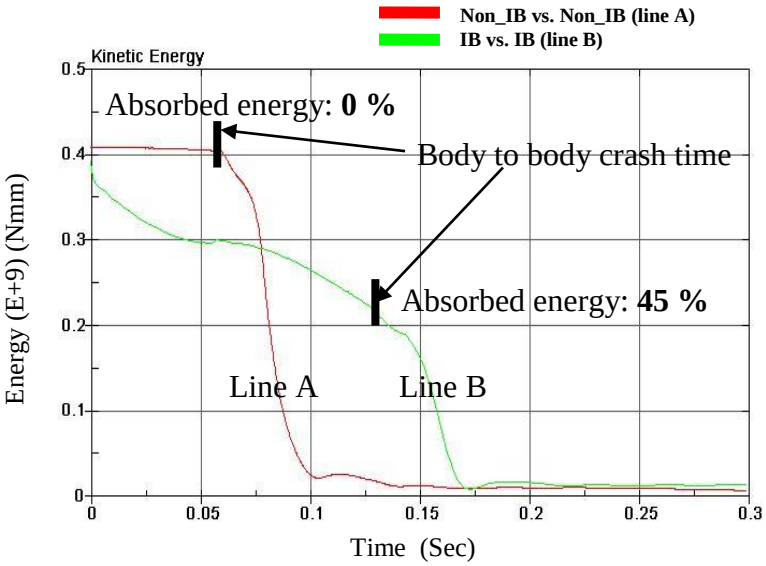

Figure 2.5 Kinetic energy curves for a collision between two cars (speed: 30 mph)

Fig. 2.5 shows a kinetic energy change curve for two cases during a collision. As shown, much more kinetic energy is absorbed before the main body collision in the case of a collision between two cars that both have an inflatable body. Fig. 2.6 shows the response surface of mass and the spring coefficient of an I-body. If a bigger mass for the bumper and a higher spring coefficient are chosen, more crash energy can be absorbed by the inflatable bumper.

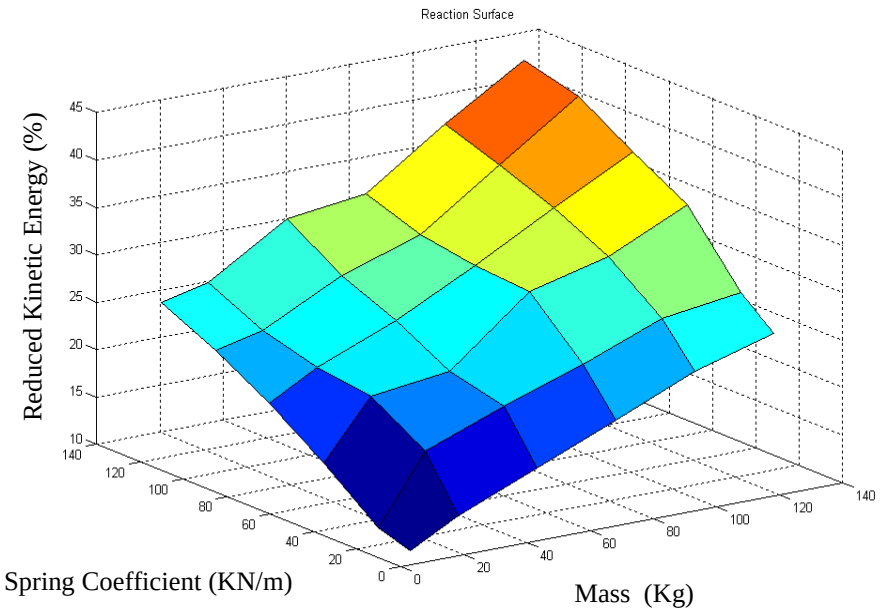

Figure 2.6 Response surface of reduced kinetic energy of each mass and spring coefficient (speed: 30 mph)

Table 2.1 and Table 2.2 show that the geometry and material of the bumper can also be design variables. It is found that the absorbed kinetic energy varies according to the shape of the bumper and the type of material.

Next, consider the offset collision of the I-bumper. Fig. 2.8 and Fig. 2.9 show a kinetic energy change curve for two cases; line B represents a case with an offset between bumpers, while line A represents a case without an offset between bumpers. More crash energy is absorbed in the case with an offset.

Table 2.1 Reduced kinetic energy for each material of bumper (speed: 30 mph)

Material Type	Young's Modulus (GPa)	Initial Kinetic Energy (Nmm)	Final Kinetic Energy (Nmm)	Reduced Kinetic Energy (%)
Al	70	398,720	306,330	23.17
Titanium	115	398,720	293,120	26.48
Steel	210	398,720	274,740	31.09

Table 2.2 Reduced kinetic energy for each shape of bumper (speed: 30 mph)

The shape of bumper	Initial KE of cars with I-bumper (Nmm)	Final KE of cars with I-bumper (Nmm)	Reduced KE with I-bumper (%)
Normal	396,899	304,690	23.23 (%)
Flat	403,317	216,220	46.39 (%)

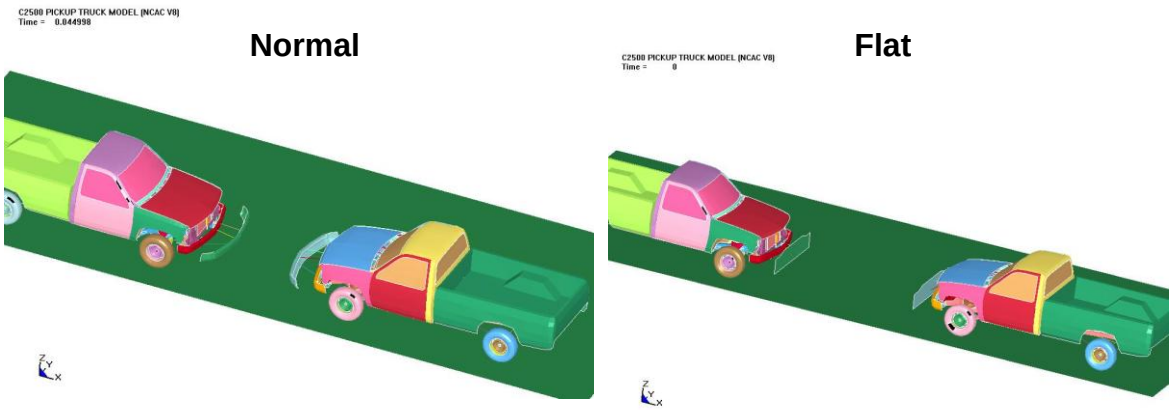

Figure 2.7 FEM model of inflatable bumper car with normal shape and flat shape

Therefore, the mass of the bumper, the spring coefficient, geometry, and the material of which the bumper is composed are all potential design variables. Figs. 2.10 and 2.11 show crash peaks and FEM models for various collisions between IB cars (cars with inflatable bodies) and non_IB cars (cars without inflatable bodies). Although these models incorporated some constraints that made it less realistic – for example, the

bumper was only able to move along the front-rear axis – the split and the distribution of the crash peaks are clearer than in Fig. 2.4, as shown in Fig. 2.10.

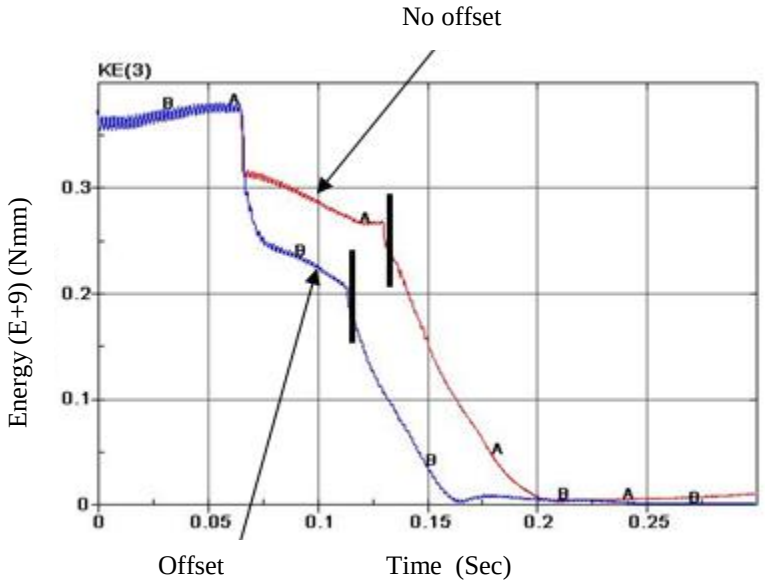

Figure 2.8 Kinetic energy curves for offset collision and non-offset collision

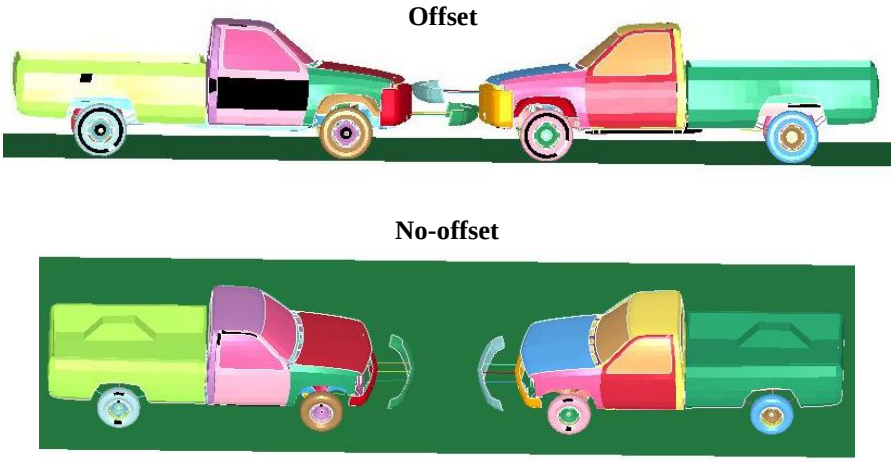

Figure 2.9 FEM model for offset collision and no-offset collision

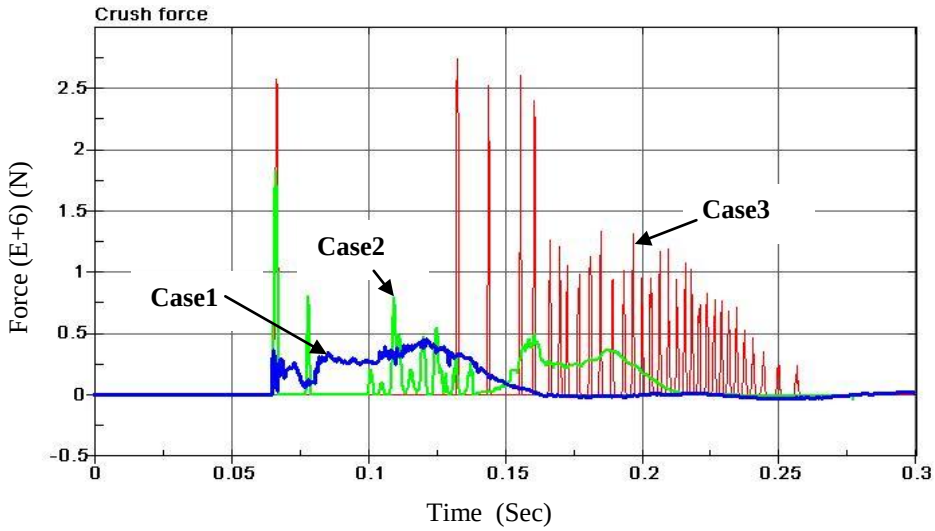

Figure 2.10 Crash peaks for various collisions

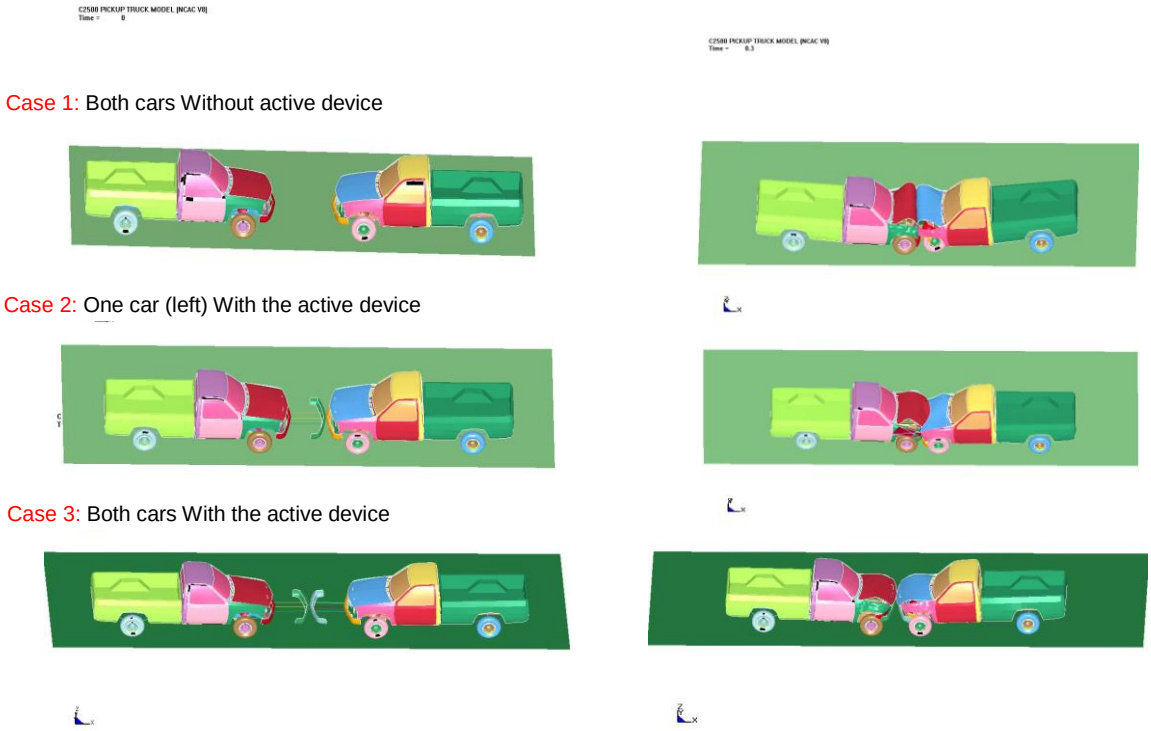

Figure 2.11 FEM models for various collisions

2.3 Preliminary analysis of active inflatable bumper with proposed design concept

2.3.1 Overview

Some modifications have been made to the previous inflatable body design shown in Fig. 2.3. This modified inflatable body is composed of airbags, a lattice structure and springs, as shown in Fig 2.12 and Fig 2.13. In particular, an explosive has been used as an airbag inflator as opposed to how it is conventionally done in airbag inflation. For passive state design, granular materials were included in the front-post.

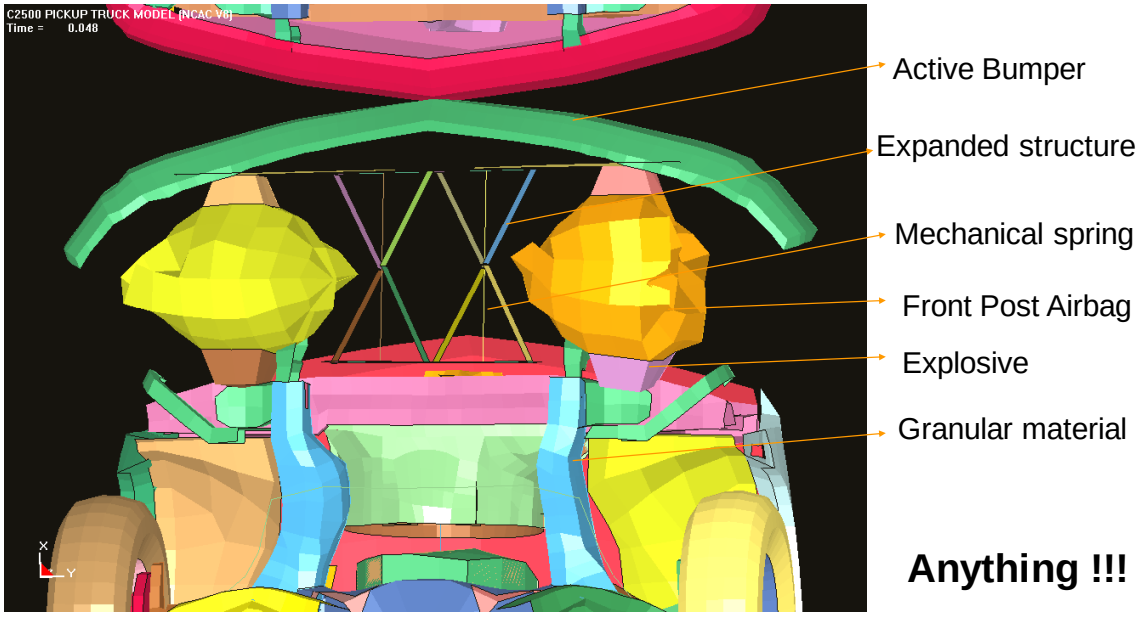

Figure 2.12 I-Bumper

Simulations were performed with this modified inflatable body. Fig. 2.14 shows a HIC number (Head Injury Criteria, a dimensionless number) for various masses and springs with the assumption that the airbag condition is fixed and that is a conventional airbag without explosive effects. It is observed that a significant reduction of the HIC number can be made using an inflatable body. HIC is defined by the equation of Fig. 2.14.

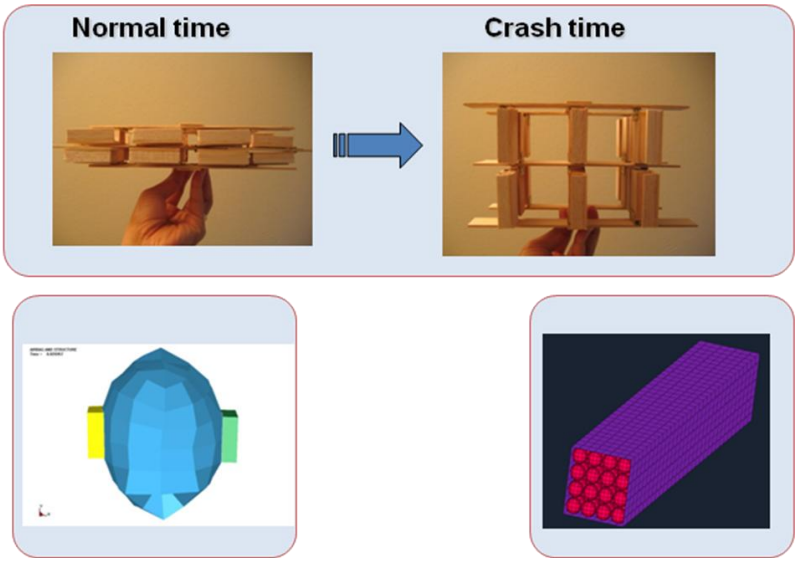

Figure 2.13 Components of active inflatable bumper

Mass & Spring Coefficient	HIC_{15}
No I-bumper	480
Bumper-20 kg, Spring-20 KN/m	300
Bumper-40 kg, Spring-40 KN/m	240

$$HIC = \max\left\{(t_2 - t_1)\left[\frac{1}{t_2 - t_1}\int_{t_1}^{t_2} a(t)dt\right]^{2.5}\right\}$$

$a(t)$: *the acceleration of head*

t_1, t_2 : *time*

Figure 2.14 HIC number for various masses and spring coefficients

2.3.2 Design and analysis

Fig. 2.15 illustrates the status of a truck FEA model (originally developed at GWU) with the innovative inflatable body before deployment. The inflatable body has several

components, including a deployable bumper, two external explosive airbags, two springs, and a lattice structure, all of which are attached to the main body. A simple dummy model of LSTC has also been implemented in the simulation model, as shown in Fig. 2.15 and 2.16, for the purpose of HIC evaluation.

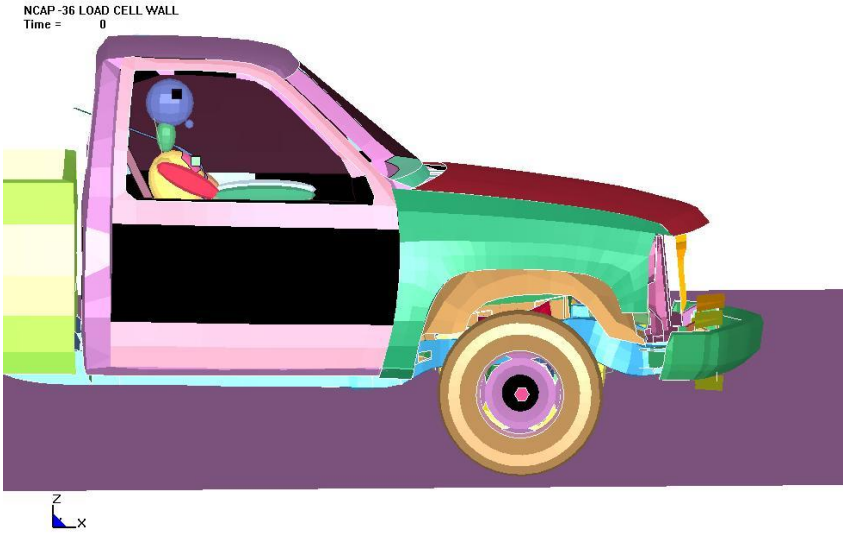

Figure 2.15 Truck with an innovative inflatable body before deployment

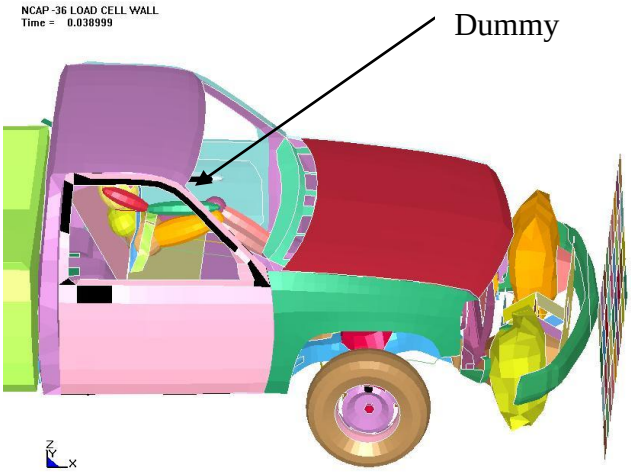

Figure 2.16 Truck body shape after deployment (side view)

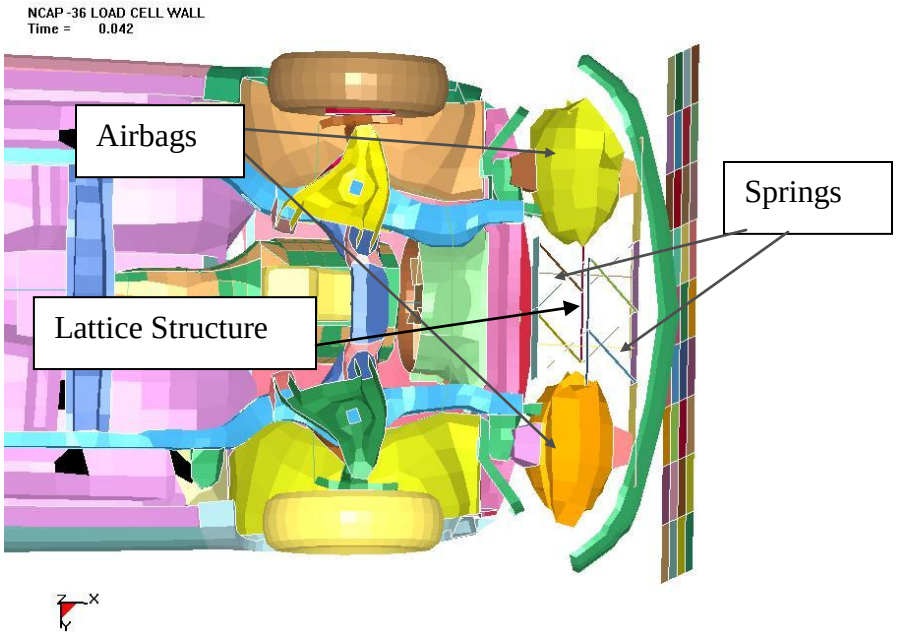

Figure 2.17 Truck body shape after deployment (bottom view)

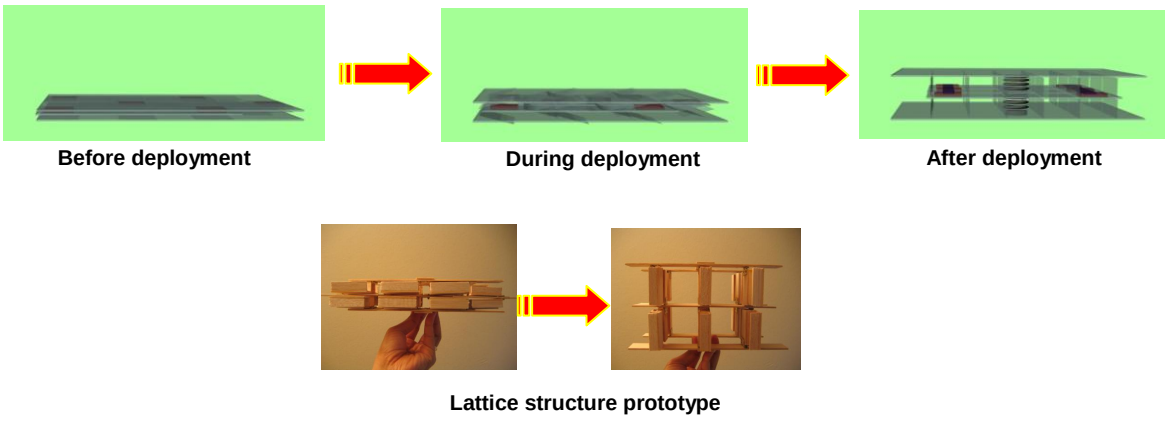

Figure 2.18 Lattice structure for locking

Fig. 2.16 and Fig. 2.17 show a bottom view and a side view of the truck FEM model after the deployment of the inflatable body, and they clearly show the composition of the airbags, springs, and lattice structure. Each component is spot-welded to the bumper and the main body. It can be seen that the new design comes much closer to being a realistic and practical design, compared to the previous design shown in Fig. 2.3.

This inflatable bumper (I-bumper) will be locked using a lattice structure after full deployment (see Fig. 2.18).

2.3.3 Validation of the C-2500 truck and dummy model

Virtual prototyping of the C-2500 (a Chevrolet truck model originally developed at George Washington University) has been performed in this study in order to validate a suitable model to be used in current inflatable body design studies. In terms of the fundamental body stiffness, since the real experimental data is not available to the public, a comparison was made with the nominal value for truck bodies. Table 2.3 illustrates the stiffness and frequency test results, which indicates that the current C-2500 model is softer in terms of bending stiffness, as well as in terms of the first eigenfrequency compared with the nominal value found from the literature, and in terms of torsional stiffness.

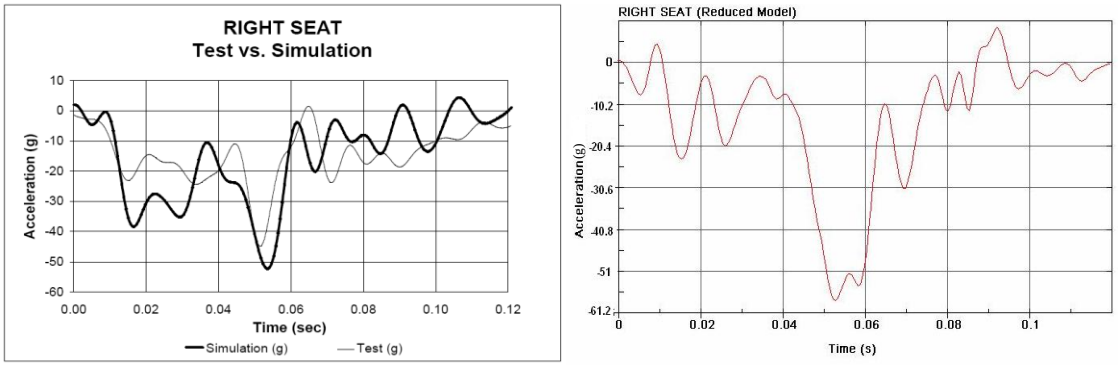

Figure 2.19 Comparison of the accelerations at the right seat for a frontal crash into a rigid wall Left figure: GWU's results Right figure: UM's result

Table 2.3 Stiffness and frequency test results

Test items	Nominal value for truck body	C-2500 model
Bending stiffness	4,000~5,000 N/mm	2,216 N/mm
Torsion stiffness	3,000~4,000 Nm/o	2,536 Nm/o
Primary frequency	Around 15 Hz	9.5 Hz

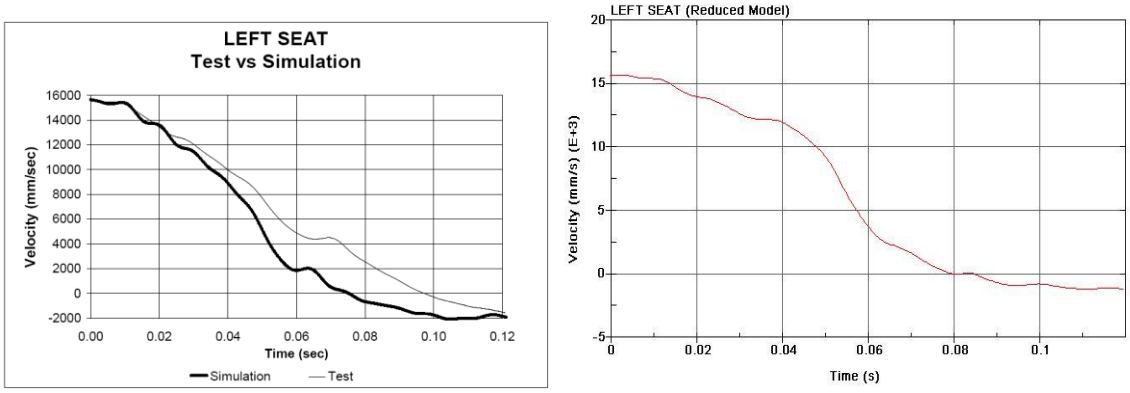

Figure 2.20 Comparison of the velocities for the frontal crash into a rigid wall
Left figure: GWU's results. Right figure: UM's result.

Table 2.4 Physical dimension and weight comparison for simplified dummy model and Hybrid III

a) Dimension comparison:

	Simplified model	Hybrid III (50^{th} percentile adult male)
Erect Sitting Height	893 mm	907 mm
Standing Height	1,742 mm	1,751 mm

b) Weight comparison:

	Simplified model	Hybrid III (50^{th} percentile adult male)
Head	4.53 kg	4.54 kg
Neck	1.48 kg	1.54 kg
Torso	38.92 kg	40.23 kg
Total	76.2 kg	78.20 kg

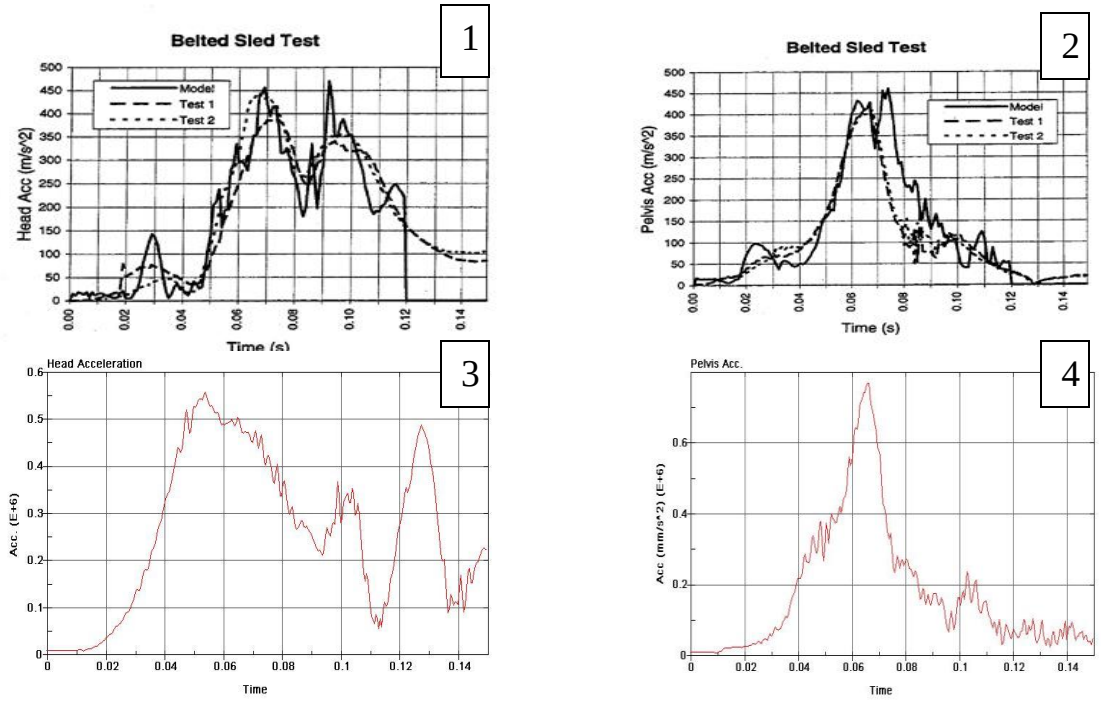

Figure 2.21 Comparison of accelerations of the head and pelvis between the simplified dummy model and Hybrid III: 1) head acceleration of Hybrid III, 2) pelvis acceleration of Hybrid III, 3) head acceleration of the simplified model, 4) pelvis acceleration of the simplified model.

In terms of crash performance, Fig. 2.19 compares the accelerations obtained in the right front seat during a frontal crash. The thick line in the left graph is a simulation result obtained at GWU (Zaouk, et al., 1996), who developed the original truck model, and the thin line in the same graph is the test result obtained at GWU. The right graph depicts the simulation results obtained at UM. It can be seen that the results are compatible in terms of major tendencies.

Fig. 2.20 further shows the velocity comparison of the measurement in the corresponding left front seat. The thick line in the left graph is the simulation result obtained at GWU and the thin line in the same graph is the test result. The right graph shows the results obtained at UM. It can be seen again that the results are compatible in terms of major tendencies.

A simplified dummy FEA model (see Fig. 2.22) was also evaluated and compared with a real dummy model, Hybrid III, using the virtual prototyping with LS-DYNA.

First, as shown in Table 2.4, the physical dimensions and weights are compared between the two models, and this comparison shows the similarity of the two models. Second, as shown in Fig. 2.21, the accelerations of the head and pelvis under a Belted Sled Test are compared between the two models. It can be observed that the tendencies and peak values are in good correlation.

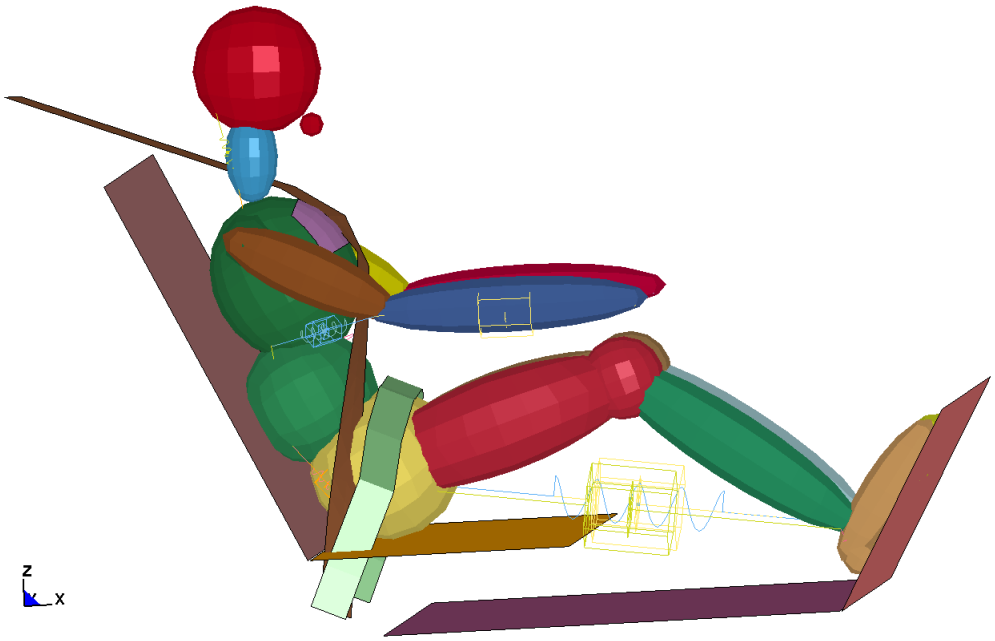

Figure 2.22 Simplified FEA dummy model

CHAPTER III

FIRST-ORDER ANALYSIS (FOA) MODEL OF AN EXPLOSIVE AIRBAG

3. 1 Introduction

In the I-bumper (inflatable bumper) concept (Kikuchi, 2007), two explosive airbags are deployed just before the main body-to-body crash in order to absorb the kinetic energy of the other vehicle. The release also actuates other components in the I-bumper, including a movable bumper and an energy absorption morphing lattice structure. A small explosive charge is used to deploy the airbag. A conventional airbag model has been used to reduce the crash energy in a controlled manner and reduce the peak impact force. An analytical model of the explosive airbag is developed in this chapter for the I-bumper system and for its optimal design, while the complete system design (I-bumper) is discussed in a separate chapter.

Analytical formulations for an explosive airbag have been developed and major design variables have been identified. These are used to determine the required amount of explosive and to predict the airbag's behavior, as well to predict the impact of the airbag on the I-bumper system. Related design guidelines and procedures have also been introduced. This new explosive airbag model has been implemented in MATLAB, and has been validated with a high fidelity model using an LS-DYNA simulation.

The concept of safety design using external airbag bumpers was introduced more than ten years ago (Clark and Young, 1995).

In this research, the advanced external airbag fitted with explosive charges for crashworthiness design is investigated. Some ideas on external airbag systems have been applied to the bumper. They are, however, still in need of development and more

theoretical grounding. In this study, some theoretical bases for the external airbag have been given, and innovative concepts including explosive charges have been investigated.

3. 2 FOA (First-order-analysis) model for an external explosive airbag model

To obtain the governing equation on the crash of a car equipped with an external explosive airbag, a simplified First-Order-Analysis (FOA) model was used in this research. Although various simplified models for vehicle collisions have been developed (Kamal, 1970; Mooi and Huibers, 1998; Lin, Kamal, and Justusson, 1975; Greene, 1977), only the three degree-of-freedom (DOF) model or the two degree-of-freedom (DOF) model has been applied in this research.

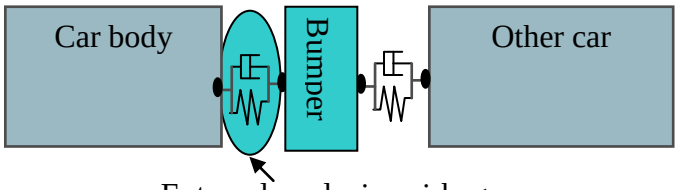

Figure 3.1 Simplified FOA model (3 DOF) for a head-on collision between cars

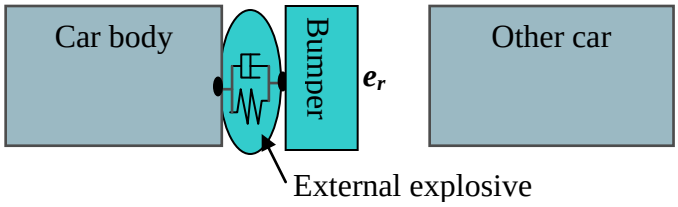

e_r: Coefficient of restitution

Figure 3.2 Simplified FOA model (2 DOF) for head-on car collision using e_r, the coefficient of restitution (COR)

Fig. 3.1 and Fig. 3.2 show the First-Order-Analysis model of a car crash with the airbags used in this study. In Fig. 3.1, a spring coefficient and a damping coefficient have been used to model both the explosive airbag and the collision between the bumper and other cars, while in Fig. 3.2, e_r, the coefficient of restitution (COR), has been used to model the collision between the bumper and other cars, and the explosive airbag has again been modeled by a spring coefficient and a damping coefficient.

The governing incremental equation of crash motion of the system (Fig. 3.1 and Fig. 3.2) can be expressed as

$$[m_i][\Delta\ddot{x}_i] + [k_i][\Delta x_i] + [c_i][\Delta\dot{x}_i] = [\Delta F_i] \tag{3-1}$$

To find the stiffness matrix and the damping matrix of equation (3-1), it is necessary to determine the spring coefficients and the damping coefficients of the external airbag, and the initial conditions (displacements and velocities after detonation) of each mass in the models shown in Figs. 3.1 and 3.2. In subsequent chapters, the analytic approach for those coefficients of airbags and initial conditions will be investigated. To obtain the spring coefficients and the damping coefficient of the airbag, the Wang-Nefske state equation was used (see chapter 3.3). The initial velocity of the car body and the bumper in equation (3-1) was obtained using a modification of Gurney's equation, a modification that was developed in this research (see chapter 3.4). In this model, typically the car bumper will have a very high speed due to the detonation of the explosive. The equation (3-1) will be solved using the step-by-step integration method (see chapter 3.5).

The spring coefficient and damping coefficient of the impact between the car bumper and other cars in Fig. 3.1 and the COR in Fig. 3.2 can be determined by experimental tests. Fig. 3.3 shows the FEA model for an external airbag using LS-DYNA. In the latter part of this chapter, the validation of the analytic model developed based on FOA (Figs. 3.1 and 3.2) using the FEA model of Fig. 3.3 has been performed.

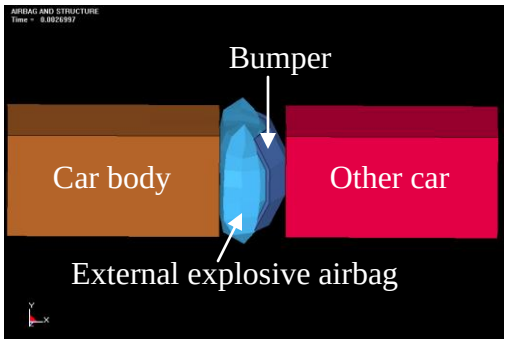

Figure 3.3 FEA model for external airbag using LS-DYNA

3.3 FOA model of a conventional airbag

As mentioned in the previous chapter, the FOA model has been used for an external explosive airbag. Therefore it is a basic necessity to know the spring coefficient and the damping coefficient for the external airbag. The development of the airbag model based on FOA is shown in this chapter. This external explosive airbag model includes both the modified conventional airbag model and the modified explosive model.

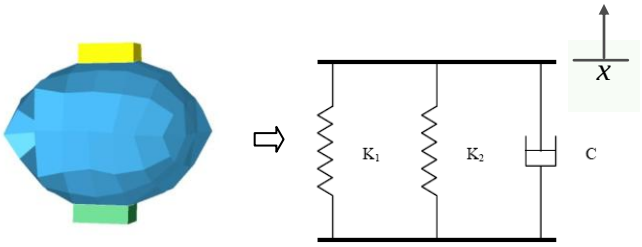

Figure 3.4 Simple airbag FOA model

Fig. 3.4 shows a simple airbag FOA model. Two spring coefficients and one damping coefficient are determined in this chapter.

3.3.1 Spring coefficients of airbag

The force of the airbag is defined by gauge pressure multiplied by the effective area

$$F_x = P_g \cdot A_e \tag{3-2}$$

where P_g denotes a gauge pressure of the airbag, and A_e denotes the effective area of the airbag, defined by the load divided by the pressure. To determine the force of the airbag at any given point, atmospheric pressure should be subtracted from the absolute pressure values to obtain the gauge pressure, giving

$$P_g = P - P_a \tag{3-3}$$

where P is absolute pressure and P_a is atmospheric pressure. The spring coefficient can be evaluated by force differentiated by displacement (Presthus, 2002). Plugging equation (3-3) into equation (3-2) and differentiating the force by displacement will give

$$\begin{aligned} K_x &= \frac{dF_x}{dx} = \frac{d}{dx}(P_g \cdot A_e) \\ &= P_g \cdot \frac{dA_e}{dx} + \frac{dP_g}{dx} \cdot A_e = P_g \cdot \frac{dA_e}{dx} + \frac{dP}{dx} \cdot A_e \end{aligned} \tag{3-4}$$

Equation (3-4) will be

$$K_x = \frac{dP}{dx} \cdot A_e + P_g \cdot \frac{dA_e}{dx} = \frac{dP}{dt} \cdot \frac{A_e}{\dot{x}} + \frac{dA_e}{dx} \cdot P_g \tag{3-5}$$

Now two spring coefficients for an airbag will be

$$K_{x\_1} = \frac{dP}{dt} \cdot \frac{A_e}{\dot{x}}, \quad K_{x\_2} = \frac{dA_e}{dx} \cdot P_g \tag{3-6}$$

where $\dot{x}$ denotes the velocity of impact mass.

3.3.2 Damping coefficient of airbag

For the damping coefficient of leakage or venting in the airbag, the Bernoulli equation is used. It is assumed that the flow between location A (inside the airbag) and location B (outside the airbag) (see Fig. 3.5) is inviscid, incompressible, free from heat transfer, and steady. Thus the Bernoulli equation between these two locations yields (White, 1994).

$$\frac{P_A}{\rho \cdot g} + \frac{v_A^2}{2g} + Z_A = \frac{P_B}{\rho \cdot g} + \frac{v_B^2}{2g} + Z_B + h \tag{3-7}$$

Assuming laminar flow gives (White, 1994)

$$h = \frac{32 \mu L v_B}{\rho g d^2} \tag{3-8}$$

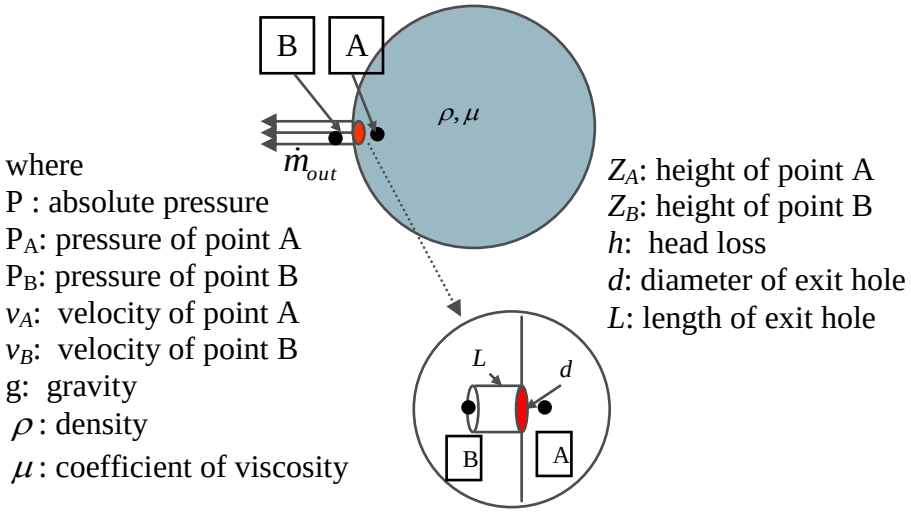

Figure 3.5 Airbag properties and geometry for the Bernoulli equation

Plugging (3-8) into (3-7) gives

$$\frac{P_A}{\rho \cdot g} + \frac{v_A^2}{2g} = \frac{P_B}{\rho \cdot g} + \frac{v_B^2}{2g} + \frac{32\mu L v_B}{\rho g d^2} \tag{3-9}$$

From equation (3-9), the pressure difference between spot A and spot B is written as

$$(P_A - P_B) = \rho \cdot g\left(\frac{v_B^2 - v_A^2}{2g} + \frac{32\mu L v_B}{\rho g d^2}\right) \tag{3-10}$$

The force generated by the pressure difference is

$$F = \rho \cdot g\left(\frac{v_B^2 - v_A^2}{2g} + \frac{32\mu L v_B}{\rho g d^2}\right) A_e \tag{3-11}$$

Finally, the viscous damping coefficient will be

$$C = F/\dot{x} = \frac{\rho \cdot g\left(\frac{v_B^2 - v_A^2}{2g} + \frac{32\mu L v_B}{\rho g d^2}\right) A_e}{\dot{x}} \tag{3-12}$$

where $\dot{x}$ denotes the velocity of the airbag compression, v_B can be expressed as $\dot{m}_{out} \Big/ \rho\left(\frac{d}{2}\right)^2 \pi$, and v_A can be assumed to be zero.

The airbag damping coefficient, usually a viscous damping coefficient, is much lower than the spring coefficient unless there is leakage or a vent hole. In that case, the damping coefficient can be neglected without detriment.

3.3.3 Wang and Nefske state variables

The spring coefficient (eq. 3-6), thus, requires knowing the pressure change at any given time. The Wang and Nefske model (Wang and Nefske, 1988) has been used to

determine the pressure change in the spring coefficient equation. For the airbag, they made three assumptions about the airbag processes: that the gas behaves as an ideal gas, that adiabatic processes are taking place, the tabular input of mass flow and the gas temperature. Based on the above assumptions, they obtained basic state equations as follows:

$$\begin{aligned}
&P_2V_2 = m_2RT_2 \\
&\frac{dm_2}{dt} = \dot{m}_{in} - \dot{m}_{out} \\
&\frac{1}{T_2}\dot{T}_2 = \frac{1}{m_2}\left(\dot{m}_{out} - \dot{m}_{in}\right) + \frac{k}{m_2}\left(\frac{T_1}{T_2}\dot{m}_{in} - \dot{m}_{out}\right) - \frac{(k-1)}{V_2}\dot{V}_2 \\
&\dot{V}_2 = V_{20}C_\beta\dot{P}_2 - \Delta\dot{V}
\end{aligned} \tag{3-13}$$

Making use of equation (3-13) results in the governing gas dynamic equations that apply after the airbag is fully inflated.

$$\begin{pmatrix} m_2V_2 & V_2T_2 & 0 & m_2T_2(k-1) \\ 0 & 1 & 0 & 0 \\ -m_2R & -RT_2 & V_2 & P_2 \\ 0 & 0 & -V_{20}c_\beta & 1 \end{pmatrix}\begin{pmatrix} \dot{T}_2 \\ \dot{m}_2 \\ \dot{P}_2 \\ \dot{V}_2 \end{pmatrix} = \begin{pmatrix} kV_2T_1\dot{m}_{in} - kV_2T_2\dot{m}_{out} \\ \dot{m}_{in} - \dot{m}_{out} \\ 0 \\ -\Delta\dot{V} \end{pmatrix} \tag{3-14}$$

Again, after performing some algebraic manipulation, equation (3-14) may be written in the form of

$$\begin{aligned}
&\dot{m}_2 = \dot{m}_{in} - \dot{m}_{out} && \text{Subscript 1: canister (inflator)} \\
&\dot{P}_2 = \frac{(kR(T_1\dot{m}_{in} - T_2\dot{m}_{out}) + kP_2\Delta\dot{V}}{(V_2 + kP_2c_\beta V_{20})} && \text{Subscript 2: airbag} \\
&\dot{V}_2 = \frac{(c_\beta V_{20}kR(T_1\dot{m}_{in} - T_2\dot{m}_{out}) + V_2\Delta\dot{V}}{(V_2 + kP_2c_\beta V_{20})} \\
&T_2 = \frac{P_2V_2}{Rm_2}
\end{aligned} \tag{3-15}$$

where

c_β : bag stretch factor

$\Delta\dot{V}$: computed bag volume change by impacting mass

V_{20} : volume of fully Inflated airbag

P_2, T_2, V_2 : pressure, temperature, volume of airbag

(P_2 is equal to P in equation $(3-3)$)

T_1 : temperature of canister

k : c_p / c_v (specific heat ratio of the gas)

R : gas constant

$\dot{m}_{in}$: mass rate of gas flowing into the airbag

$\dot{m}_{out}$: mass rate of gas flowing out from the airbag

At this point, airbag model spring coefficients can be determined by using the pressure change of the airbag obtained by using the Wang and Nefske equation (3-15). Problems involving multi-degree of freedom, including these spring coefficients (eq. 3-6) and damping coefficient (eq. 3-12) can be evaluated using the step-by-step integration method. In this method, the response is evaluated at successive increments Δt (or dt) of time. These coefficients are considered in the analysis by reevaluating at the beginning of each time increment. Details are given in chapter 3.5.

The bag's stretch factor is denoted as c_β , and this was determined experimentally. $\Delta\dot{V}$ is the bag's computed volume change rate due to the impacting mass making contact with the airbag; this can be estimated by the standard contact algorithm. To make the Wang and Nefske algorithm easier to apply to external airbags, an analytic expression for c_β and $\Delta\dot{V}$ is derived in this research.

3.3.4 Analytic solution for c_β and $\Delta\dot{V}$

According to Wang and Nefske (Wang and Nefske, 1988), the relationship between the pressure (P_2) and the volume (V_2) of the airbag will be expressed as

$$V_2 = V_{20}(1 + c_\beta (P_2 - P_a)) \tag{3-16}$$

where V_{20} is the volume of the fully inflated bag, and P_2 and V_2 denote the pressure and volume of the airbag at any given time during collision; usually, $P_2 > P_a$. The bag is considered "fully inflated" when it has attained some prescribed value V_{20} at which the bag material is taut. The volume of the airbag can be analytically found to vary with the bag pressure.

Equation (3-16) represents the volume of the airbag according to the pressure of the airbag. To find an analytic solution for c_β, some assumptions are made about the airbag. The shape of the airbag is assumed to be spherical and the thickness of the airbag is assumed to be very small relative to the radius of the airbag. So, the stress of the airbag fabric (Beer, Dewolf, and Johnston, 2002) will be shown by

$$\begin{aligned} (P_2 - P_a)\pi r^2 &= 2\pi r t \sigma \\ \sigma &= \frac{(P_2 - P_a)r}{2t} \end{aligned} \tag{3-17}$$

where r means a radius of the airbag and t means a thickness of the airbag fabric. The strain rate is expressed as

$$\varepsilon = \sigma / E = \frac{(P_2 - P_a)r}{2Et} \tag{3-18}$$

where E denotes a Young's modulus of airbag fabric. The radius of the airbag (r') according to pressure change will be given as

$$\begin{aligned} 2\pi r + \varepsilon \cdot 2\pi r &= 2\pi r' \\ 2\pi\left(r + \frac{(P_2 - P_a)r^2}{2Et} \right) &= 2\pi r' \end{aligned}$$

$$\therefore r' = r + \frac{(P_2 - P_a)r^2}{2Et} \tag{3-19}$$

where r' means a changed radius according to pressure change (see Fig. 3.6). The volume of the fully inflated airbag will be expressed by

$$V_{20} = \frac{4}{3}\pi r^3 \tag{3-20}$$

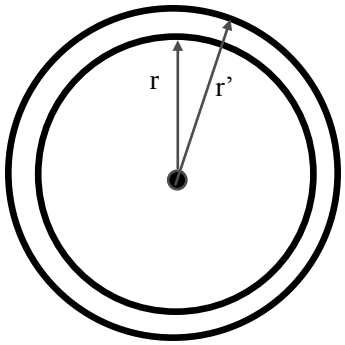

Figure 3.6 Cross section of spherical airbag

and the volume of airbag according to the pressure increase will be expressed by

$$\begin{aligned} V_2 &= \frac{4}{3}\pi r'^3 = \frac{4}{3}\pi\left(r + \frac{(P_2 - P_a)r^2}{2Et}\right)^3 \\ &= \frac{4}{3}\pi r^3\left(1 + \frac{3(P_2 - P_a)r}{2Et} + 3\left(\frac{(P_2 - P_a)}{2Et}\right)^2 r^2 + \left(\frac{(P_2 - P_a)r}{2Et}\right)^3 r^3\right) \end{aligned} \tag{3-21}$$

Finally, a volume expression that has the same format as the Wang-Nefske expression (3-16) is obtained from equation (3-21):

$$V_2 = V_{20}\left(1 + \left(\frac{3r}{2Et} + 3\left(\frac{(P_2 - P_a)}{(2Et)^2}\right)r^2 + \left(\frac{(P_2 - P_a)^2 r^3}{(2Et)^3}\right)\right)(P_2 - P_a)\right) \tag{3-22}$$

Therefore, it can be said that

$$c_\beta = 3\frac{r}{2Et} + 3\left(\frac{r}{2Et}\right)^2 (P_2 - P_a) + \left(\frac{r}{2Et}\right)^3 (P_2 - P_a)^2 \approx \frac{3r}{2Et} \qquad (3\text{-}23)$$

The analytic value for $\Delta\dot{V}$ could simply be defined by the effective area multiplied by the speed of the impacting mass.

$$\Delta\dot{V} = -(A_e v_i) \qquad (3\text{-}24)$$

where v_i denotes the speed of the impacting mass

3.3.5 Effective area (A_e)

The spring coefficient (eq. 3-6) and the damping coefficient (eq. 3-12) also require knowing the effective area. Tests for effective area and displacement were conducted by Nefske (1972).

The experimental test results of a variation of the effective area with displacement are shown in the work of Nefske (1972). It can be assumed that the relationship between the effective area and the displacement is also linear. Therefore, the effective area can be expressed as

$$A_e = A_{e\_slope} \times x + A_{e\_cons} \qquad (3\text{-}25)$$

where A_{e_slope}, A_{e_cons}, and x represent the slope of the line, the coefficient, and the displacement of impacting mass, respectively. A_{e_slope} and A_{e_cons} can be obtained from the airbag and impacting mass static tests.

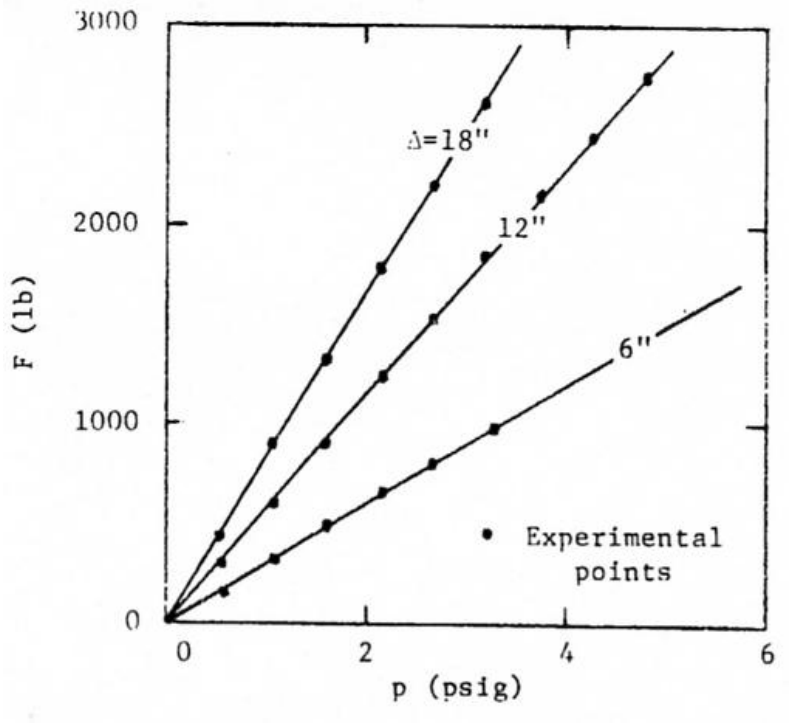

Figure 3.7(a) Force vs. bag (gauge) pressure by Nefske (1972)

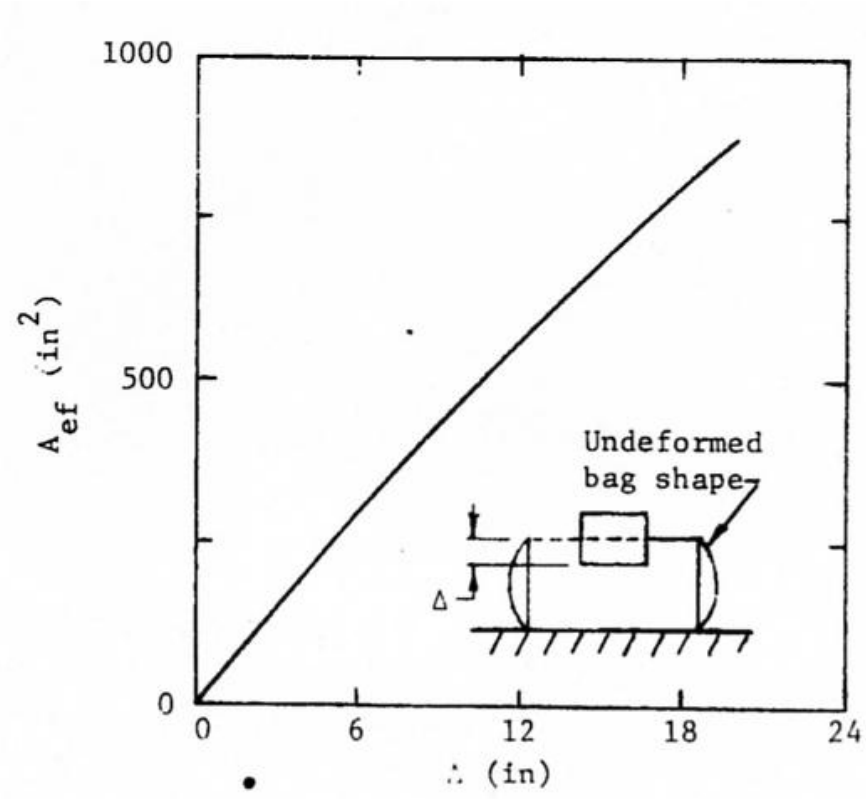

Figure 3.7(b) Effective area vs. displacement by Nefske (1972)

3.3.6 Prediction of airbag failure

To estimate the time when the airbag is flattened after a crash, it is assumed that the airbag will be compressed in such a way that when the center part of the airbag is compressed, the upper part and lower part of the airbag will be forced into a cylindrical shape, as shown in Fig 3.8. Therefore, maximum stress will appear in the upper part or the lower part of the cylinder. The volume of one cylinder is given as

$$\pi \cdot r^2 \cdot a = (V - A_e x)/2 \tag{3-26}$$

where r, a, V, x represent the radius of the cylinder, the length of the cylinder, the volume of the airbag, and the intrusion distance of the impacting mass, respectively. The radius and stress (Beer, Dewolf, and Johnston, 2002) of the cylinder becomes

$$r = \sqrt{\frac{V - A_e x}{2\pi a}}, \qquad \sigma = \frac{P \cdot r}{t} \tag{3-27}$$

Thus, if the stress obtained by the equation (3-27) exceeds the yield stress of the airbag fabric, then the airbag will flatten.

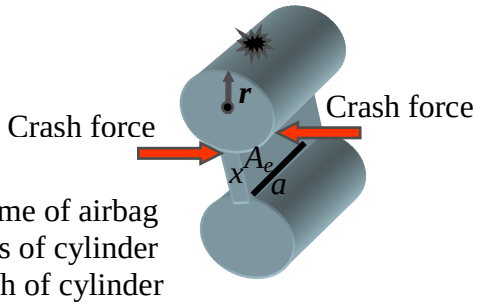

V: volume of airbag
r: radius of cylinder
a: length of cylinder
x: intrusion distance of impacting mass
A_e: effective area

Figure 3.8 Estimated shape of airbag during compression

3.4 Explosive model in an airbag for the system with an initial velocity

3.4.1 Airbag bumper equipped with an explosive charge and Gurney's model (Jones, Kennedy, and Bertholf, 1980; Zukas and Walters, 1998)

Flat sandwich

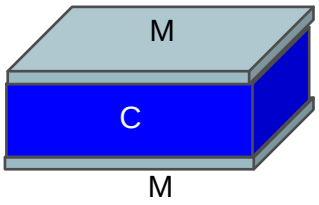

$$v_M = \sqrt{2E_T}\left[\frac{2M}{C}+\frac{1}{3}\right]^{-1/2}$$

Cylindrical case

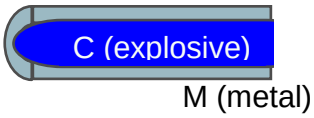

$$v_M = \sqrt{2E_T}\left[\frac{M}{C}+\frac{1}{2}\right]^{-1/2}$$

Spherical case

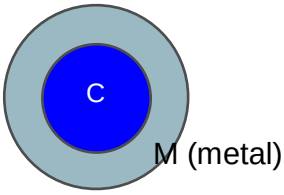

$$v_M = \sqrt{2E_T}\left[\frac{M}{C}+\frac{3}{5}\right]^{-1/2}$$

Asymmetric Flat sandwich

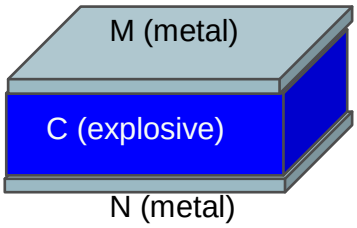

$$v_M = \sqrt{2E_T}\left[\frac{1+A^3}{3(1+A)}+\frac{N}{C}A^2+\frac{M}{C}\right]^{-1/2}$$

Open-face Flat sandwich

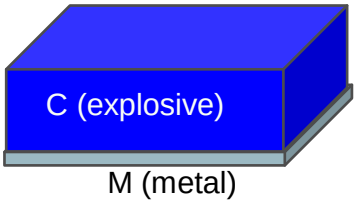

$$v_M = \sqrt{2E_T}\left[\frac{\left(1+2\frac{M}{C}\right)^3+1}{6(1+\frac{M}{C})}+\frac{M}{C}\right]^{-1/2}$$

$$where,\ A=\frac{1+2\frac{M}{C}}{1+2\frac{N}{C}}$$

C : *mass per unit area of explosive*
E_T : *energy per unit mass of explosive*
M : *mass per unit area of metal layer*
v : *max. velocity of metal after detonation*

Figure 3.9 Examples of Gurney's equation

In this study, it is necessary to determine the effect of the explosive in deploying the airbag as opposed to the effect of deploying it with compressed gas. To do this, Gurney's model for the explosive has been applied. The explosive will be positioned in the airbag between the bumper and the main body of the car.

The explosive model of the airbag is based on Gurney's model that estimates the velocity or the kinetic energy of materials driven by detonation expansion. Gurney's approach is outstanding for its versatility and simplicity. Extensions and new applications continue to appear because the physical framework is intuitively satisfying and mathematically easy to handle even at very advanced and complex levels.

The basic equation is derived based on the assumption that the potential energy characterizing the explosive charge before detonation is equal to the sum of the kinetic energies of the detonation product gases and the metal after detonation expansion.

Fig. 3.9 shows Gurney's equation for certain cases that denote the maximum velocity of masses after detonation. The velocity of the bumper and the car after detonation (but before the collision) can be determined from Gurney's equation as the system's initial velocity in Figs. 3.1 and 3.2. After detonation, the external airbag will work like an ordinary dynamic airbag or a static air spring as modeled by FOA in Figs. 3.1 and 3.2. The external explosive airbag can be modeled using the explosive model (the modified Gurney model for the system's initial velocities) and the conventional model (the Wang and Nefske model for the state variables of the spring coefficients).

3.4.2 Modified Gurney's model with initial velocity (for velocity and pressure during detonation)

Gurney's equation was developed through treating the mass to be driven as a stationary object. In a car crash, usually the cars have an initial non-zero velocity before the crash. To apply Gurney's model to an external explosive airbag, some modifications must be made to Gurney's original equation with respect to initial velocity v_0 (see Fig. 3.10).

Additionally, it is necessary to know the velocity history during detonation, as well as the maximum velocities of the masses, because a collision could occur before the

driven mass reaches the maximum velocity. To do this, an energy conservation equation and momentum conservation equation will be applied.

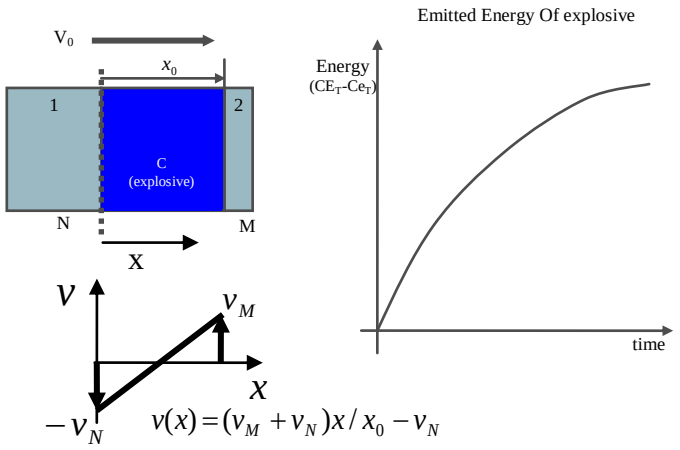

Figure 3.10 Asymmetric sandwich configuration with initial velocity v_0 for modified Gurney's model

Jones (Jones, Kennedy, and Bertholf, 1980) developed the velocity history equation (v'_M) and pressure history equation (P') of an airbag during detonation for stationary case ($v_0 = 0$) with respect to displacement (x_M)

$$v_M'^2 = \frac{2E_T}{B}\left\{1-\left[\left(\frac{x_M}{x_{M0}}\right)(A+1)-A\right]^{-B(\gamma-1)/(M/C)(A+1)}\right\}$$

$$P' = \left(CE_T - \frac{1}{2}v_M^2 BC\right)(\rho(\gamma-1))/C \qquad (3\text{-}28)$$

$$\rho = \frac{C}{x_M - x_N} = \frac{C}{x_M(1+A) - x_{M0}A}$$

where

$$B = \frac{N}{C}A^2 + \frac{M}{C} + \frac{(1+A^3)}{3(1+A)},\quad A = \frac{M+\frac{C}{2}}{N+\frac{C}{2}},\quad x_{M0} = \frac{C}{\rho_0}$$

x_M : position coordinate of plate M x_{M0} : initial position coordinate of plate M

γ : the ratio of specfic heat ρ : mass density of the gas

From these equations (3-28), the velocity of mass N and mass M after detonation for the stationary case can be computed.

Now the equation (3-28) must be modified for a case where the initial velocity is not zero. The linear gas velocity profile assumption (see Fig. 3.10) allows us to write the principle of energy conservation as

$$\frac{1}{2}(N+M+C)v_0^2 + CE_T = Ce_T + \frac{1}{2}Mv_M^2 + \frac{1}{2}Nv_N^2 + \frac{1}{2}\int_{x=0}^{x=x_0}\rho(x)[v(x)]^2\,dx \tag{3-29}$$

where

$\rho(x) = C/x$

$v(x) = (v_M + v_N)x/x_0 - v_N$

x_0 : initial distance of metal

x : distance of metal

v_M : velocity of metal M

v_N : velocity of metal N

e_T : internal energy per unit mass remaining in the explosive

which reduces to

$$\frac{1}{2}(N+M+C)v_0^2 + \left[CE_T - Ce_T\right] = \frac{1}{2}Mv_M^2 + \frac{1}{2}Nv_N^2 + \frac{C}{6}\frac{\left(v_M^3 + v_N^3\right)}{\left(v_M + v_N\right)} \tag{3-30}$$

It is assumed that the emitted energy and the time relationship for the explosive are not associated with the initial velocity, so the emitted energy during detonation for the case with the initial non-zero velocity can be obtained from the stationary case ($v_0 = 0$) (Jones, Kennedy, and Bertholf, 1980); that is,

$$CE_T - Ce_T = \frac{1}{2}Mv_M'^2 + \frac{1}{2}Nv_N'^2 + \frac{C}{6}\frac{\left(v_M'^3 + v_N'^3\right)}{\left(v_M' + v_N'\right)} \tag{3-31}$$

where

v_M', v_N' : velocities of masses with zero initial velocity during detonation with same explosive energy (Equation (3-28))

Therefore, plugging equation (3-31) into equation (3-30) will give

$$\frac{1}{2}(N+M+C)v_0^2 + \left[\frac{1}{2}Mv_M'^2 + \frac{1}{2}Nv_N'^2 + \frac{C}{6}\frac{\left(v_M'^3 + v_N'^3\right)}{\left(v_M' + v_N'\right)}\right]$$
$$= \frac{1}{2}Mv_M^2 + \frac{1}{2}Nv_N^2 + \frac{C}{6}\frac{\left(v_M^3 + v_N^3\right)}{\left(v_M + v_N\right)} \tag{3-32}$$

Momentum conservation can be expressed by

$$(M+N+C)v_0 = Mv_M + Nv_N + \int_{x=0}^{x=x_0}\rho(x)[v(x)]dx \tag{3-33}$$

which reduces to

$$(M+N+C)v_0 = Mv_M + Nv_N + \frac{C}{2}\left(v_M + v_N\right) \tag{3-34}$$

Thus, equation (3-34) will be

$$v_N = \frac{(M + C/2)v_M - (M+N+C)v_0}{(N + C/2)} \tag{3-35}$$

Finally, the velocity equation from equations (3-32) and (3-35) can be expressed as

$$\alpha v_M^2 + \beta v_M + \gamma \tag{3-36}$$

where

$$\alpha = \frac{1}{2}\frac{N(M + C/2)^2}{(N + C/2)^2} + \frac{1}{2}M + \frac{C}{6}\left[1 - \frac{M + C/2}{N + C/2} + \frac{(M + C/2)^2}{(N + C/2)^2}\right]$$

$$\beta = \frac{-Nv_0(M + N + C)(M + C/2)}{(N + C/2)^2} + \frac{C}{6}\left[\frac{-2v_0(M + N + C)(M + C/2)}{(N + C/2)^2} + \frac{v_0(M + N + C)}{(N + C/2)}\right]$$

$$\gamma = \frac{(M + N + C)^2 v_0^2}{(N + C/2)^2}\left(\frac{C}{6} + \frac{N}{2}\right) - \frac{C}{6}\left(v_M'^2 + v_M' v_N' + v_N'^2\right) - \frac{1}{2}\left[(M + N + C)v_0^2 + Mv_M'^2 + Nv_N'^2\right]$$

This equation is a function of v_M' and v_N' (see equation (3-28)) which are functions of displacement (x_M). So it can be said that equation (3-36) is a function of displacement (x_M).

Finally, the velocity of mass M for the case with initial non-zero velocity according to the displacement can be found from the equation (3-36). The velocity of mass N can be found in the same way. The ideal gas equation is

$$e_T = \frac{P}{\rho(\gamma - 1)} \tag{3-37}$$

Therefore, the pressure (P) equation for the case with initial non-zero velocity with respect to displacement, from equations (3-30) and (3-37), can be given as

$$P = \left[\frac{1}{2}(N + M + C)v_0^2 + CE_T - \frac{1}{2}Mv_M^2 - \frac{1}{2}Nv_N^2 - \frac{C}{6}\frac{\left(v_M^3 + v_N^3\right)}{\left(v_M + v_N\right)}\right]\rho(\gamma - 1)/C \tag{3-38}$$

The inside pressure of the airbag after the collision between the bumper and the other cars will be increased by the reflection of the air shock in the airbag. Reflected pressure in the airbag for a solid surface and a zero angle of incidence will be (Kinney and Graham, 1985)

$$P_r = \frac{P(8P - P_a)}{P + 6P_a} \tag{3-39}$$

where P_a is atmospheric pressure. This pressure will be the initial value for equation (3-13).

3.4.3 Volume calculation during detonation using the effective explosive mass

Now, consider the effective explosive mass in driving the bumper. It cannot be assumed that the whole mass of the explosive is fully employed to drive the bumper. The explosive that is effective in driving the bumper plate is the core of the explosive nearest to the mass (Zukas and Walters, 1998). The effective explosive in driving the plate can be calculated by discounting angle (k_a) (see Fig. 3.11).

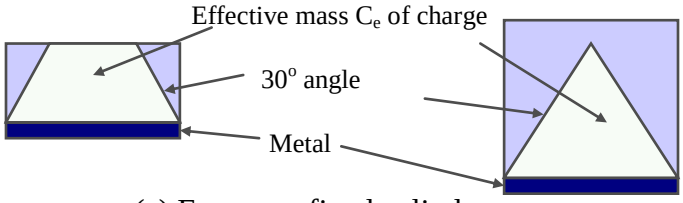

(a) For unconfined cylinders

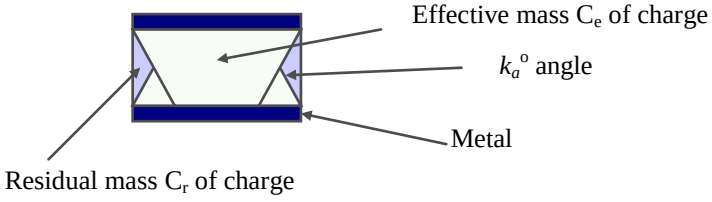

(b) For confined cylinders

Figure 3.11 Effective explosive mass in driving the plate

The discounting angle (Zukas and Walters, 1998) for confined cylinders to account for side losses in a cylindrical charge can be given as

$$k_a = \frac{30^o}{\sqrt{2}\left(\frac{M_a}{C} + \frac{1}{2}\right)^{1/2}} \tag{3-40}$$

where

M_a = mass of airbag fabric

C = explosive mass

The total explosive mass (C) will be expressed as a summation of the effective explosive (C_e) in driving a mass and residual explosive (C_r). It can be assumed that the effective explosive mass will be effective in driving in the bumper, and the residual explosive mass will produce the lateral expansion of the airbag.

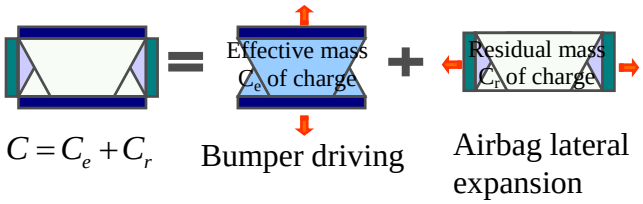

Figure 3.12 Effective explosive mass in driving the plate and residual explosive mass in lateral inflation

Therefore the airbag volume calculation during detonation will be performed by lateral expansion with residual explosive mass, and by longitudinal expansion with effective explosive mass, using the modified Gurney's equation (see Fig. 3.12). This volume will be the initial value for equation (3-15).

Fig. 3.13 shows a comparison between Gurney's original equation and modified equation in this study.

$$v = \sqrt{2E_T}\left[\frac{2M}{C} + \frac{1}{3}\right]^{-1/2} = 96.73$$

Result of Gurney's original equation

Explosive	v_0 *(m/s)*	*N(kg)*	*M(kg)*	*C(kg)*	v_N *(m/s)*	v_M *(m/s)*
TNT	0	30	30	0.1	-96.73	96.73

Result of modified equation

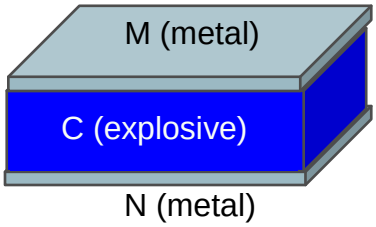

$$v_M = \sqrt{2E_T}\left[\frac{1+A^3}{3(1+A)} + \frac{N}{C}A^2 + \frac{M}{C}\right]^{-1/2} = 135.74 \quad where,\ A = \frac{1+2\frac{M}{C}}{1+2\frac{N}{C}}$$

$$v_N = \sqrt{2E_T}\left[\frac{1+A^3}{3(1+A)} + \frac{M}{C}A^2 + \frac{N}{C}\right]^{-1/2} = 2.04 \quad where,\ A = \frac{1+2\frac{N}{C}}{1+2\frac{M}{C}}$$

Result of Gurney's original equation

Explosive	v_0 *(m/s)*	*N(kg)*	*M(kg)*	*C(kg)*	v_N *(m/s)*	v_M *(m/s)*
TNT	0	2,000	30	0.1	-2.04	135.74

Result of modified equation

Figure 3.13 Comparison between original Gurney's equation and modified Gurney's equation

3.4.4 Collision time issue

In this section, the effect that the collision time has on absorbing the kinetic energy of the cars is investigated. Fig. 3.14 shows the velocity and deployment distance of the bumper with an explosive airbag. It says that the bumper will reach the steady-state

velocity (120 m/s) before it deploys 1 cm. Considering that the usual full deployment distance is more than 30 cm, it can be said that the collision will barely begin to happen during the transition region (within 1 cm of deployment). This means that there is no need to account for the collision occurring prior to when the steady state velocity of the bumper is reached.

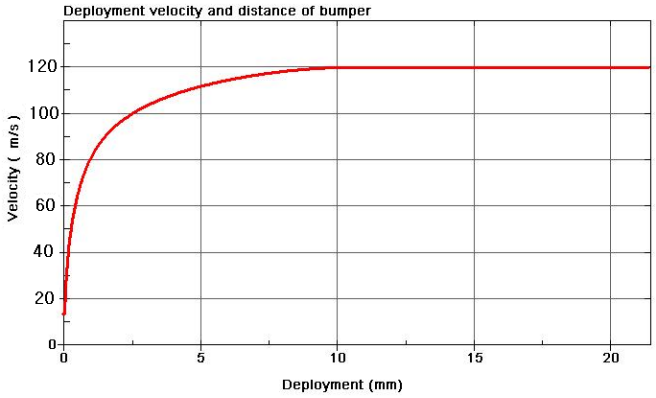

Figure 3.14 Deployment velocity and distance of bumper from an LS-DYNA simulation

Table 3.1 Total reduced kinetic energy according to the deployment distance

Deployment Distance (m)	Total Reduced KE of Mass 1 & 3 (%)
0.05	35.3514
0.1	35.3520
0.15	35.3535
0.2	35.3559
0.25	35.3594
0.3	35.3637

TNT- 100 g

The simulation results of Table 3.1 will further demonstrate this. Given the mass of TNT, the total of the kinetic energy absorbed by the explosive bumper is almost constant regardless of where the collision happens during the inflation of the airbag, as shown in Table 3.1. Again, Table 3.1 tells us that the position (inflated distance) of the projected

bumper is not critical to the reduced kinetic energy. Therefore it is not necessary to consider the collision time and position of the bumper in relation to the external airbag.

3.4.5 Issues of explosive design

The basic concept to project a bumper with explosives can be derived from the principles of the shaped charge of Rocket Propelled Grenade (RPG) based on the Munroe effect. The Munroe effect refers to the partial focusing of blast energy caused by a hollow or void cut into a piece of explosive, a property which is exploited by a shaped charge. Explosive energy is released directly away from (normal to) the surface of an explosive, so shaping the explosive will concentrate the explosive energy in the void. If the void is properly shaped, a high-velocity and safe projection will be obtained.

Safety is also a very important concern here, as a car loaded with explosives could be very dangerous. It should normally be very stable and should not explode if the car impacts with a human rather than another vehicle. Furthermore, when it explodes, it should not destroy any other parts of the car. These will be very challenging and vital tasks. In the future, the safety of the design must also be considered.

3.5 Integrated airbag-vehicle model and its solution

The spring and damping coefficient was investigated based on the Wang and Nefske equation for the stiffness matrix and the damping matrix of equation (3-1) and mass velocity driven by the explosive, based on Gurney's equation for the system's initial velocity of equation (3-1). As can be seen in Fig. 3.15, two kinds of models (the Gurney model and the Wang and Nefske model) for an airbag with explosives (as opposed to an airbag with a conventional gas canister as an inflator) were used.

Finally, the external airbag model can be combined and completed, incorporating both the explosive and the conventional airbag models (see Fig. 3.16). The initial pressure and volume of the airbag for equation (3-15) can be obtained from equation (3-39) and Fig. 3.11, respectively. The effective area (equation (3-25)) and the mass flow rate of the vent can be obtained from a static test of the airbag.

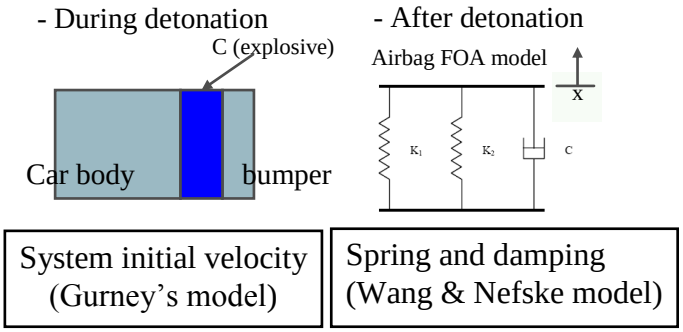

Figure 3.15 Explosive model and FOA model of airbag

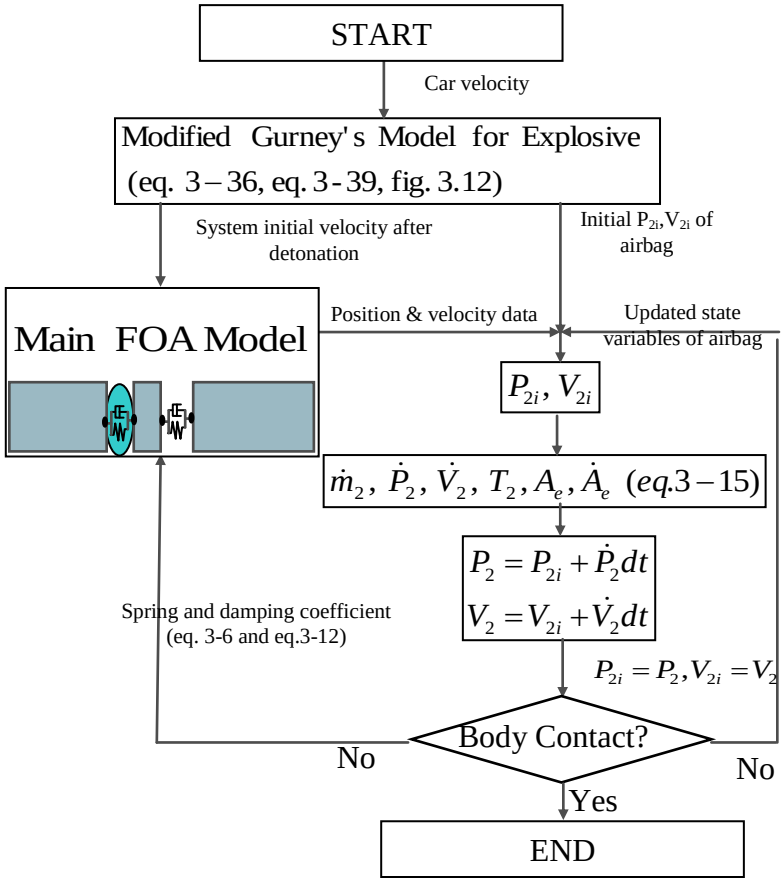

Figure 3.16 Process flow of the complete airbag model including explosive

To solve the nonlinear equation that appeared in the FOA model (equation (3-1) and Fig. 3.16), the step-by-step integration method for multi-degree of freedom systems using the linear acceleration method and the Wilson-θ method is applied. For details, see chapter 6.1.3

3.6 Validation of the integrated airbag and vehicle model

To validate the analytic model, a comparison between the analytic model and the FEA model using LS-DYNA has been made. Figure 3.17 shows an analytic model and an FEA model for validation. To simulate the effect of the explosive in the airbag, the CONWEP function of LS-DYNA was used.

The methodology for the complete airbag model was implemented using MATLAB. Now, the velocities of each mass are shown in Figs. 3.18, 3.19, and 3.20, for the velocity of mass1, the velocity of mass 3, and the velocity of mass 2, respectively. The results are compatible in terms of their major tendencies

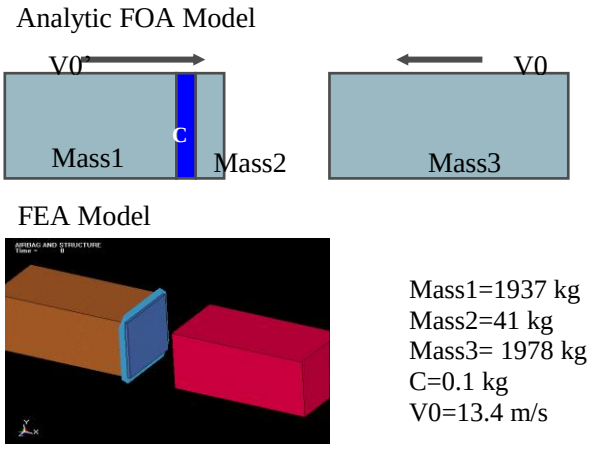

Figure 3.17 Analytic FOA model and FEA model for the complete airbag model

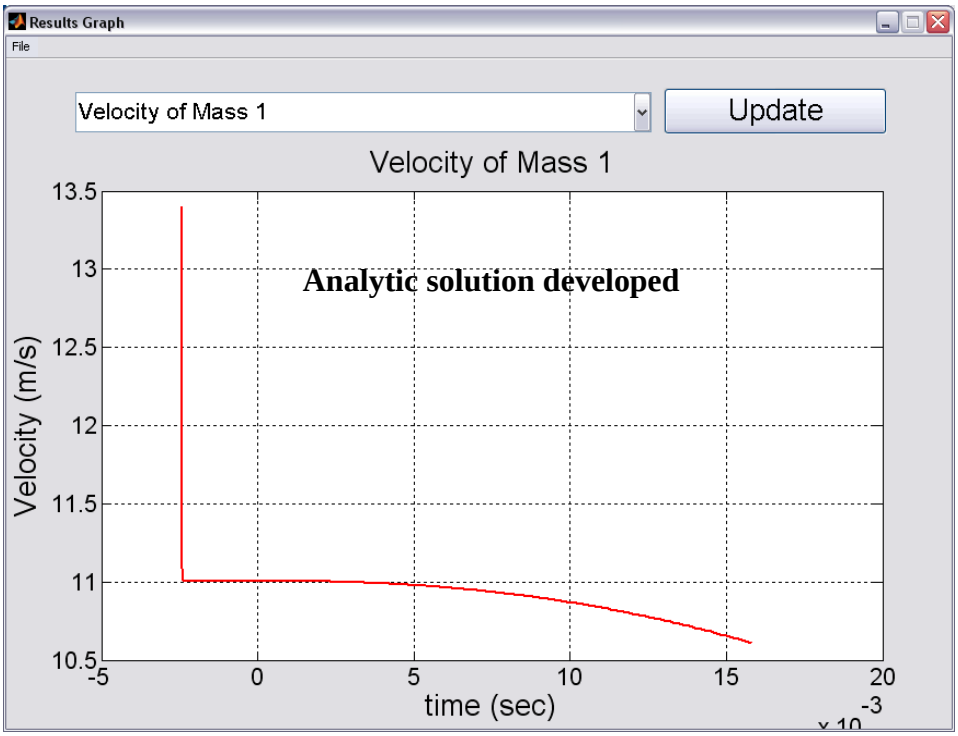

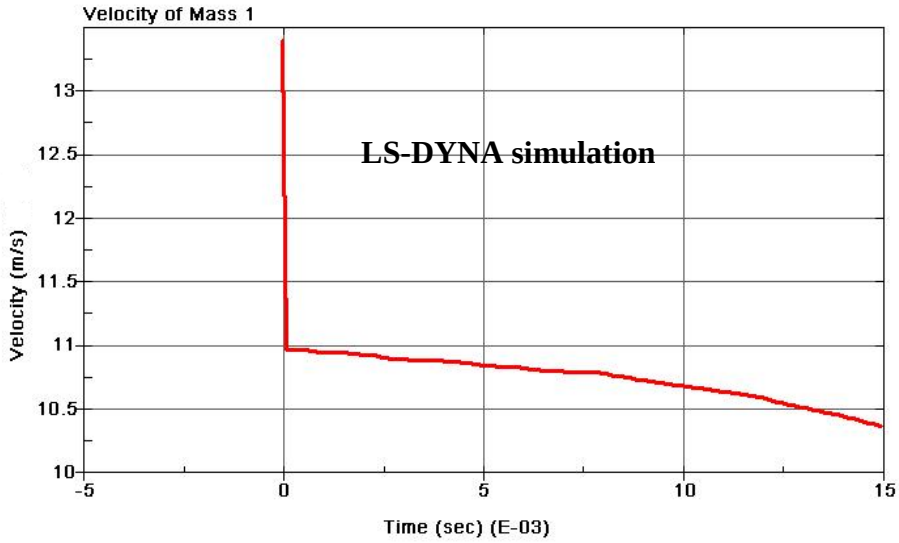

Figure 3.18 Velocity of Mass1

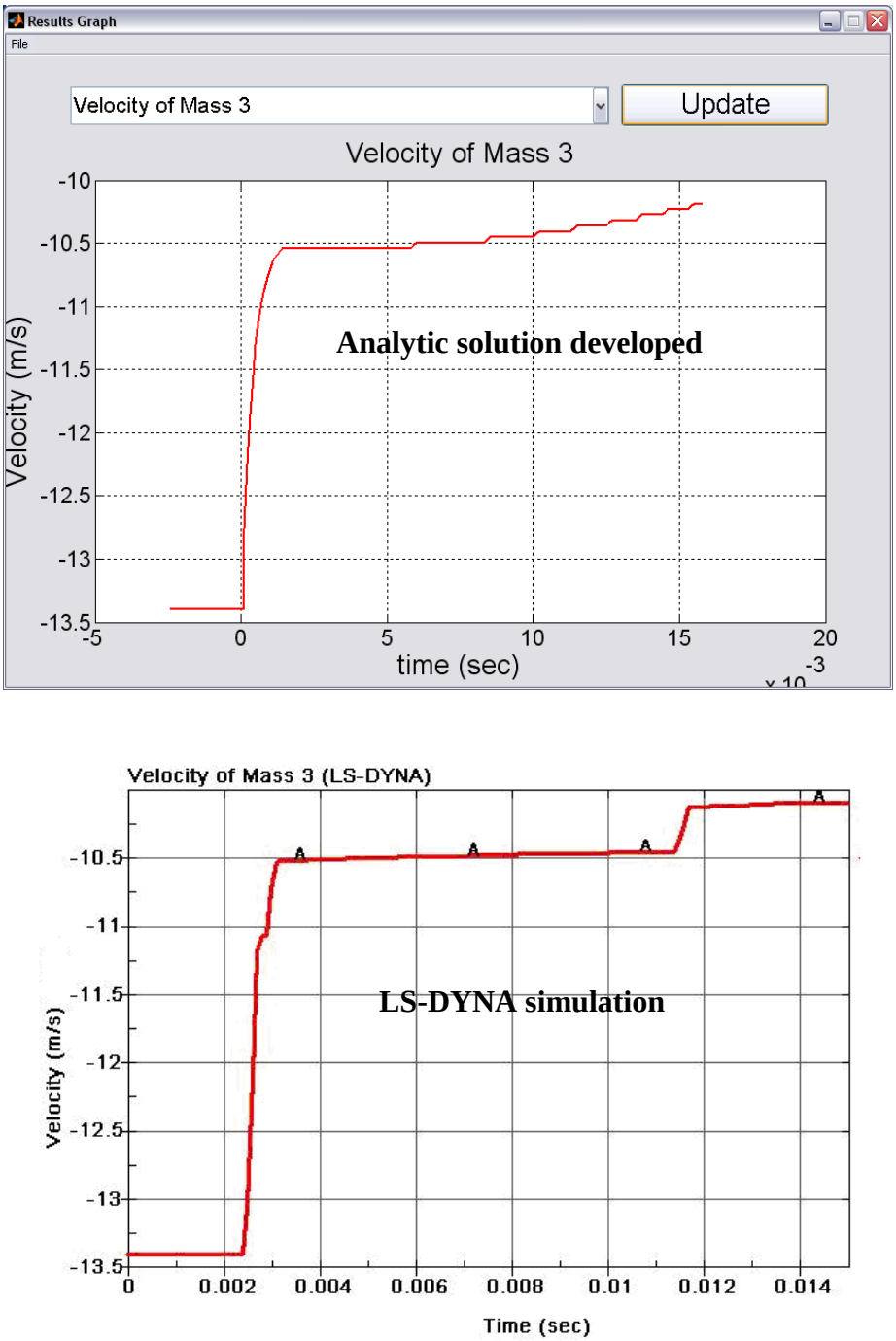

Figure 3.19 Velocity of Mass 3

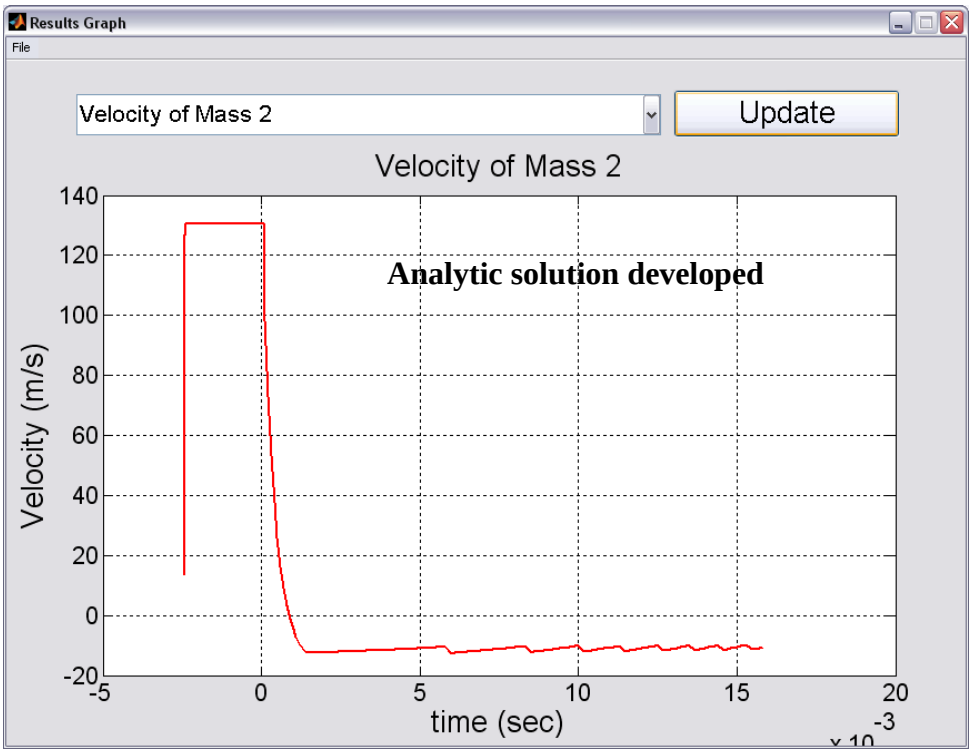

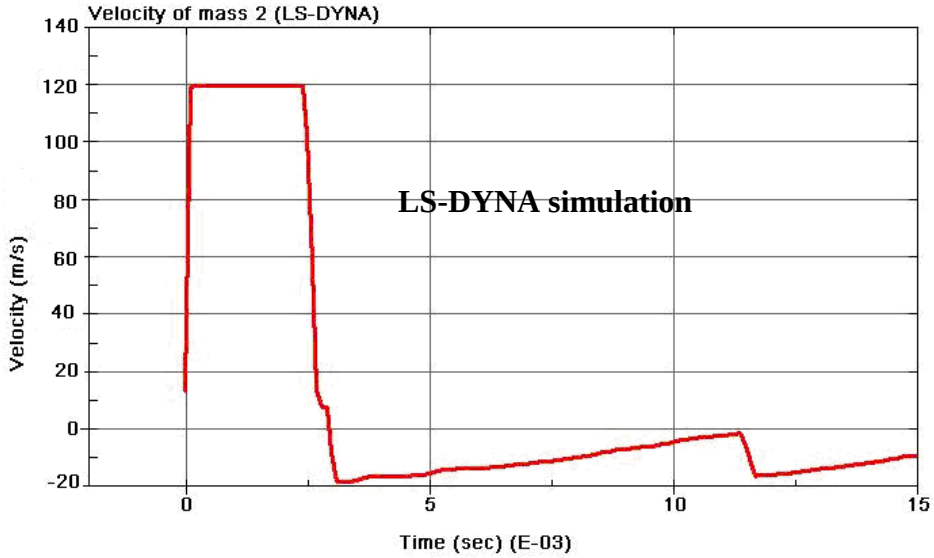

Figure 3.20 Velocity of Mass 2 (bumper)

3.7 Design variables for the explosive airbag

Input parameters or design variables are composed of the physical data from the cars, the explosive mass, and the airbag properties. The output results include the reduced kinetic energy of each mass, the displacement and velocity of each mass and the airbag state values, such as pressure and volume. Mass1, mass2, and mass3 denote the mass of the car body to be designed, the bumper mass of car to be designed and the mass of the other car, respectively.

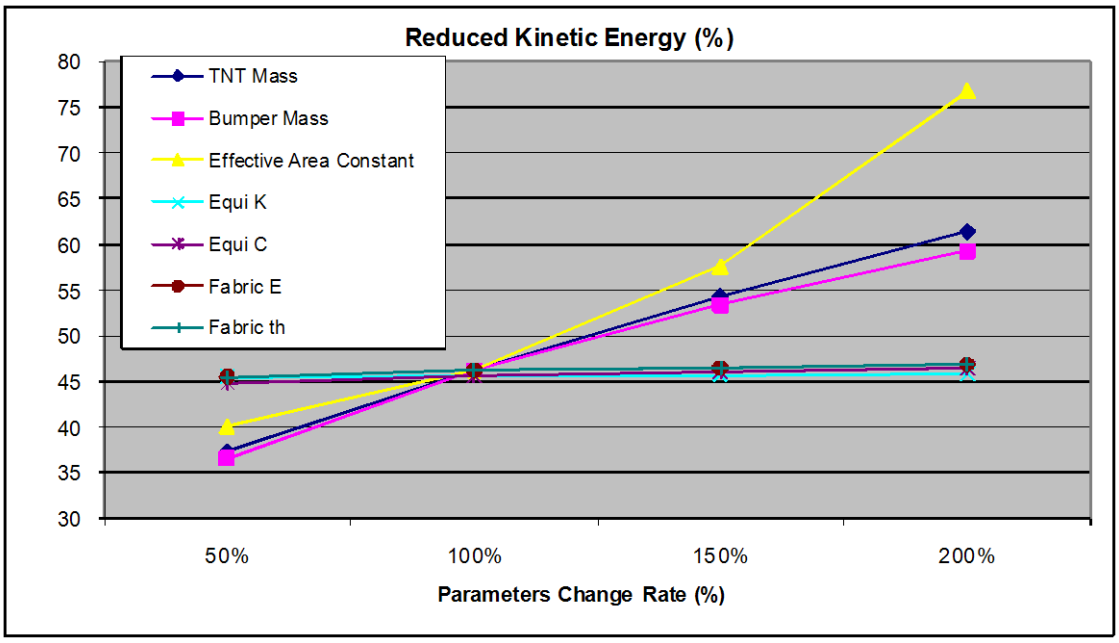

Figure 3.21 Design variable sensitivity

Fig. 3.21 shows the sensitivity of several design variables. The variable expected to be most sensitive was picked based on experience. It can be seen that some design variables are more sensitive and important for explosive design than other variables. Those are the variables for an effective area, explosive mass, and bumper mass.

3.8 Closure

In this chapter, the spring coefficients of an airbag were expressed by volume and pressure changes. The Wang and Nefske airbag model was used to find the value of pressure and volume changes. Airbag model spring coefficients can be computed using iteration processes and the interaction with the FOA model. The analytic expression for c_β and $\Delta\dot{V}$ in the Wang and Nefske model were shown in this chapter. The stress and radius of an airbag according to the pressure change was obtained as well.

A modified Gurney's equation was introduced for the velocity of moving mass with non-zero initial velocity after detonation, based on the energy conservation equation and the momentum conservation equation.

Finally, a combined and complete airbag model, including the explosive and the conventional model, was developed in this research. From the explosive model, the velocity of car and bumper after detonation was obtained. From the conventional airbag model, the spring coefficient of an airbag can be calculated.

In this paper, it is assumed that the bumper mass was concentrated on the area that is in contact with the explosives. However, to obtain a more realistic and effective analytic tool, the secondary mass of the bumper (outside the explosive contact area) should also be considered (Kennedy et al.. 1996). This will be addressed in the future.

CHAPTER IV

DESIGN OF LATTICE STRUCTURE

A crash energy absorbing (CEA) lattice structure with a locking mechanism has been investigated as a way of providing rigidity and energy absorption capability during a vehicular collision. An analytical model for the CEA lattice structure design has been developed. The proposed CEA structure is composed of a morphing lattice structure with movable thin-walled members for morphing purposes, members that will be locked in designated positions either before or during the crash. What will be described here is how to model the CEA structure analytically based on the energy absorbed by the CEA structure.

4.1. Introduction

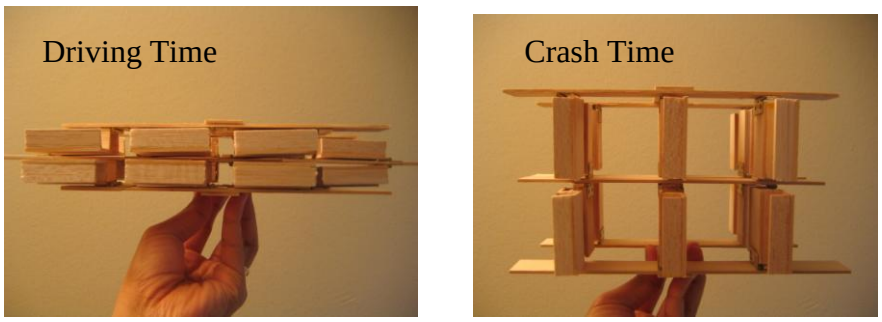

Figure 4.1 Prototype of expandable lattice structure for crashworthiness

In this research, analytic modeling of an active (foldable and expendable) lattice structure (see Fig. 4.1) was conducted. This structure is used to absorb the crash energy of colliding cars that have active bumpers. The structure is folded while driving, and is expanded and locked during the crash in order to absorb the crash energy. The car is

equipped with a sophisticated sensor and radar system to detect an impending collision. Usually in mechanical or civil engineering, a lattice structure utilizes beam elements or bar elements; analytic modeling of the lattice structure has been performed for strength and stiffness (Pedersen and Nielsen, 2003; Sedaghati et al., 2001; Kawamura, Ohmori, and Kito, 2002) or for frequency constraints to avoid resonance (Lingyun et al., 2005). Pedersen (Pedersen, 2004) has studied the crashworthiness design of frame structures, but his work is also for passive (fixed) structures.

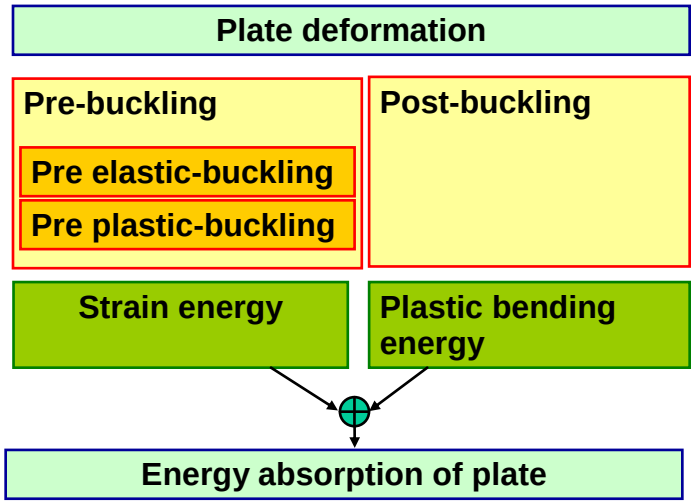

Figure 4.2 Pre-buckling region and post-buckling region in plate crush behavior

The thin-walled member of the proposed lattice structure is composed of plates. Therefore analytic modeling should be performed for the plates instead of beams or bars. It is assumed that the pressure is evenly distributed between the upper and lower plates; that every thin-walled member in the lattice structure is under the same boundary and loading conditions; and that every thin-walled member has the same shape and size. To calculate the crash energy absorbed in the lattice structure, the deformation region can be separated into a pre-buckling region and a post-buckling region (see Fig. 4.2). For the pre-buckling region, a strain energy of superimposed thin-walled member elements in parallel and series can be used, based on the single plate theory. For the post-buckling region, this research applies the theory of plastic limit analysis to an absorbed energy in the lattice structure. The methods of plastic limit analysis have been widely used to solve

practical engineering problems. Final energy absorption by the lattice structure can be obtained by summation of the absorbed energies in the pre-buckling region and the post-buckling region.

Two kinds of elements for thin-walled members in the lattice structure have been considered in this research. Those are the U shape of the thin-walled member (see Fig. 4.3 (a)) and the rectangular jagged thin-walled member (see Fig. 4.3 (b)). Analytic modeling in this research is based on the U shape of the thin-walled member. The analytic model that was developed can be applied to the rectangular jagged member with minor changes like boundary conditions. For the material properties, it is assumed to be elastic-perfect plastic material.

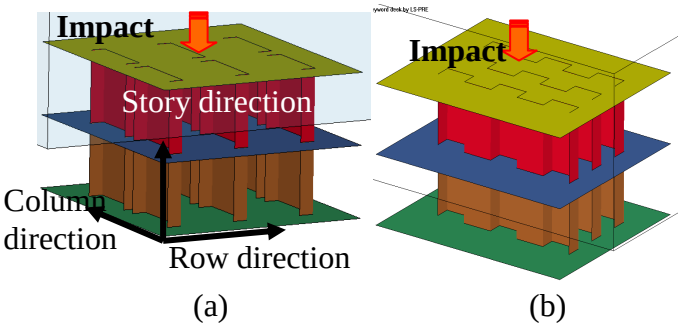

Figure 4.3 Lattice structure with the U shape of a thin-walled member (a) and rectangular jagged member (b)

Many materials are strain rate sensitive, and the yield stress increases as the strain rate increases. In this research, the strain rate effect has been neglected.

4.2 Absorbed energy in the pre-buckling region based on the strain energy

4.2.1 Strain energy of lattice structure in pre-elastic buckling

In this section, an analytic expression for strain energy of the lattice structure in the state of pre-elastic buckling is found.

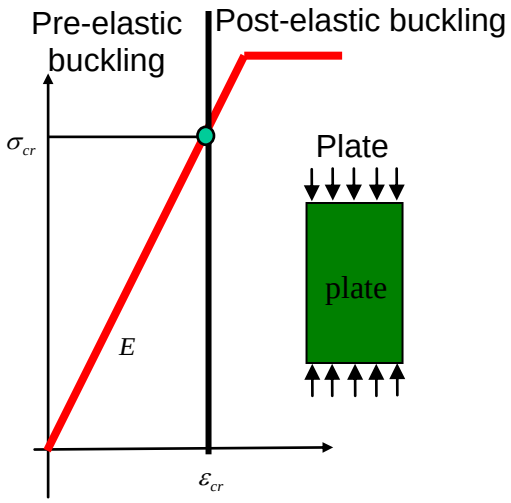

Figure 4.4 Stress and strain curve for elastic buckling

Fig. 4.4 shows a stress and strain curve for the elastic buckling of a plate in lattice structure. Elastic buckling means that the buckling will happen before the stress reaches the elastic limit. During pre-elastic buckling, the energy absorbed by plate deformation can be determined by the strain energy stored in the plate. The strain energy density is simply the area under the stress-strain curve in Fig. 4.4. The strain energy can be obtained by multiplying the strain energy density by the volume of the plate. Considering only the longitudinal stress, the strain energy of a single plate (Hibbeler, 2005) will be expressed by

$$U = \int \sigma d\varepsilon dV = \frac{\sigma_{cr}{}^2 abt}{2E} \tag{4-1}$$

where σ_{cr}, E, a, b, and t denote a critical stress, Young's modulus, the width of the plate, the length of the plate, and the thickness of the plate, respectively. If it is assumed that the element in the lattice structure is the U shape of a thin-walled member like Fig. 4.3, then the U section can be isolated using boundary conditions as in Fig. 4.5. Therefore the critical stress for each plate in the U section element can be obtained separately (Schafer, 2002). The strain energy of the element will be given as

$$U_{pre}^{1} = \frac{(\sigma_{cr\_web})^2 abt}{2E} + 2\frac{(\sigma_{cr\_flange})^2 (flange\_h)bt}{2E} \tag{4-2}$$

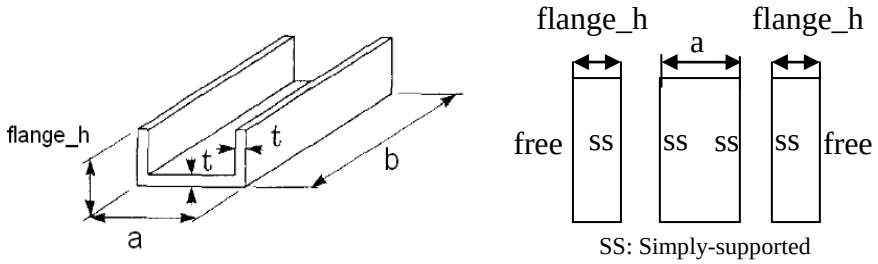

Figure 4.5 Element to be repeated in lattice structure and plate edge condition for buckling coefficient *k*

where σ_{cr_web} and σ_{cr_flange} are the critical stress for the web part and the critical stress for the flange part, respectively. The first term represents the strain energy of the web and the second term shows the strain energy of two flanges. Generally, buckling-critical stress for a single plate (Yu, 2000) will be given as

$$\sigma_{cr} = k\frac{E\pi^2}{12(1-\mu^2)(w/t)^2} \tag{4-3}$$

where k, E, μ, w, and t denote the constant for the boundary condition of a single plate, Young's modulus, Poisson's ratio, the width of a single plate, and the thickness of a single plate, respectively. Now, the critical stress for web and flanges can be determined by equation (4-3) and boundary conditions for the web and flange are shown in Fig. 4.5. Plugging the critical stress obtained by equation (4-3) into equation (4-2) gives a strain energy of one element (see Fig. 4.5). That is,

$$U^1{}_{pre} = \frac{\left(k_{web}\frac{E\pi^2}{12(1-\mu^2)(a/t)^2}\right)^2 abt}{2E} + 2\frac{\left(k_{flange}\frac{E\pi^2}{12(1-\mu^2)(flange\_h/t)^2}\right)^2 (flange\_h)bt}{2E} \quad (4\text{-}4)$$

where k_{web} is a constant for the boundary condition of the web plate and k_{flange} is a constant for the boundary condition for the flange plate. Therefore, the total strain energy stored in the lattice structure will be the sum of the individual strain energies in each element of the lattice members. That is,

$$U_{pre} = \sum_{1}^{n\_row}\sum_{1}^{n\_column}\sum_{1}^{n\_story} U^1{}_{pre} = U^1{}_{pre} \times n\_row \times n\_column \times n\_story \quad (4\text{-}5)$$

where n_row, n_column, and n_story are the number of elements in the direction of the row, the number of elements in the direction of the column, and the number of elements in the direction of height, respectively (see Fig. 4.3). $U^1{}_{pre}$ is the same for each of the elements in the lattice structure, because the elements are identical.

4.2.2. Strain energy of lattice structure in pre-plastic buckling

Next, the strain energy of pre-buckling in the case of plastic buckling will be described. Fig. 4.6 shows the stress-strain curve for plastic buckling. The plastic buckling will happen in the plastic region over the elastic limit. To obtain the strain energy of pre-plastic buckling, it is necessary to know the area under the graph in Fig. 4.6. It is not easy, however, to directly calculate the area under the graph of Fig. 4.6.

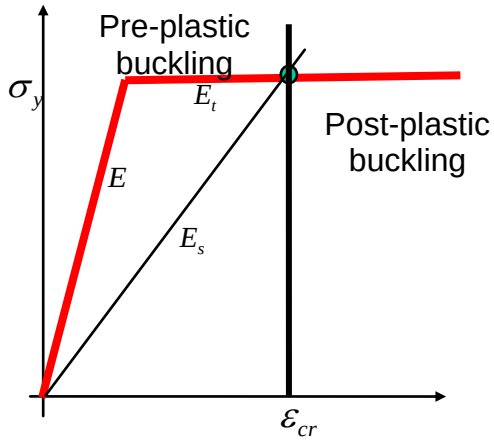

Figure 4.6 Stress and strain curve for plastic buckling

Therefore, the reduced modulus or double modulus (von Karman, 1947; Shanley, 1947; Pride and Heimerl 1949; Bloom and Coffin 2001) for plastic buckling will be introduced here. Reduced modulus is effective at the plastic buckling and can be expressed as

$$E_r = \eta E \tag{4-6}$$

The non-dimensional coefficient η is a reduction factor for plastic buckling and $\eta = 1$ is for stresses in the elastic range, whereas $\eta < 1$ is for above the elastic range. Values of η can be determined by various theories. In this research, the theory of Stowell (1948) will be used to determine η. This theory is applicable to plates having various edge support and constraints.

$$\eta = \frac{E_s}{E}\left(\frac{1}{2} + \frac{1}{2}\sqrt{\frac{1}{4} + \frac{3}{4}\frac{E_t}{E_s}}\right) \tag{4-7}$$

where E, E_s, and E_t represent Young's modulus, the secant modulus, and the tangent modulus, respectively. By using the reduced modulus, the graph of Fig. 4.6 can be modified into the graph shown in Fig. 4.7. Therefore, the strain energy for the pre-plastic

buckling of one element can be found by repeating equation (4-4) and switching the critical stress and the elastic modulus. It will be shown as

$$U^1{}_{pre} = \left[\frac{(\sigma_Y)^2 abt}{2E_r} + \frac{(\sigma_Y)^2 (flange\_h) bt}{E_r} \right] \tag{4-8}$$

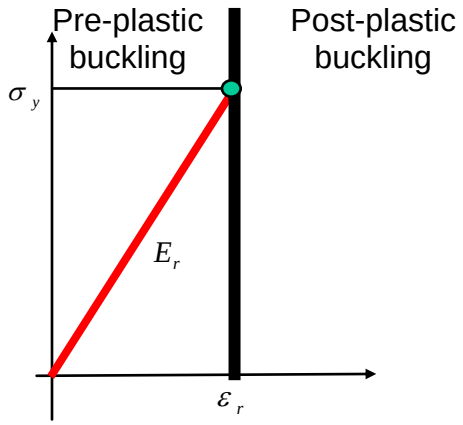

Figure 4.7 Modified stress and strain curve using reduced modulus for plastic buckling

So the total strain energy stored in the lattice structure will be the sum of the individual strain energies in each element of the lattice members. That is,

$$\begin{aligned} U_{pre} &= \sum_{1}^{n\_row} \sum_{1}^{n\_column} \sum_{1}^{n\_story} U^1{}_{pre} \\ &= U^1{}_{pre} \times n\_row \times n\_column \times n\_story \end{aligned} \tag{4-9}$$

Finally, the general expression for absorbed energy in the pre-buckling of the lattice structure can be written as

$$\begin{aligned} U_{pre} &= \sum_{1}^{n\_row} \sum_{1}^{n\_column} \sum_{1}^{n\_story} U^1{}_{pre} \\ &= U^1{}_{pre} \times n\_row \times n\_column \times n\_story \end{aligned} \tag{4-10}$$

where

$$U^{1}{}_{pre} = \left[\frac{(\sigma_{cr\_web})^2 abt}{2E^*} + \frac{(\sigma_{cr\_flange})^2 (flange\_h) bt}{E^*} \right] \tag{4-11}$$

$$E^* = \begin{cases} E & for\ elastic\ buckling \\ E_r = \eta E & for\ plastic\ buckling \end{cases} \tag{4-12}$$

$$\sigma_{cr\_web} = \begin{cases} k_{web} \dfrac{E\pi^2}{12(1-\mu^2)(\frac{a}{t})^2} & for\ elastic\ buckling \\ \sigma_y & for\ plastic\ buckling \end{cases} \tag{4-13}$$

$$\sigma_{cr\_flange} = \begin{cases} k_{flange} \dfrac{E\pi^2}{12(1-\mu^2)(\frac{flange\_h}{t})^2} & for\ elastic\ buckling \\ \sigma_y & for\ plastic\ buckling \end{cases} \tag{4-14}$$

4.3 Absorbed energy in the pre-buckling region based on the stiffness approach

In this chapter, another approach for energy absorption in the pre-buckling region based on the stiffness theory is investigated.

4.3.1 Stiffness of a single plate in the lattice structure

A plate of the lattice structure will undergo plate buckling during failure. In this section, another approach to estimate the absorbed energy in the pre-buckling region is investigated based on stiffness theory derived from the plate buckling theory. Once it has

buckled, a beam will lose the ability to carry increased load. However, a plate can carry an increased load even after buckling (see Fig. 4.8).

Another method for measuring the absorbed energy in the lattice structure of a pre-plastic buckling region has been investigated (see Fig. 4.8). It is assumed that every plate in the lattice structure have the same shape and size, and the structure is constructed by repeating the same plate obtained from optimization. In this section, equations for estimating stiffness of a single plate (see Figs. 4.9 and 4.10) in the lattice structure before and after buckling are developed.

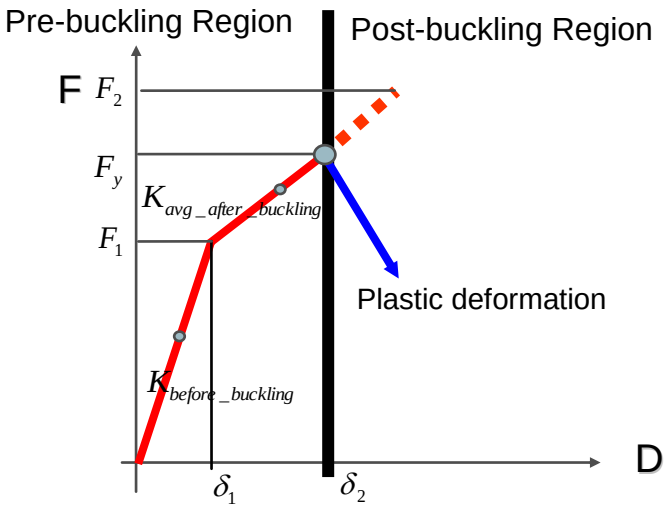

Figure 4.8 Elastic region and plastic region in plate crush behavior

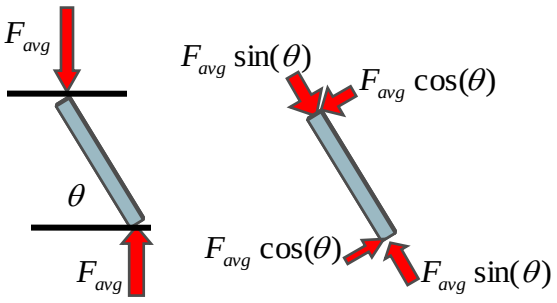

Figure 4.9 Load path of a single plate in lattice structure

Fig. 4.9 shows the load path of a single plate in the lattice structure. Load (F_{avg}) in Fig. 4.9 (a) can be divided into load in the longitudinal direction ($F_{avg}\sin(\theta)$) and load in the lateral direction ($F_{avg}\cos(\theta)$) of the plate in Fig. 4.9 (b). Actually, the load in lateral direction has no influence on the deformation of the plate, and the lock device and horizontal plates are stiff enough to withstand the lateral load. Considering only the load in longitudinal direction yields Fig. 4.10.

Figure 4.10 Plate under longitudinal force and declined by θ

Work done by external force ($F_{avg}\sin(\theta)$) is the same as strain energy stored in the structure, which is,

$$\frac{1}{2}F_{avg}\Delta = U_{strain\_energy} \tag{4-15}$$

where $\Delta = \dfrac{F_{avg}}{K}$

Therefore, stiffness of a single plate can be expressed as

$$K = F_{avg}^2/(2U_{strain\_energy}) \tag{4-16}$$

The strain energy stored in a single plate can be given simply as

$$U = \int \sigma d\varepsilon dV = \int \frac{\sigma^2}{2E} dV = \frac{\sigma^2 abt}{2E} \tag{4-17}$$

Now, it is necessary to find the stress of a plate in order to determine the absorbed strain energy *U*. This stress can be considered in two cases: before buckling and after buckling. First, the stress of plate before buckling will be expressed by

$$\sigma = F_{avg}\sin(\theta)/(at) \tag{4-18}$$

The strain energy stored by the plate will be

$$U = \frac{\sigma^2 abt}{2E} = \frac{F_{avg}^2 \sin^2(\theta) b}{2Eat} \tag{4-19}$$

Therefore, the stiffness of the plate before buckling can be expressed as

$$K_{before\_buckling} = \frac{Eat}{b\sin^2(\theta)} \tag{4-20}$$

Consider the stress of plate after buckling. This will be written as

$$\sigma_s = F_{avg}\sin(\theta)/(a_e t) \tag{4-21}$$

where

$$a_e = \frac{a}{2}\left(1+\frac{\sigma_{cr}}{\sigma_s}\right): \text{by effective thickness theory}$$
$$\sigma_s = \sigma_{cr} : \text{at the point where buckling begins}$$
$$\sigma_s = \sigma_y : \text{at the point where failure begins}$$

So, the strain energy stored in the plate yields

$$U = \frac{\sigma_s^2 a_e bt}{2E} \tag{4-22}$$

The average effective thickness will be

$$a_e = \frac{a}{2}(1+\frac{2\sigma_{Cr}}{\sigma_{Cr}+\sigma_y}) \tag{4-23}$$

Therefore, the stiffness of the plate right before failing can be given by

$$K_{avg\_after\_buckling} = \frac{a_e tE}{b\sin^2(\theta)} = a\left(1+\frac{2\sigma_{cr}}{\sigma_{cr}+\sigma_y}\right)Et/(2b\sin^2(\theta)) \qquad (4\text{-}24)$$

Fig. 4.11 shows the comparison of stiffness obtained by our measurements and those of Rhodes. As can be seen, the stiffness ($K_{before\_buckling}$ and $K_{avg\_after\_buckling}$) before buckling and after buckling is almost the same in both studies.

Our Work

$$K_{before\_buckling} = \frac{Eat}{b}$$

$$K_{avg\_after\_buckling} = \frac{aEt}{b}\times\left(\frac{1}{2}+\frac{\sigma_{cr}}{\sigma_{cr}+\sigma_y}\right)$$

Rhodes's work

$$K_{before\_buckling} = \frac{Eat}{b}$$

$$K_{avg\_after\_buckling} = \frac{aEt}{b}\times(1-K_l)$$

$*(1-K_l)=18/35$

for unloaded edges fixed – fixed

Figure 4.11 Stiffness of a single plate (90 degree simply supported)

4.3.2 Stiffness of lattice structure

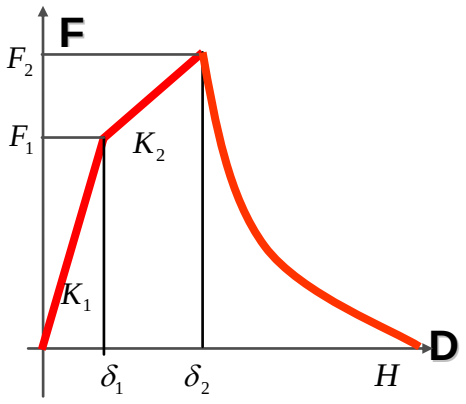

Figure 4.12 F-D curve of lattice structure

The stiffness of one plate is obtained for the whole range: before buckling, after buckling, and after failure. To find the stiffness (represented by K_1 and K_2 in the F-D curve in Fig. 4.12) of a lattice structure composed of many identical plates represented by K_1 and K_2, plates are superimposed using the serial and parallel theories of connected springs.

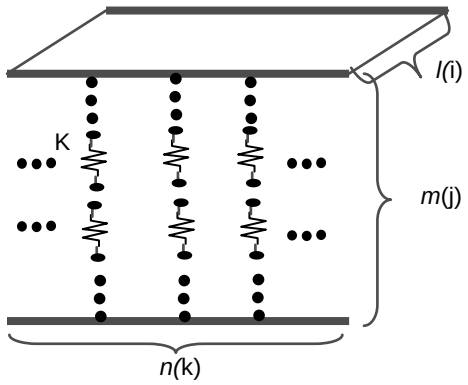

$$K = \sum_{i=1}^{l}\sum_{k=1}^{n}\left(1\Big/\sum_{j=1}^{m}\frac{1}{K_{ijk}}\right) \qquad K = K_p \times (n)(l)/(m)$$

K_p: spring constant of a single plate

l: # of columns m: # of stories n: # of rows

Figure 4.13 Serial and parallel combination of lattice structure

Considering the U-shape section of Fig. 4.5 results in:

$$K_1 = \frac{n_{row}n_{column}}{n_{story}}\left(\frac{Eat + 2\cdot E\cdot flange\_h\cdot t}{b\sin^2(\theta)}\right)$$

$$K_2 = \frac{n_{row}n_{column}}{n_{story}}\left(\frac{\left(at\left(1+\frac{2\sigma_{cr\_web}}{\sigma_{cr\_web}+\sigma_y}\right)+ flange\_h\cdot t\left(1+\frac{2\sigma_{cr\_flange}}{\sigma_{cr\_flange}+\sigma_y}\right)\right)E}{(2b\sin^2(\theta))}\right) \qquad (4\text{-}25)$$

4.3.3 Absorbed energy in lattice structure

Usually, force can be obtained by stress multiplied by area.

$$F = \sigma A \tag{4-26}$$

At the buckling start point,

$$\sigma = k \frac{E\pi^2}{12(1-\mu^2)(a/t)^2} \tag{4-27}$$

The critical force at the buckling start point (F_1) can be expressed as

$$F_1 = \frac{n_{row} n_{column}}{\sin(\theta)} \left(\begin{array}{l} k_{web} \dfrac{E\pi^2}{12(1-\mu^2)(a/t)^2} at \\ + 2k_{flange} \dfrac{E\pi^2}{12(1-\mu^2)(flange\_h/t)^2} flange\_h \cdot t \end{array} \right) \tag{4-28}$$

At the point where failure begins,

$$A = a_e t, \quad \sigma = \sigma_y, \quad where \quad a_e = \frac{a}{2}\left(1 + \frac{\sigma_{cr}}{\sigma_y}\right) \tag{4-29}$$

The critical force at the point where failure begins (F_2) can be expressed as

$$F_2 = \frac{\sigma_Y n_{row} n_{column} t}{\sin(\theta)} \left(\begin{array}{l} \dfrac{a}{2}\left(1 + \dfrac{k_{web} \dfrac{E\pi^2}{12(1-\mu^2)(a/t)^2}}{\sigma_Y}\right) \\ + flange\_h \left(1 + \dfrac{k_{flange} \dfrac{E\pi^2}{12(1-\mu^2)(flange\_h/t)^2}}{\sigma_Y}\right) \end{array} \right) \tag{4-30}$$

And, the critical displacements under the critical forces become

$$\delta_1 = \frac{F_1}{K_1} \quad \delta_2 = \frac{F_1}{K_1} + \frac{F_2 - F_1}{K_2} \tag{4-31}$$

Using the above equations, the absorbed energy of a lattice structure can be obtained as

$$U_{pre} = \frac{1}{2} K_1 \delta_1^2 + F_1(\delta_2 - \delta_1) + \frac{1}{2} K_2 (\delta_2 - \delta_1)^2 \tag{4-32}$$

4.4 Absorbed energy in the post buckling region

In this section, absorbed energy for the post buckling region is investigated. In the post buckling region, the plate will be deformed and some part of the plate will go through the plastic bending as shown in Fig. 4.14. The absorbed energy for post buckling will be the same as the plastic bending energy. To obtain the plastic bending energy, the plastic limit analysis can be applied.

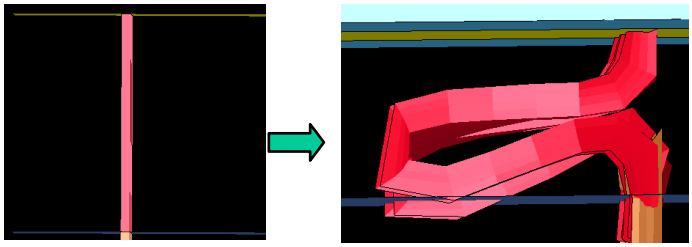

Figure 4.14 Deformation of a plate

The energy absorbed by the plastic deformation of one element can be given by

$$U^1{}_{post} = M_p \times \theta_{final} \tag{4-33}$$

where M_p means a full plastic bending moment and θ_{final} means an average distortion angle in the final position.

To obtain the value of equation (4-33), it is necessary to know the full plastic bending moment and the amount of distortion of the elements in plastic bending. Consider the full plastic bending moment. If it is assumed that the plate is a solid rectangle, the full plastic bending moment (Crandall, Dahl, and Lardner, 1978) can be expressed by

$$M_p = \frac{3}{2} M_y = \frac{3}{2} \frac{at^2}{6} \sigma_y = \frac{at^2}{4} \sigma_y \tag{4-34}$$

where M_y, expressed by $\left(at^2/6\right)\sigma_y$ (Crandall, Dahl, and Lardner, 1978), denotes a bending moment that corresponds to the onset of yielding in the plate. σ_y, a, and t are yield stress, the width of a plate, and the thickness of a plate, respectively. For the elements in the lattice structure (Fig. 4.5), the full plastic bending moment can be modified as

$$M_p = \frac{a_e t^2}{4} \sigma_y \tag{4-35}$$

where a_e means an effective width for plastic moments determined by the summation of the width of web, the height of flange, and the extra elongation. It can be expressed by

$$a_e = a + 2 \times flange\_h + 2 \times \beta_{lattice} \times flange\_h \tag{4-36}$$

where $\beta_{lattice}$ is an elongation factor for plastic bending, the value of which can be determined by a simulation test. As shown in Fig. 4.15, after plastic bending, the total width for the element will be increased by some amount. In this research, it is assumed that the width of the web is bigger than the height of the flange; it can then be assumed that an elongated length is proportional to flange height, like $\beta_{lattice} \times flange\_h$.

Now, consider the amount of distortion of the elements. To find the analytic expression for the amount of distortion, the shape of deformation has been assumed to be a circle or any other polygon that has one loop and two hinges like Fig. 4.16. It is necessary to know the total deformation angle for the loop and the hinges around the polygon that is modeled.

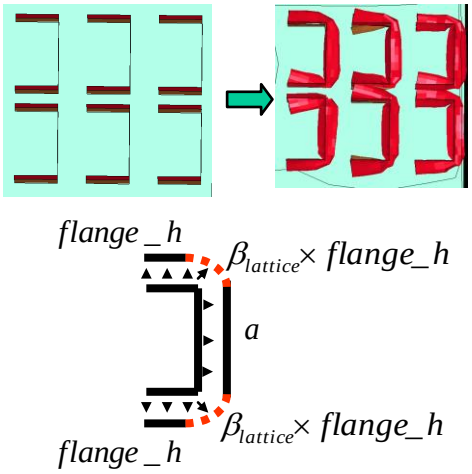

Figure 4.15 The cross section shape of plates before and after buckling

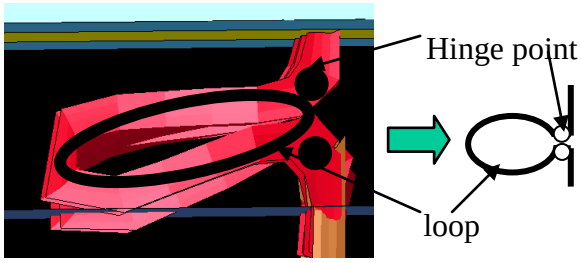

Figure 4.16 The shape of the deformation of a plate (one loop and two hinges)

The deformation angle (exterior angle) for one polygon (loop) that has n sides will be given as the constant

$$\left(\pi - \frac{\pi(n-2)}{n}\right) \times n = 2\pi \qquad (4\text{-}37)$$

Therefore, it can be said that the deformation angle in any polygon is always 2π (see Fig. 4.17). So, regardless of loop shape, the loop can be assigned 2π for its deformation angle, and the hinge can be assigned π for its deformation angle. Then the total deformation angle for elements with one loop and two hinges will be

$$\left(\pi - \frac{\pi(n-2)}{n}\right) \times n + 2\pi = 4\pi \tag{4-38}$$

The deformation angle of an element depends on the number of loops and the number of hinges. In this research, those numbers are determined by a simulation using LS-DYNA. For a U section thin-walled member, one loop and two hinges are appropriate for almost all cases. In future research, those numbers will be determined by an analytic approach.

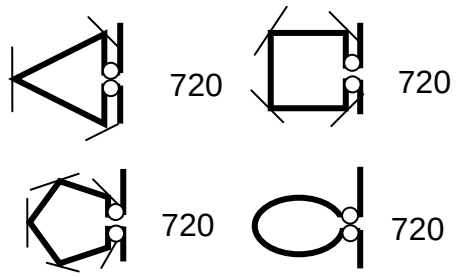

Two hinges and one loop

Figure 4.17 Deformation angle of some polygons

The absorbed energy in the post-buckling region by the lattice structure during a crash will be the sum of the individual plastic bending energies in each of the lattice members. The resulting equation (4-33) will be

$$U^1{}_{post} = \frac{(a + 2\times flange\_h + 2\times \beta_{lattice} \times flange\_h)t^2}{4} \sigma_y \times 4\pi \tag{4-39}$$

So, the total strain energy stored in the lattice structure will be the sum of individual plastic bending energies in each element of the lattice structure. That is,

$$\begin{aligned} U_{post} &= \sum_{1}^{n\_row} \sum_{1}^{n\_column} \sum_{1}^{n\_story} U^{1}{}_{post} \\ &= U^{1}{}_{post} \times n\_row \times n\_column \times n\_story \end{aligned} \tag{4-40}$$

Finally, the energy absorbed by the lattice structure during elastic and plastic deformation can be described as

$$U_{lattice} = U_{pre}\,(eq.4-10 \; or \; eq.4-32) + U_{post}\,(eq.4-40) \tag{4-41}$$

Now, the equivalent spring constant can be determined by

$$\begin{aligned} U_{lattice} &= \frac{1}{2} K_{eq\_lattice}\, x^{2}_{expanded} \\ K_{eq\_lattice} &= \frac{2U_{lattice}}{x^{2}_{expanded}} \end{aligned} \tag{4-42}$$

where, $x_{expanded}$ denotes an expanded distance of the lattice structure.

4.5 Maximum force (ultimate compressive load) of lattice structure

Maximum force can be calculated using the effective width theory of plate buckling. Some references (Yu, 2000; Malen and Kikuchi, 2006) demonstrate this procedure, so, results for maximum force are given here without additional proof or derivation. The maximum force (ultimate compressive load) of one element for elastic buckling will be at the onset of yield for a U section. That is,

$$F^{1}{}_{\max\_elasic\_buckling} = \left(a_{e\_web}\, t + 2a_{e\_flange}\, t\right) \times \sigma_{y} \tag{4-43}$$

So, the maximum force for lattice structure will be the sum of the individual maximum force in each element connected in parallel in the lattice structure.

$$F_{\max\_elasic\_buckling} = \left(a_{e\_web}\, t + 2a_{e\_flange}\, t\right)\times \sigma_y \times n\_row \times n\_column \tag{4-44}$$

where

$$a_{e\_web} = \frac{a}{2}\left(1+\frac{\sigma_{cr\_web}}{\sigma_y}\right)$$

$$a_{e\_flange} = \frac{flange\_h}{2}\left(1+\frac{\sigma_{cr\_flange}}{\sigma_y}\right)$$

In plastic buckling, the yield will start before buckling and the maximum stress will be at the yield uniformly. So the maximum force of plate for plastic buckling will be

$$F_{\max\_plastic\_buckling} = \left(a\times t + 2\times flange\_h \times t\right)\times \sigma_y \times n\_row \times n\_column \tag{4-45}$$

4.6 Optimization of lattice structure's shape and size

Now the amount of energy absorbed by the lattice structure during elastic and plastic deformation can be found. The absorbed energy will be maximized. So, the objective function will be

$$MAXIMIZE \quad U_{total} = U_{pre} + U_{Post} \tag{4-46}$$

The constraint functions for geometry (see Fig. 4.18) and mass are:

$$n_{column} a = L \tag{4-47}$$

$$n_{story}\, b \sin(\theta) = H \tag{4-48}$$

$$2abtn_{row}n_{column} \le M \tag{4-49}$$

$$b < W \tag{4-50}$$

Equation (4-47) is the relationship between a width of the element and *L*. Equation (4-48) is the relationship between a length of the element and *H*. Equation (4-49) is a constraint on total mass of the lattice structure. Equation (4-50) indicates that the length of the element should be less than *W*.

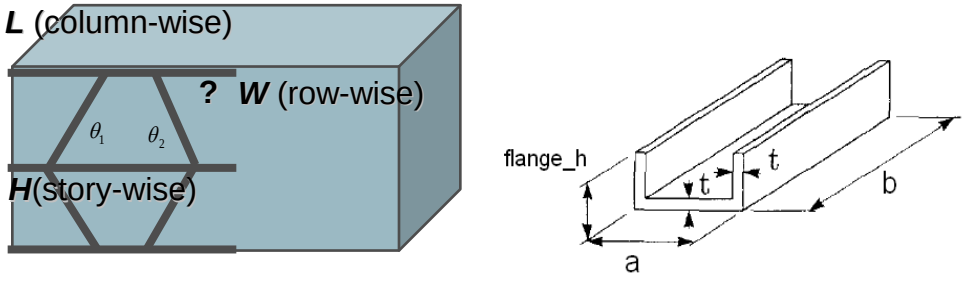

Figure 4.18 Given volume for lattice structure and size of element

An optimization process has been implemented using a MATLAB function (fminbnd). This optimization process can be used to predict the optimum shape of the plate as well as average stiffness of the lattice structure and the absorbed energy by the lattice structure during the crash. Variables of the objective function include integer numbers and real numbers. In this research, to simplify the optimization process, some pairs were made for integer numbers with the number of rows, the number of stories and the number of columns using a For-loop. The optimization was performed in each For-loop and the results of each loop were compared to find the optimized value.

4.7 Validation of the analytic model of a crash energy absorption structure using LS-DYNA

The analytic model has been verified simply by using LS-DYNA. For the lattice structure crash simulation, the impact mass is 1962 kg and the speed of the mass is 13.4 m/s. The material used in this test is steel that is assumed to be elastic-perfect plastic.

Three kinds of elements (see Fig. 4.19) were applied to this test: the U shape of the thin-walled member with a short flange, the U shape of a thin-walled member with a long flange, and the rectangular jagged thin-walled member. The masses of the structure for each element are same.

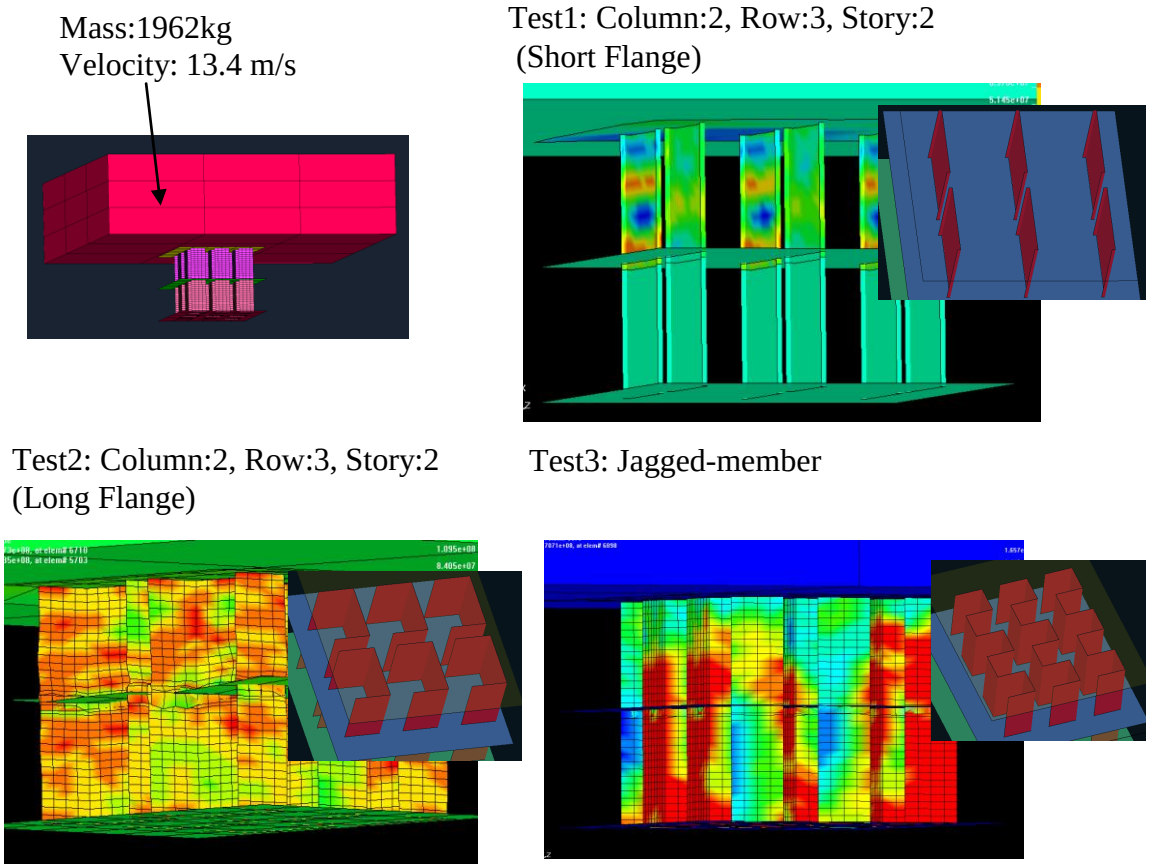

Figure 4.19 FEM model for verification of analytic solution

Fig. 4.20 demonstrates the total absorbed energy for the three kinds of elements. Fig. 4.21 shows the maximum force of lattice structure for each element.

As seen in Fig. 4.20 and Fig. 4.21, the values of the total absorbed energy during the crash and the maximum load of the analytic model and simulation for the lattice structure are in good agreement with each element. Fig. 4.20 shows that the jagged-member gives better results than the isolated U section thin-walled member in terms of energy absorption.

There is still information to be learned through future research. In this research, the number of lobes, the secant modulus (E_s), and the elongation factor β have been obtained by simulation. For this method to be faster and more economical, these values should be determined by analytic expression. These will be researched in the future.

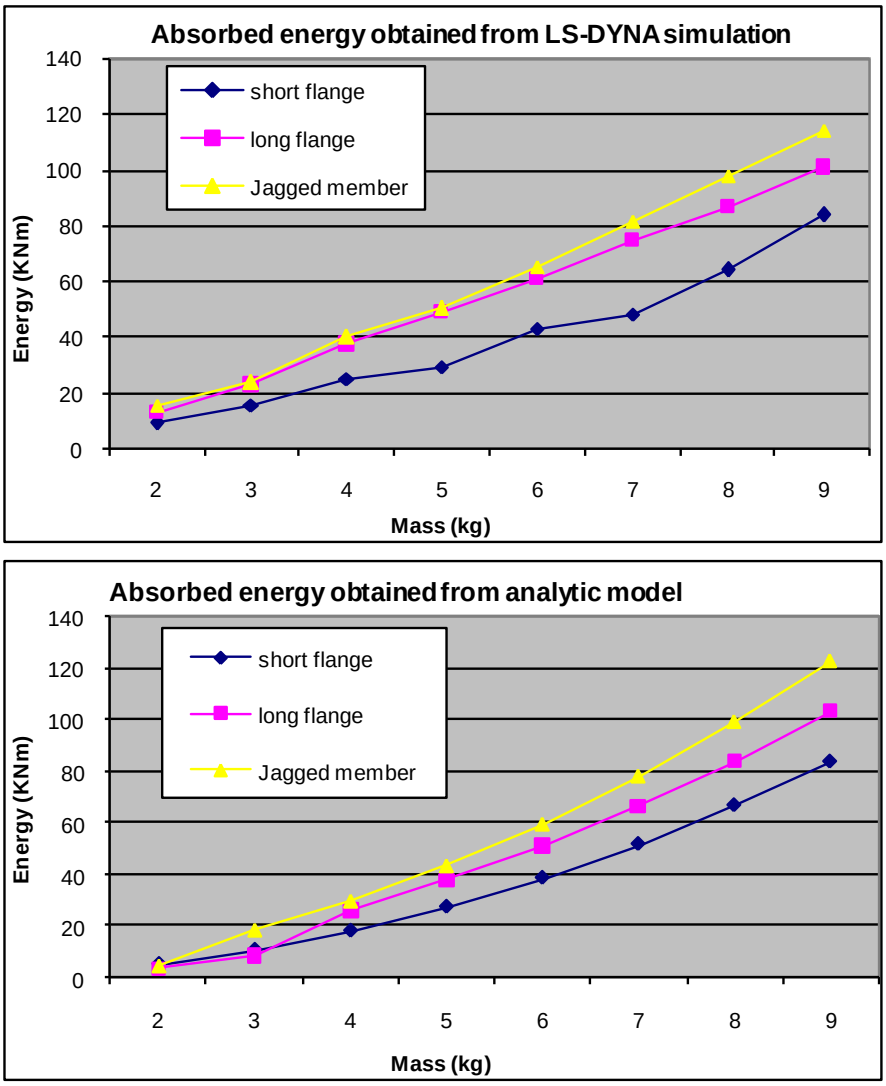

Figure 4.20 Absorbed energy of analytic model and LS-DYNA simulation (X axis: mass of lattice structure (kg), Y axis: energy (KNm))

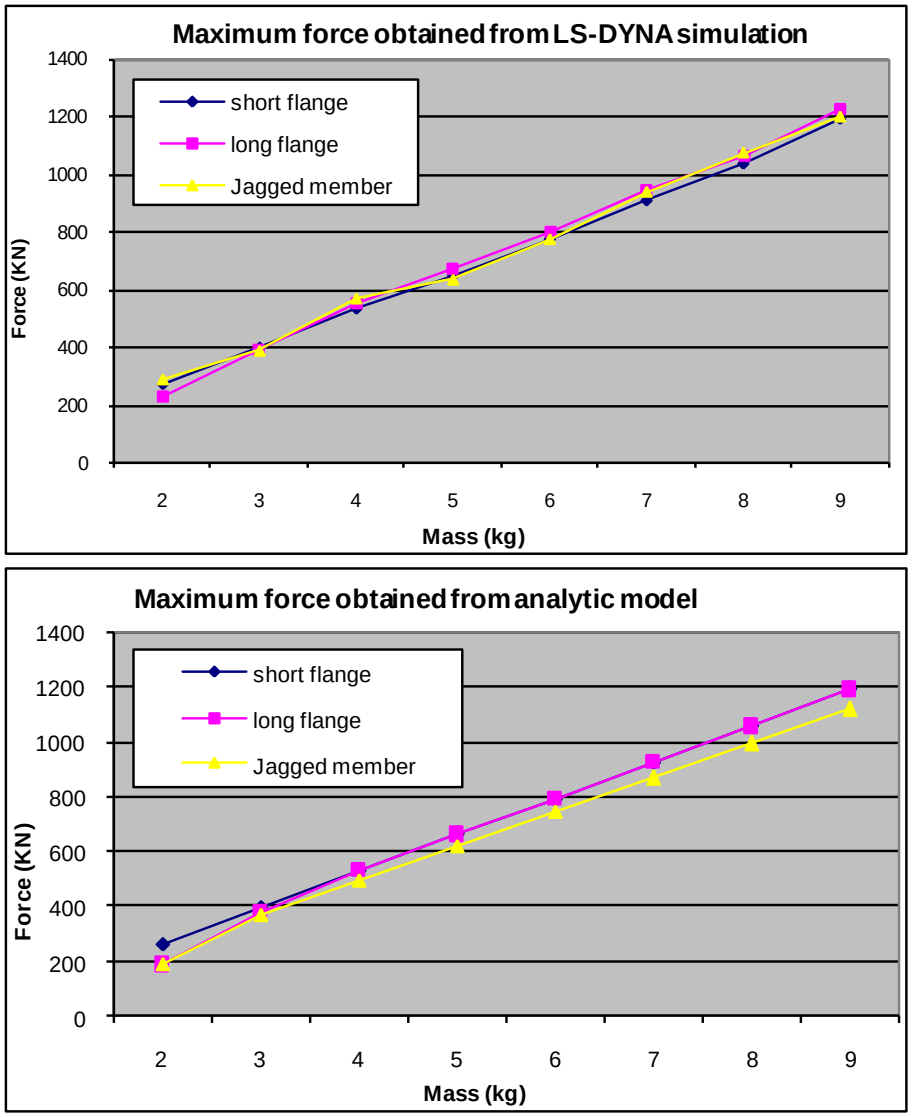

Figure 4.21 Maximum force of analytic solution and LS-DYNA simulation (X axis: mass of lattice structure (kg), Y axis: force (KN))

4.8 Closure

The objective of this chapter was to develop a reconfigurable lattice structure for the improved crashworthiness of vehicles, and to develop an analytic model for crash energy absorption of an expandable lattice structure. The available space and total mass for a lattice structure have been pre-determined and this space has been filled with an expandable lattice structure. The structure is folded while driving and is expanded at the

moment of impact. In this structure, an identical element has been repeated in the direction of story, row, and column. In this research, two kinds of elements have been considered. The absorbed energy in this structure was determined from summation of the strain energy and the plastic bending energy. To maximize the absorbed energy, the shape and size of this element, and the numbers of story, row, and column, were optimized. The values of the total absorbed energy during the crash of the analytic model and simulation for the lattice structure were in good agreement with each element. Practically, this lattice structure should have a support structure like a cross member between the engine and the bumper. Therefore, the means by which the lattice structure will be supported by the vehicle body should be examined in the future.

CHAPTER V

APPLICATION OF TUBES FILLED WITH GRANULES FOR CRASHWORTHY DESIGN OF AUTOMOBILES

An innovative means for improving crashworthiness is to use tubes filled with a granular material to absorb energy during the process of a crash. In this research, how to use granular materials in the tubes found in the front posts of automobiles for improved safety has been studied. The focus has been on a specific design of tubes filled with a granular material. Granular particles can create enormous friction through their interactions; therefore a tube filled with a granular material can absorb much more crash energy than an empty tube. The application of granular materials to a crashworthiness design is very challenging but highly effective. In this research, an analytic model has been developed based on the effective thickness theory of a tube filled with granules.

5.1 Introduction

In the previous section, a crashworthiness design for the active state using explosives and airbags was presented. In this section, a crashworthiness design for the passive state using granular materials is presented. Granular materials are currently the subject of a very active line of research in various scientific fields: physics, mechanics, geophysics, chemistry, and pharmacy. In engineering, static granular materials under gravitationally induced stress (i.e. a grain silo) and flowing granular material like fluid (i.e. an avalanche) used to be the main subjects of analysis. Many approaches for analyzing flowing granular material originated from the field of fluid mechanics. In this section, the application of granular materials to vehicle crashworthiness design is researched.

© Bureau of Land Management

Figure 5.1 Example of granular material: sand

In this research, an approach is introduced that is more general and more directly applicable to automotive bodies, an approach called the “effective thickness approach,” that is applied to a tube filled with granular material.

The material properties in this research were assumed to be elastic-perfect plastic material. Many materials are strain-rate sensitive, and the yield stress increases as the strain rate increases. In this research, the strain-rate effect has been neglected.

5.2 Effective thickness of a tube filled with granules

In this chapter, the concept of the effective thickness of a tube equivalent to a tube filled with granules is introduced. The effective thickness has been found separately for axial deformation (see Fig. 5.7(a)) and global bending deformation (see Fig. 5.7(b)). In the latter part of this chapter, the effective thickness of a tube filled with granules is used in the simple crashworthiness design of automotive rails. First, consider the case of axial deformation. It has been assumed that during the deformation, the tube would undergo

plastic deformation. This assumption is reasonable for elastic-perfect material and it can be confirmed from the LS-DYNA simulation. Therefore, the axial peak crush force for a square tube will be given by

$$P_{t\_\max} = 4\sigma_{t\_y} bt \tag{5-1}$$

where σ_{t_y} is a yield stress, b is a section width and t is the thickness of a square tube. Peak crush force for granules in the tube will be given by

$$P_{g\_\max} = b^2 \sigma_{g\_y} \tag{5-2}$$

where σ_{g_y} denotes a yield stress of granules and b denotes the section of a square tube. Therefore, the peak crush force for a tube filled with granules (see Fig. 5.2) can be expressed by

$$P_{tg\_\max} = b^2 \sigma_{g\_y} + 4\sigma_{t\_y} bt = 4\sigma_{t\_y} b\left(t + \frac{1}{4}\frac{b\sigma_{g\_y}}{\sigma_{t\_y}} \right) \tag{5-3}$$

Now an effective thickness for a tube filled with granules can be defined from equation (5-3) as

$$t_e = \left(t + \frac{1}{4}\frac{\sigma_{g\_y}}{\sigma_{t\_y}} b \right) \tag{5-4}$$

In the same way, the effective thickness of a non-square tube filled with granules for axial deformation can be obtained. That is,

$$t_e = \left(t + \frac{\sigma_{g\_y}}{\sigma_{t\_y}} \frac{ab}{2(b+a)} \right) \tag{5-5}$$

where a and b mean section widths for non-square tube.

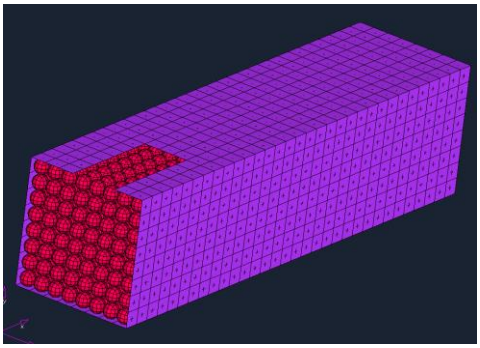

Figure 5.2 Tubes filled with granules

Next consider the case of global bending deformation. The full plastic bending moment (Crandall, Dahl, and Lardner, 1978) for the square tube will be given by

$$M_b = \frac{3}{2}\sigma_{t\_y} b^2 t \tag{5-6}$$

The full plastic bending moment for the square tube filled with granules can be given as

$$\begin{aligned} M_b &= \frac{3}{2}\sigma_{t\_y} b^2 t + \sigma_{g\_y} b^3 / 8 \\ &= \frac{3}{2}\sigma_{t\_y} b^2 t + \frac{3}{2}\sigma_{t\_y}\left(\frac{\sigma_{g\_y}}{\sigma_{t\_y}} b^2 / 12\right) \\ &= \frac{3}{2}\sigma_{t\_y} b^2\left(t + \frac{1}{12}\frac{\sigma_{g\_y}}{\sigma_{t\_y}} b\right) \end{aligned} \tag{5-7}$$

where only the upper half of the granules will be compressed, having been subjected to bending deformation. This is because the lower half of the granules will go through tensile stress and there is no tensile stress between granules. Therefore, the bending moment of granules about the neutral axis of a tube will be expressed by $\sigma_{g\_y} b^3 / 8$. Now

the effective thickness of a square tube filled with granules for bending deformation can be defined as

$$t_e = \left(t + \frac{1}{12} \frac{\sigma_{g\_y}}{\sigma_{t\_y}} b \right) \tag{5-8}$$

Consider a non-square tube undergoing bending deformation. The full plastic bending moment for the non-square tube (Malen and Kikuchi, 2006) will be given as in Fig. 5.3.

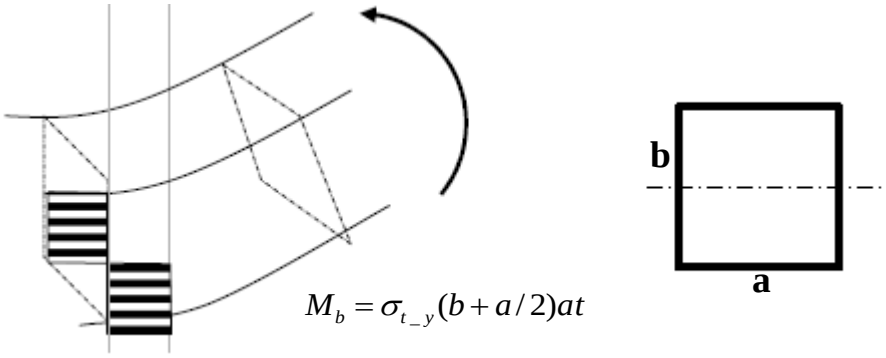

Figure 5.3 Non-square thin-walled section for plastic bending

Just as in the square tube, the full plastic bending moment for the non-square tube filled with granules will be given as

$$\begin{aligned} M_b &= \sigma_{t\_y}(b + \frac{1}{2}a)at + \sigma_{g\_y}a^2 b/8 \\ &= \sigma_{t\_y}(b + \frac{1}{2}a)a\left(t + \frac{\sigma_{g\_y}}{\sigma_{t\_y}} \frac{ab}{8(b + a/2)} \right) \end{aligned} \tag{5-9}$$

Therefore the effective thickness of a non-square tube filled with granules for bending deformation can be defined as

$$t_e = \left(t + \frac{\sigma_{g\_y}}{\sigma_{t\_y}} \frac{ab}{8(b + a/2)} \right) \tag{5-10}$$

Various effective thicknesses for tubes filled with granules are shown in Table 5.1. This effective thickness will be used in the simple crashworthiness design of automotive rails in the latter part of this chapter.

Table 5.1 Effective thickness of tubes filled with granules

Loading	Square tubes filled with granules	Non-square tubes filled with granules
Axial deformation	$t_e = \left(t + \frac{1}{4} \frac{\sigma_{g\_y}}{\sigma_{t\_y}} b \right)$	$t_e = \left(t + \frac{\sigma_{g\_y}}{\sigma_{t\_y}} \frac{ab}{2(b+a)} \right)$
Bending deformation	$t_e = \left(t + \frac{1}{12} \frac{\sigma_{g\_y}}{\sigma_{t\_y}} b \right)$	$t_e = \left(t + \frac{\sigma_{g\_y}}{\sigma_{t\_y}} \frac{ab}{8(b + a/2)} \right)$

In this research, the stress for granules has been obtained using an LS-DYNA simulation test. The simple analytic expression of stress for granules has been investigated by Walton (Walton, 1987). In future research, the general stress expression for granules in the tube will be developed.

If the tube is to undergo only axial deformation (see Fig. 5.7(a)), all granules in the tube will be in compression. Therefore the effective thickness for axial deformation will be effective for the tube. On the other hand, if the tube is to undergo only bending deformation (see Fig. 5.7(b)), some of the granules in the tube will be in compression and the effective thickness for bending deformation will be effective for the tube. Real tubes will go through both axial deformation and global bending deformation during a crash. Therefore, the effective thickness for the crashworthiness in a tube will vary according to the deformation mode. The portion of the axial deformation and the bending deformation during the crash can be expressed by deformation mode factors, α_{tube} and β_{tube}, which are values between zero and one, and where $\alpha_{tube} + \beta_{tube}$ is equal to one. Generally, the effective thickness for crashworthiness of tubes will be expressed as

$$t_e = \begin{cases} \alpha_{tube}\left(t + \frac{1}{4}\frac{\sigma_{g\_y}}{\sigma_{t\_y}}b\right) + \beta_{tube}\left(t + \frac{1}{12}\frac{\sigma_{g\_y}}{\sigma_{t\_y}}b\right) \\ \qquad \text{for square tubes:} \\ \alpha_{tube}\left(t + \frac{\sigma_{g\_y}}{\sigma_{t\_y}}\frac{ab}{2(b+a)}\right) + \beta_{tube}\left(t + \frac{\sigma_{g\_y}}{\sigma_{t\_y}}\frac{ab}{8(b+a/2)}\right) \\ \qquad \text{for non-square tubes} \end{cases} \tag{5-11}$$

Now it will be shown how to use the effective thickness of a tube filled with granules to calculate the energy absorbed in a square tube. The energy absorbed by a square tube can be obtained from the equation developed by Mahmood and Paluszny (1981). Note that this relationship was developed for a square steel section loaded by static force. They said that the relationship between mean crush force and peak crush force can be expressed as $P_{\max} = 1.42P_{mean}$. $P_{\max}$ can be expressed as $\sigma_{t\_y}(4bt_e)$ for a square tube filled with granules. So the mean crush force (P_{mean}) can be expressed by

$$P_{mean} = \sigma_{t\_y}(4bt_e) \Big/ 1.42 \tag{5-12}$$

Therefore the energy absorbed by a tube filled with granules for the axial deformation will be

$$\begin{aligned} U_{axial} &= P_{mean} \times deformation\ length \\ &= \sigma_{t\_y}(4bt_e) \Big/ 1.42 \times deformation\ length \end{aligned} \tag{5-13}$$

Now consider the case of bending deformation. The energy absorbed by the tube for bending deformation can be given by

$$U_{bend} = M_b \times \theta \tag{5-14}$$

where M_b (eq. 5-6) means a full plastic bending moment and θ means a deformation angle in the hinge. Therefore, the energy absorbed by a tube filled with granules during bending deformation will be

$$U_{bend} = \frac{3}{2}\sigma_{t\_y} b^2 t_e \times \theta \tag{5-15}$$

where the values of θ in an actual crash of tubes must be determined by simulation or an through analytic approach. In this research, the value will be assumed.

Therefore, the absorbed energy in a tube filled with granules will be

$$U_{tube} = \alpha_{tube} U_{axial} + \beta_{tube} U_{bend} \tag{5-16}$$

where, α_{tube} and β_{tube} express the portion of the axial deformation and the bending deformation during the crash by deformation mode factors.

Now, the equivalent spring constant can be determined by

$$U_{tube} = \frac{1}{2} K_{eq\_tube} x_{tube}^2$$

$$K_{eq\_tube} = \frac{2U_{tube}}{x_{tube}^2} \tag{5-17}$$

where x_{tube} denotes the deformation length of a front post filled with granules.

5.3 Stress on granular material (Walton, 1978 and 1987)

The stress of granular material packing has been derived from the elastic moduli developed by Walton (1978 and 1987). In Walton's paper, the sphere material is assumed to be homogenous and elastically isotropic and the spheres are identical in that they are of the same size and have the same elastic moduli (see Fig. 5.4). In his research, for

simplicity, only two special cases were taken into consideration to examine the effect of friction, namely those in which there is infinite friction and those in which there is no friction. Packing is assumed to be random. The center of the *n*th sphere and *m*th sphere initially in contact with each other will undergo a displacement (see Fig. 5.5). From this initial deformation state, some vectors will be derived.

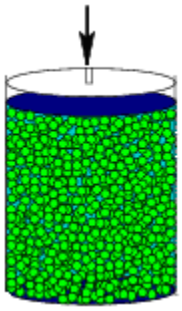

Figure 5.4 Random packing of granular spheres

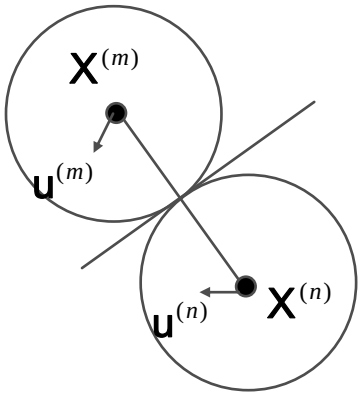

Figure 5.5 The initial deformation

The position vector of the contact point is

$$1/2(\mathbf{X}^{(n)} + \mathbf{X}^{(m)}) \tag{5-18}$$

Displacement of the contact point is

$$1/2(\mathbf{u}^{(n)} + \mathbf{u}^{(m)}) \tag{5-19}$$

The unit vector along the line of center reduces to

$$\mathbf{l}^{(nm)} = \frac{\mathbf{X}^{(n)} - \mathbf{X}^{(m)}}{2R} \tag{5-20}$$

$$R: radius\ of\ \ granule$$

The normal component w_0 of the relative displacement of the upper sphere will be

$$w_0 = 1/2(\mathbf{u}^{(m)} - \mathbf{u}^{(n)}) \cdot \mathbf{l}^{(nm)} \tag{5-21}$$

The remainder of the relative displacement is:

$$u_0 + v_0 = 1/2(\mathbf{u}^{(m)} - \mathbf{u}^{(n)}) - [1/2(\mathbf{u}^{(m)} - \mathbf{u}^{(n)}) \cdot \mathbf{l}^{(nm)}]\mathbf{l}^{(nm)} \tag{5-22}$$

It was assumed that the displacement of the sphere centers was consistent with the applied uniform field:

$$u_i^{(n)} = e_{ij} X_j^{(n)} \tag{5-23}$$

The effective moduli will be obtained from the relationship between incremental stress and incremental strain

$$\left\langle \delta\sigma_{ij} \right\rangle = -\frac{3\phi n}{2\pi^2 B(2B+C)} \left\{ B\left\langle (-e_{pq}I_pI_q)^{1/2}\left(\delta e_{ik}I_kI_j + \delta e_{jk}I_kI_i\right)\right\rangle - C\left\langle (-e_{pq}I_pI_q)^{1/2} I_kI_lI_iI_j \right\rangle \delta e_{kl} \right\} \tag{5-24}$$

where,

$$B=\frac{1}{4\pi}\left\{\frac{1}{\mu}+\frac{1}{\lambda+\mu}\right\},\quad C=\frac{1}{4\pi}\left\{\frac{1}{\mu}-\frac{1}{\lambda+\mu}\right\}$$

where, λ and μ denote the Lame moduli of sphere material

Since the effective moduli are defined by

$$\left\langle \delta\sigma_{ij}\right\rangle = C^{*}_{ijkl}\left\langle \delta e_{kl}\right\rangle \tag{5-25}$$

The general expression for the effective moduli is

$$C^{*}_{ijkl}=-\frac{3\phi n}{4\pi^{2}B(2B+C)}\left\{\begin{array}{l} B\left\langle(-e_{pq}I_pI_q)^{1/2}I_jI_l\right\rangle\delta_{il}+B\left\langle(-e_{pq}I_pI_q)^{1/2}I_iI_k\right\rangle\delta_{jl}+B\left\langle(-e_{pq}I_pI_q)^{1/2}I_jI_l\right\rangle\delta_{ik} \\ +B\left\langle(-e_{pq}I_pI_q)^{1/2}I_iI_l\right\rangle\delta_{jk}+2C\left\langle(-e_{pq}I_pI_q)^{1/2}I_iI_jI_kI_l\right\rangle \end{array}\right\} \tag{5-26}$$

$$where,\ \alpha=\frac{\phi n(-e_3)^{1/2}}{32\pi^{2}B},\ \beta=\frac{\phi n(-e_3)^{1/2}}{32\pi^{2}(2B+C)}$$

$$\phi(volume\ concentrat\ ion)=\frac{4\pi R^{3}N}{3V}$$

V : *total volume*

N : *the number of spheres within volume V*

n: *the average number of contact points per sphere*

For the case where the spheres are infinitely rough:

$$\begin{aligned} &C_{1111}=3(\alpha+2\beta),\ C_{1122}=\alpha-2\beta,\ C_{1133}=C_{2233}=2C^{*}_{12}, \\ &C_{3333}=8(\alpha+\beta),\ C_{1313}=C_{2323}=\alpha+7\beta \end{aligned} \tag{5-27}$$

For the case where the sphere are perfectly smooth:

$$C_{1111}=3\alpha,\ C_{1122}=C_{1313}=C_{2323}=\alpha,\ C_{1133}=C_{2233}=2\alpha,\ C_{3333}=8\alpha \tag{5-28}$$

To extend the above spring constant from a specific case to a more general case, multi-axial compression, general friction, a plastic case, non-identical spheres, composite materials, and non-sphere materials should be considered.

5.4 Validation of effective thickness approach for tubes filled with granules using LS-DYNA

In this section, the validation of effective thickness approach for tubes filled with granules using LS-DYNA is performed (see Fig. 5.6). Two cases of deformation are considered. The first one is an axial deformation (see Fig. 5.7(a)). The second one is a global bending deformation (see Fig. 5.7(b)). A pre-V-shaped tube with a small angle has been used to reconstruct the global bending deformation of Fig. 5.7(a).

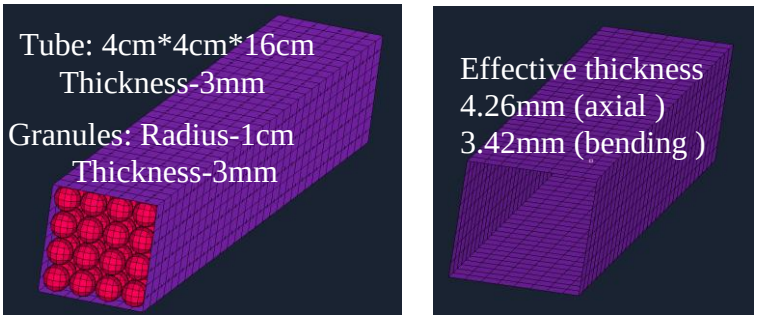

* Impact mass: 1962 kg, Impact speed: 13.4 m/s

* One end is fixed and the other end is struck by the impact mass

Figure 5.6 Tubes filled with granules and the effective tube

For the axial deformation, $\alpha_{tube}=1, \beta_{tube}=0$, and for the global bending deformation, $\alpha_{tube}=0, \beta_{tube}=1$. In Figs. 5.8 – 5.11, "A" in the legend denotes the results of a tube filled with granules, using LS-DYNA; "B" denotes the results of the tube with effective thickness, using LS-DYNA; and "C" denotes the results using the developed analytic model. The X-axis refers to the deformation length of the tube and the Y-axis refers to the corresponding force or energy. It is assumed that the tube is made of steel,

that granules are made of polyester (PBT) and that the two materials are elastic-perfect plastic materials that have no strain rate effect.

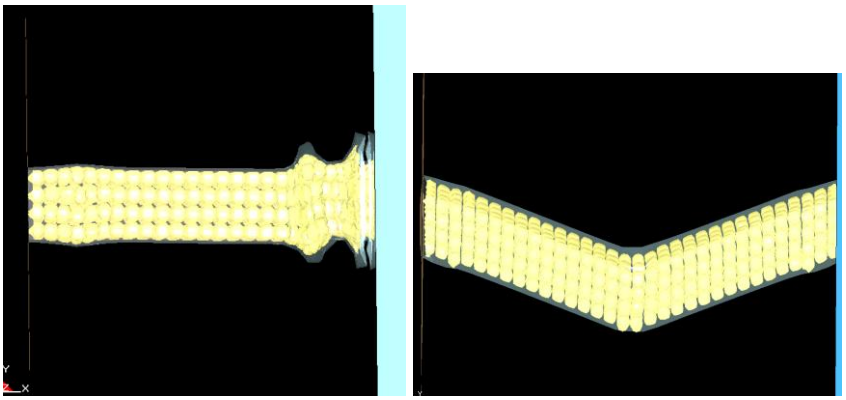

(a) (b)

Figure 5.7 Axial deformation (a) and global bending deformation (b) of tubes with filled with granules

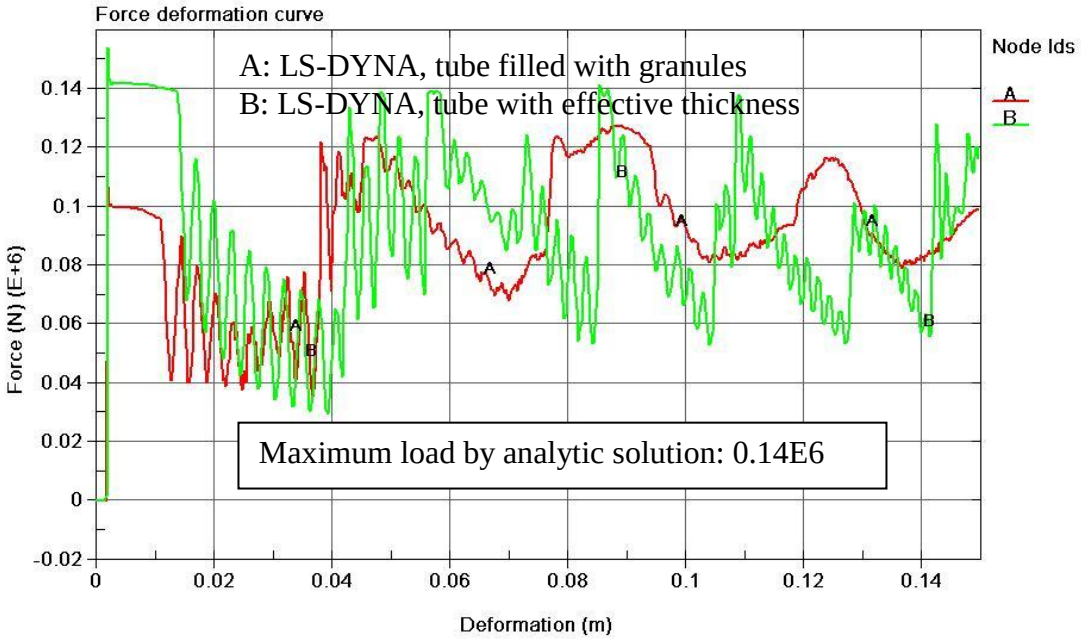

Figure 5.8 Force and deformation curve for an effective tube and a tube filled with granules (axial deformation)

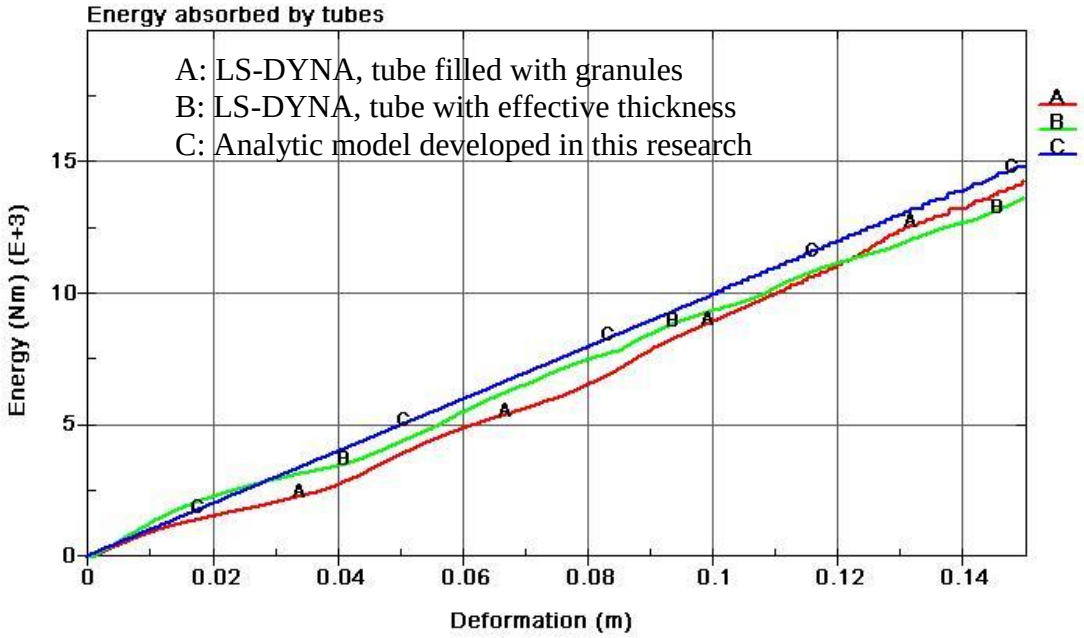

Figure 5.9 Energy absorbed by an effective tube and a tube filled with granules and obtained by analytic model (axial deformation)

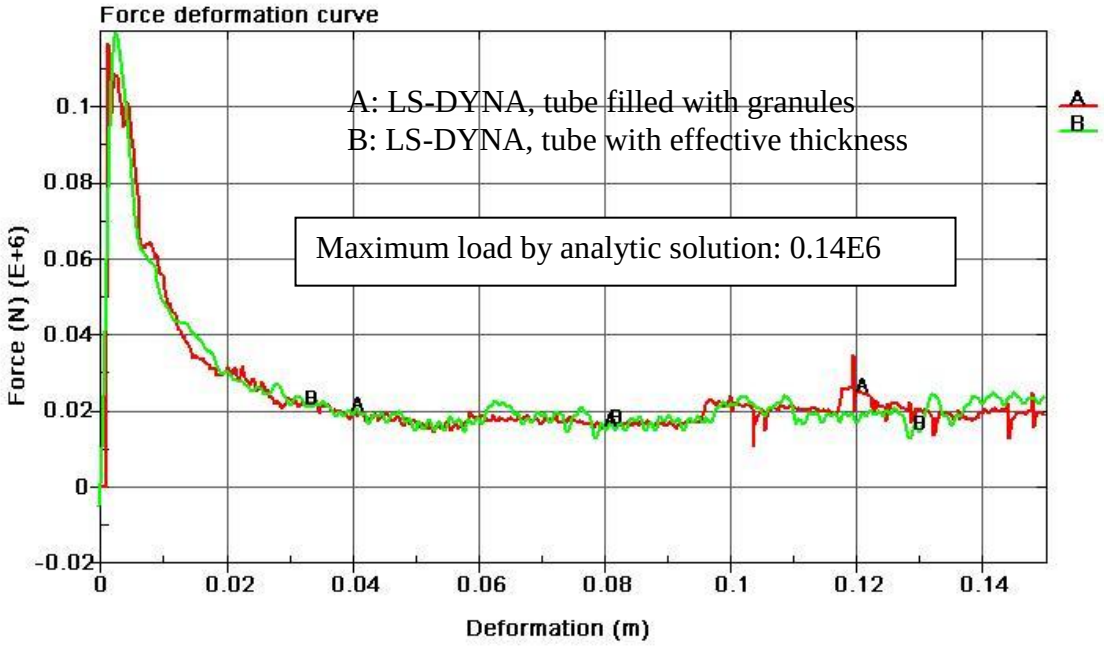

Figure 5.10 Force and deformation curve for an effective tube and a tube filled with granules (global bending)

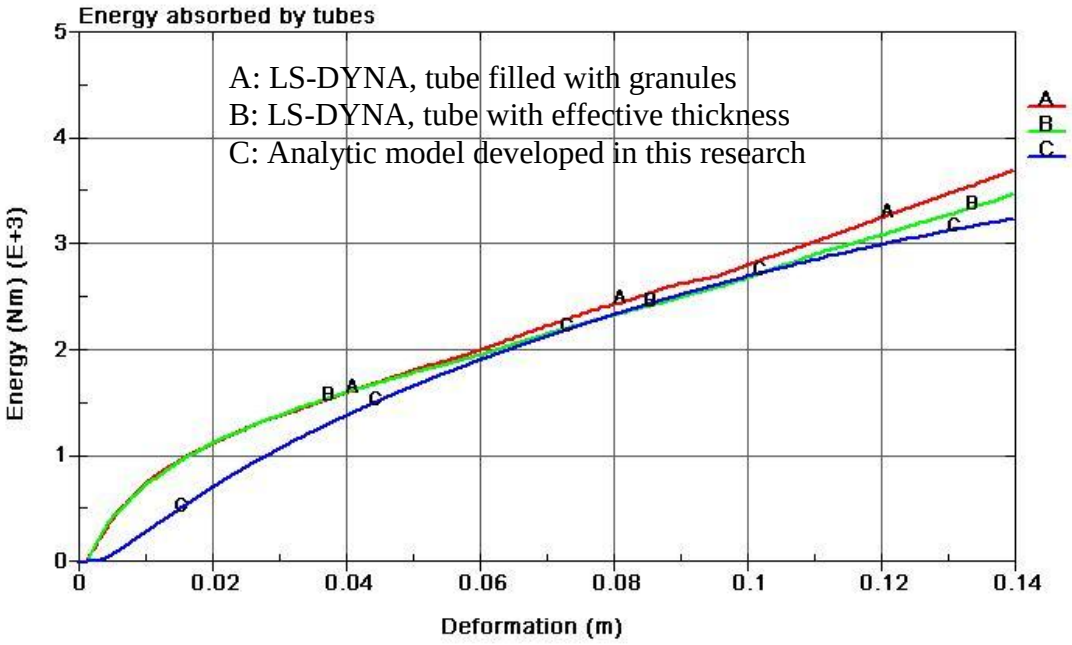

Figure 5.11 Energy absorbed by an effective tube and a tube filled with granules and obtained by analytic model (global bending)

Fig. 5.8 shows a force and deformation curve of an effective tube and a tube filled with granules for axial deformation. Fig. 5.9 shows energy absorbed by an effective tube and a tube filled with granules using LS-DYNA and obtained by the analytical model.

Fig. 5.10 shows a force and deformation curve of an effective tube and a tube filled with granules for global bending deformation. Fig. 5.11 shows the energy absorbed by an effective tube and a tube filled with granules and obtained by the developed analytic model.

As seen in Figs 5.8 through 5.11, the results of the analytic model and the simulation test are in good agreement with each other.

According to Fig. 5.12, which shows the absorbed energy in the tube filled with granular material and the absorbed energy in the empty tube, the tube filled with granules can absorb more energy than the empty tube for both axial deformation and global bending deformation.

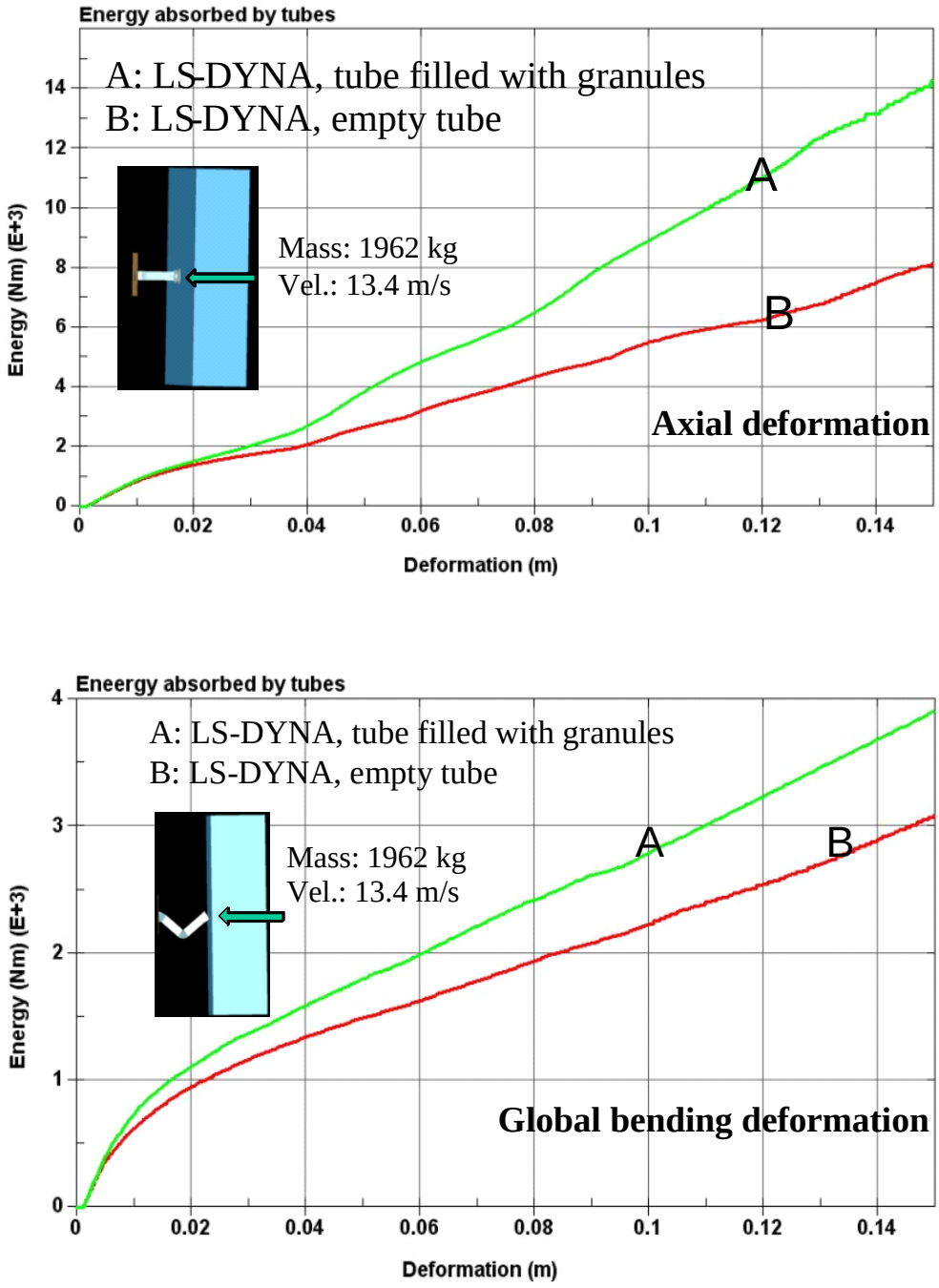

Figure 5.12 Comparison of energy absorbed by a tube filled with granules and empty tube for axial and global bending deformation

5.5 Comparisons of crashworthiness of typical sections of motor compartment rails with empty tubes and tubes filled with granules

In this section, comparisons of typical sections of motor compartment rails are made for empty tubes and for tubes filled with granules using a simple method (Malen and Kikuchi 2006). Those results have been compared to show the suitability of tubes filled with granules. In this analysis, Young's modulus (E) is 2.0E5 N/mm^2, Poisson's ration (μ) is 0.3 and yield stress (σ_{t_y}) is 300 N/mm^2 for the properties of a steel tube. The stress for bulk of granules can be assumed or obtained using Walton's equations (see chapter 5.3) before using it.

5.5.1 Motor compartment side rails – front crash load

In this section, the design of a side rail for crashworthiness is discussed. Assuming the maximum allowable acceleration to be 20g's, and the vehicle mass to be 1,423.7 kg, the allowable maximum crush force will be given by

$$F_{\max} = ma_{\max} = 1{,}423.7 \cdot 20 \cdot 9.81 = 279{,}330N \tag{5-29}$$

Therefore, assuming a crush efficiency factor to be 0.7, the allowable average crush force will be given as

$$F_{avg} = \eta F_{\max} = 0.7 \cdot 279{,}330 = 195{,}531N \tag{5-30}$$

where η is a crush efficiency factor (Malen and Kikuchi, 2006) expressed by

$$\eta = \frac{F_{avg}}{F_{\max}} \tag{5-31}$$

Assuming that in the motor compartment, the two rails will account for 50% of the crush force, then the crash force for two rails will be 97,765.5N. So, 48,882.8N will be the crash force for one rail. Equation (5-12) will give

$$\sigma_{t\_y}(4bt_e) \Big/ 1.42 = 48{,}882.8 \tag{5-32}$$

Assuming the thickness to be 1 mm and σ_{t_y} to be 300 N/mm^2, the section width of a square tube will be

$$b = \frac{1.42 \times 48{,}882.8}{4\sigma_{t\_y}t} = 5.78\ cm \tag{5-33}$$

Now, a rail section size for a square tube filled with granules will be determined. Assuming that $\sigma_{g\_y} = 0.1\sigma_{t\_y}$, $\sigma_{t\_y} = 300\,N/mm^2$ and $t = 1mm$, then equation (5-4) and equation (5-12) will give

$$4\sigma_{g\_y}b^2 + 4\sigma_{t\_y}tb - 1.42 \times 48{,}882.8 = 0 \tag{5-34}$$

From equation (5-34), the section width b is 1.95 cm. It is shown that using the tube filled with granules, the side rails can be more slender, leaving more space for the engine or the wheels.

5.5.2 Under-floor longitudinal rails: reaction crash loads

Now the under-floor longitudinal rails will be considered. The limit analysis will be done for reaction crash loads of under-floor longitudinal rails. Taking the deformation model of under-floor longitudinal rails as given in Fig. 5.13 and using the work and energy equation, the reaction force and bending moment relationship is given as

$$F_P\delta = \frac{\delta M_b}{\sin(\phi_1)L_1} + M_b\left[\frac{\delta}{\sin(\phi_1)L_1} + \frac{\delta\cos(\phi_1)}{\sin(\phi_1)L_2}\right] \tag{5-35}$$

where M_b denotes a full plastic bending moment (Crandall, Dahl, and Lardner, 1978) in the joints and ϕ_1 and ϕ_2 denote a deformation angle in the joints. For an empty square tube, the plastic bending moment (Crandall, Dahl, and Lardner, 1978) is expressed as

$$M_b = \frac{3}{2}\sigma_{t\_y}b^2t \tag{5-36}$$

where σ_{t_y}, b, and t are the yield stress of tube, the section width, and the thickness of a tube, respectively. Assuming that t=1mm and b=120mm

$$M_b = \frac{3}{2}\sigma_{t\_y}b^2 = \frac{3}{2}\cdot 300\cdot 120^2 = 6.48E6\,Nmm \tag{5-37}$$

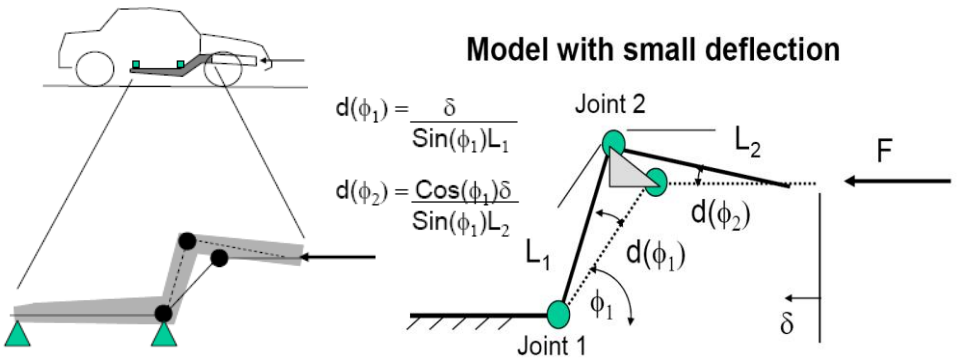

Figure 5.13 Deformation model of under-floor longitudinal rails with small deflection (from the course pack of an automotive body class at the University of Michigan)

If L1=350mm, and L2=300mm, then equation (5-35) will give

$$F_P = 73{,}974.2\ N \tag{5-38}$$

Now, consider the square tube filed with granules; the plastic bending moment will be expressed (eq. 5-7) as

$$M_b = \frac{3}{2}\sigma_{t\_y} b^2 \left(t + \frac{1}{12}\frac{\sigma_{g\_y}}{\sigma_{t\_y}} b \right) \tag{5-39}$$

Assuming that $\sigma_{g\_y} = 0.01\sigma_{t\_y}$, $t = 1mm$ and $b = 120mm$, then $M_b = 1.296E7\ Nmm$. Therefore the plastic bending moment in the case of a tube filled with granules will be twice as large as the plastic bending moment of an empty tube. So, the reaction force (F_P) will be twice as high as in the case of an empty square tube

$$F_P = 147{,}948\ N \tag{5-40}$$

The results of the rail analysis for empty tubes and tubes filled with granules are summarized in Table 5.2. As can be seen, a significant increase in body performance can be made by using tubes filled with granules.

Table 5.2 Numerical structural values for an empty-tube body and a granule-filled tube body

	Empty tubes	Tubes filled with granules
Motor compartment side rail size	5.78 cm	1.95 cm **(66.3% decrease)**
Reaction force of mid rail	73,974.2 N	147,948 N **(100% increase)**

5.6 Closure

The objective of this chapter was to develop an analytic model for the energy absorption of a tube filled with granules based on the effective thickness theory developed in this research, and to validate the analytic model and show the effectiveness and availability of a tube filled with granules for crashworthiness. In this research, the tube filled with granules has been investigated in view of its crashworthiness design, and the analytic expression of absorbed energy in a tube filled with granular material has been proposed. However, it was not straightforward to obtain that value directly from a tube filled with granules, so an effective thickness theory of a tube filled with granules has been developed. Effective thickness is the thickness of an empty tube which provides crash energy absorption capabilities equivalent to a tube filled with granules. Absorbed energy has been obtained from this equivalent tube instead of from the tube filled with granular materials. The results of the analytic model and the simulation test are in good agreement with each other. Therefore, it can be said that the absorbed energy in this effective empty tube would be equivalent to the one in the tube filled with granules.

CHAPTER VI

INTEGRATION, VALIDATION, DEVELOPED SOFTWARE, AND APPLICATION OF I-BUMPER TO HIGH-SPEED CRASH

6.1 Integration of I-bumper and vehicle

6.1.1 FOA model for a system with an explosive airbag, lattice structure, and mechanical spring (I-bumper at active state)

To analyze and predict the collision of a car with the I-bumper, a simplified FOA model is investigated in this study. Although some authors have already developed a simplified model for car collisions (Kamal, 1970; Mooi and Huibers, 1998; Lin, Kamal, and Justusson, 1975; Greene, 1977), only the three degree-of-freedom (DOF) model or two DOF model has been used in this research.

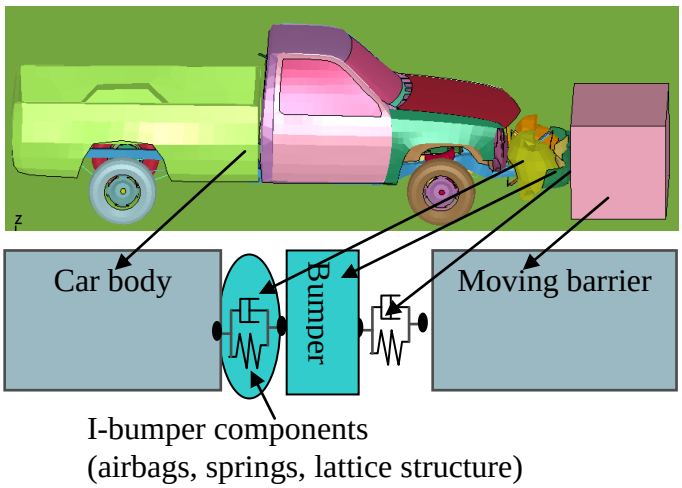

Figure 6.1 Simplified First-Order-Analysis model (3 DOF) for car head-on collision in active state

Fig. 6.1 and Fig. 6.2 illustrate the FOA model of crash between an I-bumper-car and a moving barrier used in this study. In Fig. 6.1, I-bumper components and the impact between the bumper and a moving barrier have been modeled using a spring coefficient and a damping coefficient.

In Fig. 6.2, however, the impact between the bumper and the moving barrier has been modeled by e_r, the coefficient of restitution (COR), but the I-bumper components are again modeled by a spring coefficient and a damping coefficient.

The incremental differential equation of crash motion for the system (Fig. 6.1 and Fig. 6.2) can be expressed as

$$[m_i][\Delta\ddot{x}_i] + [k_i][\Delta x_i] + [c_i][\Delta\dot{x}_i] = [\Delta F_i] \tag{6-1}$$

To determine the stiffness matrix and the damping matrix in equation (6-1), it is necessary to find the spring coefficients and damping coefficients of the I-bumper components. It is also necessary to know the initial conditions (displacements and velocities) for each mass in the models of Figs. 6.1 and 6.2. In the previous chapters, the analytic approaches for those coefficients of I-bumper components and initial conditions were derived.

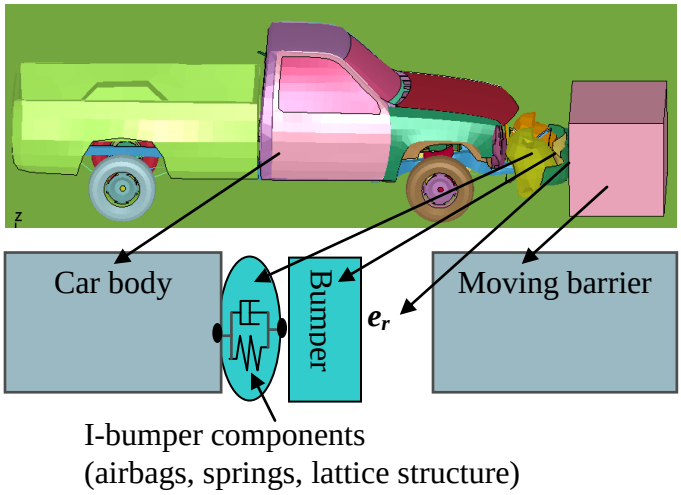

Figure 6.2 Simplified First-Order-Analysis model (2-DOF) for a car head-on collision using e_r, the coefficient of restitution (COR), in active state

The system's initial velocity of the car body and bumper, as well as the velocity after detonation, has been determined by a developed using the modified Gurney's equation (see chapter 3.4). In this model, in most cases, the bumper will have a very high speed due to the detonation of the explosive. Equation (6-1) can be solved using a step-by-step integration method. The spring coefficient and the damping coefficient of the impact between the car bumper and the moving barrier in Fig. 6.1 and COR in Fig. 6.2 can be determined by experimental testing.

6.1.2 FOA model for a system with a front-post filled with granules (I-bumper at passive state)

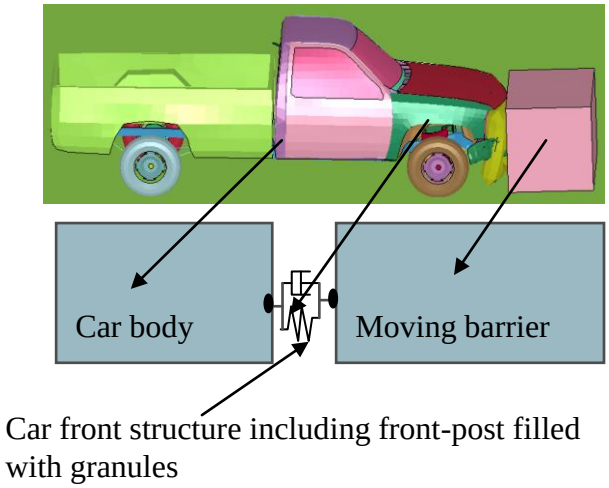

Figure 6.3 Simplified First-Order-Analysis model (2-DOF) for a car head-on collision in the passive state

In the passive state, the front structure, including a front post filled with granules, will account for the remaining energy left over from the active state. The FOA model for the passive state, including a front-post filled with granules, can be simply two DOF, as shown in Fig. 6.3.

6.1.3 The integrated I-bumper and vehicle model

This research investigated the spring and damping coefficients for an airbag (eq. 3-6 and eq. 3-12); lattice structure (eq. 4-42); tubes filled with granules (eq. 5-17), by which the spring and damping matrix in equation (6-1) can be determined; and mass velocity driven by an explosive, based on Gurney's equation for initial velocity (eq. 3-36) in the previous chapters. These were summarized in Table 6.1.

Table 6.1 Spring coefficients and damping coefficient for I-body components

I-body components	Spring coefficients
Airbag	$K_{airbag\_1} = \frac{dP}{dt} \cdot \frac{A_e}{\dot{x}}$ $K_{airbag\_2} = \frac{dA_e}{dx} \cdot P_g$
Lattice structure	$K_{eq\_lattice} = \frac{2U_{lattice}}{x^2_{expanded}}$
Front post filled with granules	$K_{eq\_tube} = \frac{2U_{tube}}{x^2_{tube}}$

* Damping coefficient for airbag $C_{airbag} = F/\dot{x} = \frac{\rho \cdot g\left(\frac{v_B^2 - v_A^2}{2g} + \frac{32\mu L v_B}{\rho g d^2}\right)A_e}{\dot{x}}$

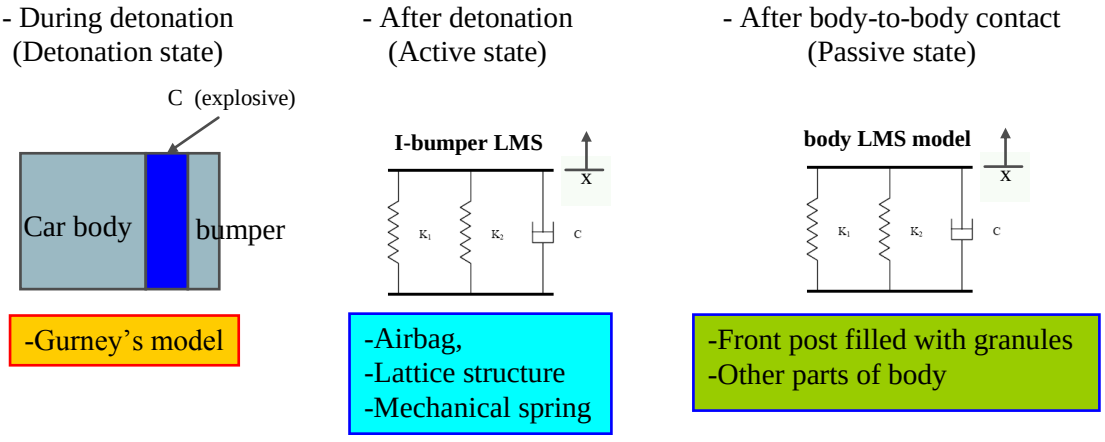

Figure 6.4 Explosive model and FOA model of I-bumper

The I-bumper system comprises the detonation state, the active state, and the passive state (see Fig. 6.4). In the detonation state, the I-bumper will be deployed by the explosive in the airbag, and the bumper will be projected with high kinetic energy after the impending crash is anticipated. In this state, the projected bumper will reduce the kinetic energy of other cars by colliding with them. In the active state, expanded front structures including the airbag, the lattice structure, and the mechanical spring will absorb the crash energy (see Figs. 6.1 and 6.2). In the passive state, the automotive front structure including a front-post filled with granules will absorb the crash energy remaining from the active state (see Fig. 6.3).

To solve the nonlinear equation that appears in the FOA model (equation (6-1) and Fig. 6.5), the step-by-step integration method (Paz, 1997) can be applied. In this method, the equation is solved at successive increments Δt (or dt) of time.

For computational advantage, the increment is usually taken at equal lengths of time. At the beginning of each interval, the initial conditions (such as displacements and velocities of the dynamic equilibrium) are updated. Then, the solution of the equation for a time increment Δt is obtained approximately on the assumption that the spring and damping coefficients are constant during the increment Δt. The nonlinear characteristics of the spring and damping coefficients are taken into account in this method by updating these coefficients at the beginning of each time increment using the equations (3-6), (3-12), (4-42), and (5-17) (see Fig. 6.5). The response is obtained using the displacement and velocity calculated at the end of the time interval as the initial conditions for the next time step. The system's initial velocity can be determined using the modified Gurney's equation (3-36) (see Fig. 6.5). Many procedures are available for implementing this step-by-step integration. In this study, the linear acceleration method with a modification known as the Wilson-θ method (Paz, 1997) has been used. The basic assumption of the Wilson-θ method is that the acceleration varies linearly over the time interval from t to $t+\theta\Delta t$. The value of the factor θ is determined so as to obtain optimum stability of the numerical process and accuracy of the solution. It was shown by Wilson that for $\theta \geq 1.38$ the method becomes unconditionally stable.

The equation of motion (equation (6-1)) would be the incremental equation of motion, which is

$$\mathbf{M}\Delta\ddot{\mathbf{x}} + \mathbf{K}\Delta\mathbf{x} + \mathbf{C}\Delta\dot{\mathbf{x}} = \Delta\mathbf{F} \tag{6-2}$$

Equations for each time step are as follows (Paz, 1997):

Initialization

$$\tau = \theta\Delta t,\ a_1 = 3/\tau,\ a_2 = 6/\tau,\ a_3 = \tau/2,\ a_4 = 6/\tau^2$$

For each time step ($i-th$ *time step*)

$$\Delta\bar{\mathbf{F}}_i = \Delta\mathbf{F}_i + (a_2\mathbf{M} + 3\mathbf{C})\dot{\mathbf{x}}_i + (3\mathbf{M} + a_3\mathbf{C})\ddot{\mathbf{x}}_i$$
$$\bar{\mathbf{K}}_i = \mathbf{K}_i + a_4\mathbf{M} + a_1\mathbf{C}$$
$$\hat{\Delta}\mathbf{x}_i = \frac{\Delta\bar{\mathbf{F}}_i}{\bar{\mathbf{K}}_i}$$
$$\hat{\Delta}\ddot{\mathbf{x}}_i = a_4\hat{\Delta}\mathbf{x}_i - a_2\dot{\mathbf{x}}_i - 3\ddot{\mathbf{x}}_i$$
$$\Delta\ddot{\mathbf{x}}_i = \frac{\hat{\Delta}\ddot{\mathbf{x}}_i}{\theta}$$
$$\Delta\dot{\mathbf{x}}_i = \ddot{\mathbf{x}}_i\Delta t + 1/2(\Delta\ddot{\mathbf{x}}_i)\Delta t$$
$$\Delta\mathbf{x}_i = \dot{\mathbf{x}}_i\Delta t + 1/2(\ddot{\mathbf{x}}_i\Delta t^2) + 1/6(\Delta\ddot{\mathbf{x}}_i\Delta t^2)$$
$$\mathbf{x}_{i+1} = \mathbf{x}_i + \Delta\mathbf{x}_i$$
$$\dot{\mathbf{x}}_{i+1} = \dot{\mathbf{x}}_i + \Delta\dot{\mathbf{x}}_i$$
$$\ddot{\mathbf{x}}_{i+1} = \mathbf{M}^{-1}\left(\mathbf{F}_E(t_{i+1}) - \mathbf{F}_K(\mathbf{x}_{i+1}) - \mathbf{F}_C(\dot{\mathbf{x}}_{i+1})\right)$$

(6-3)

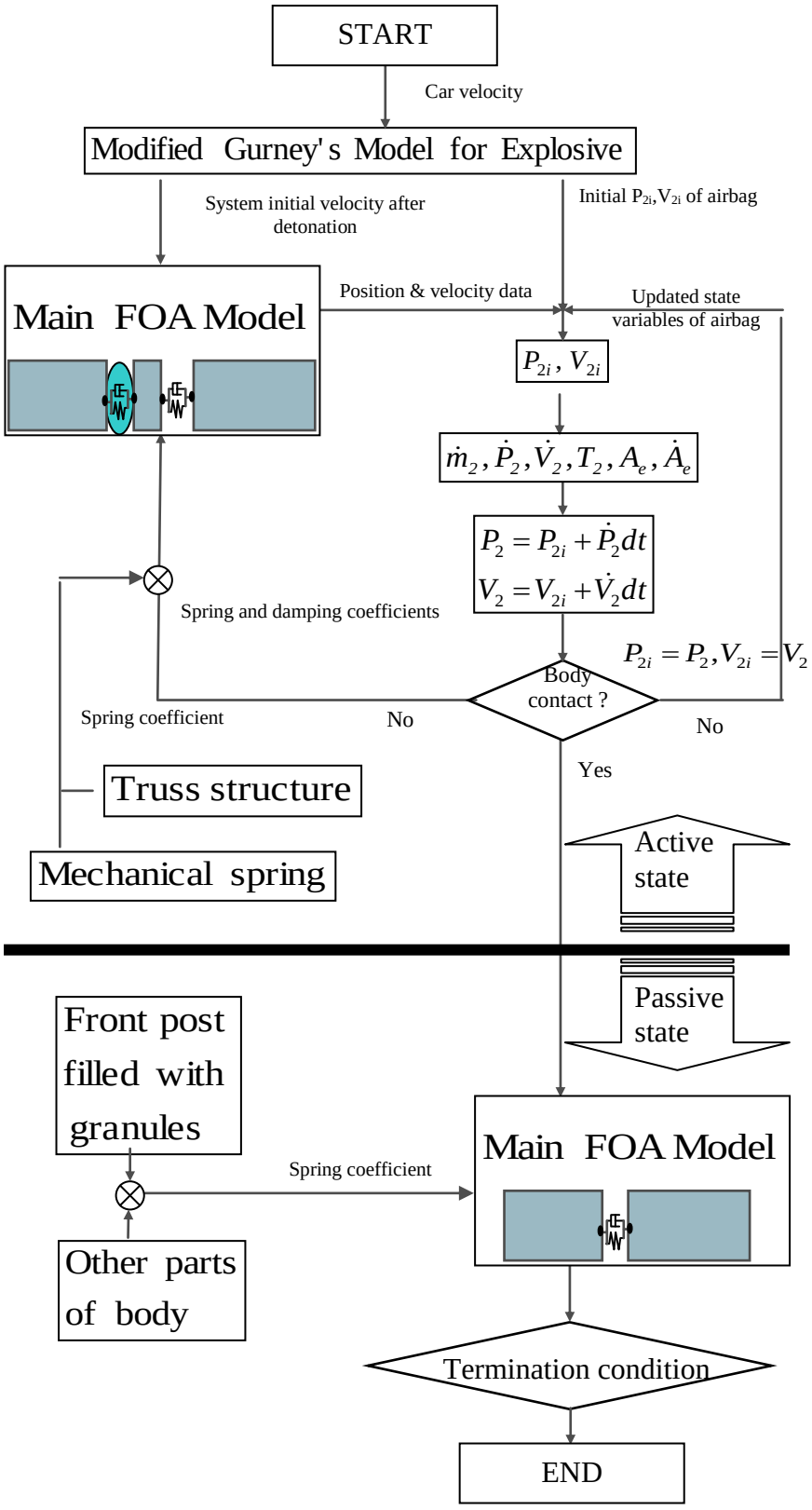

Figure 6.5 Process flow of a complete collision model for a car with an I-bumper

6.2 Validation of the FOA model of the I-bumper

To validate the FOA model, a comparison between the developed FOA model and the FEA model using LS-DYNA has been made. Figure 6.6 shows an FOA model and an FEA model for validation.

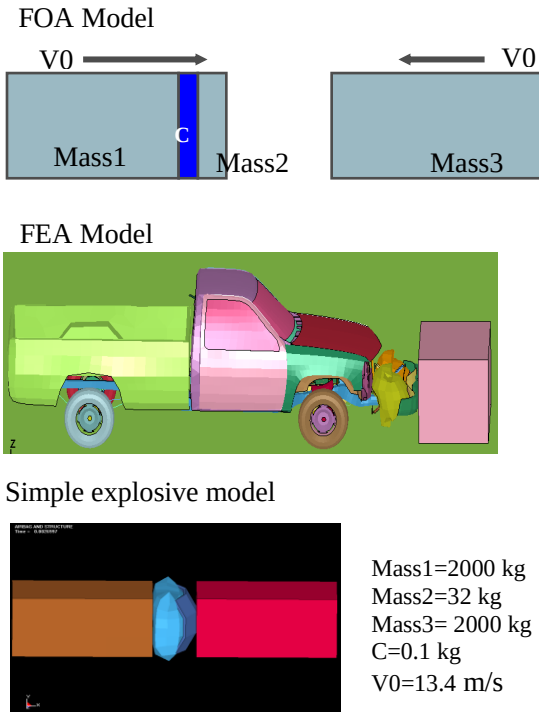

Figure 6.6 FOA model and FEA model for a complete I-bumper model

To simulate the explosive effect, the velocities of the bumper and the car after detonation, as well as the airbag pressure obtained from the simple explosive model (Fig. 6.6) using the CONWEP function of LS-DYNA, were entered simply as initial conditions of simulation. For a tube filled with granules made of polyester (PBT), an effective tube with effective thickness (Lee, Ma, and Kikuchi, 2007) was used.

The method for the complete airbag model was implemented using MATLAB. The velocity of each mass is shown in Figs. 6.7, 6.8, and 6.9, for velocity of mass 1, velocity of mass 3, and velocity of mass 2, respectively. The results are compatible in terms of major tendencies.

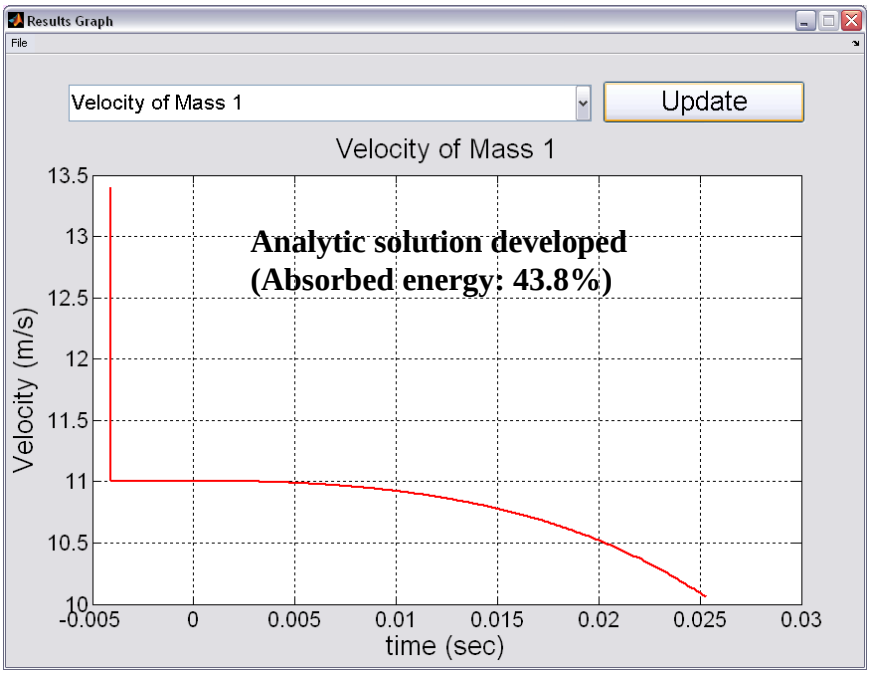

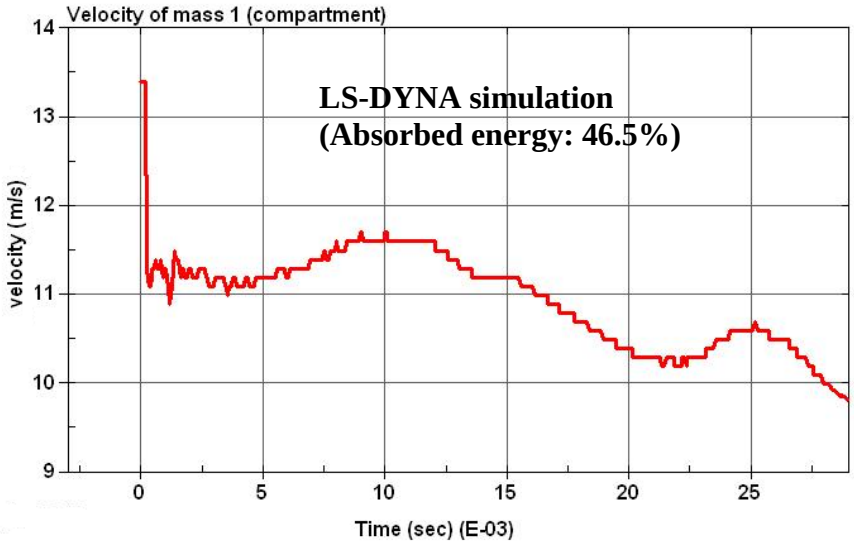

Figure 6.7 Velocity of Mass1

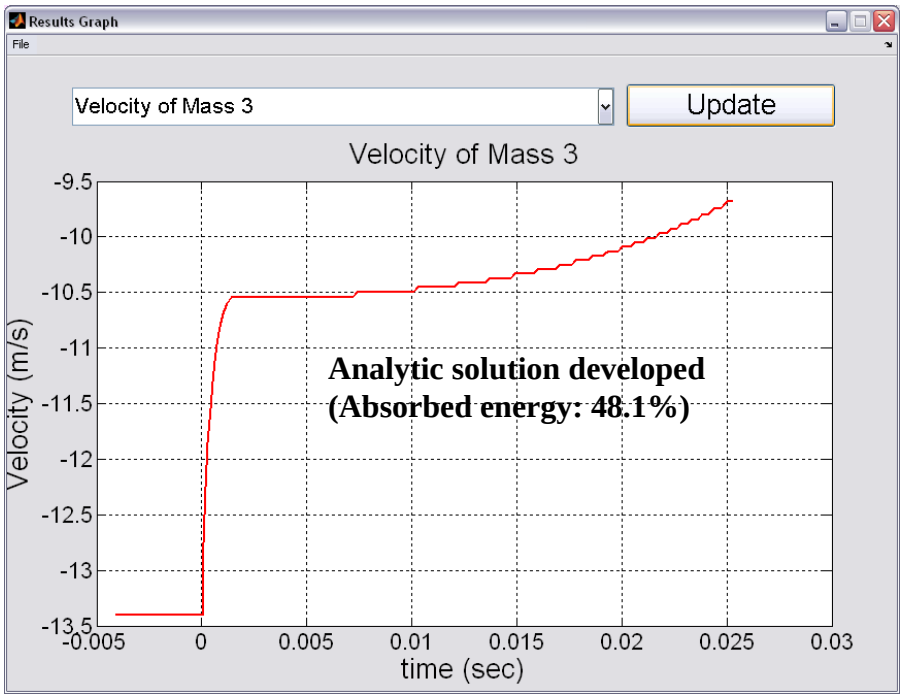

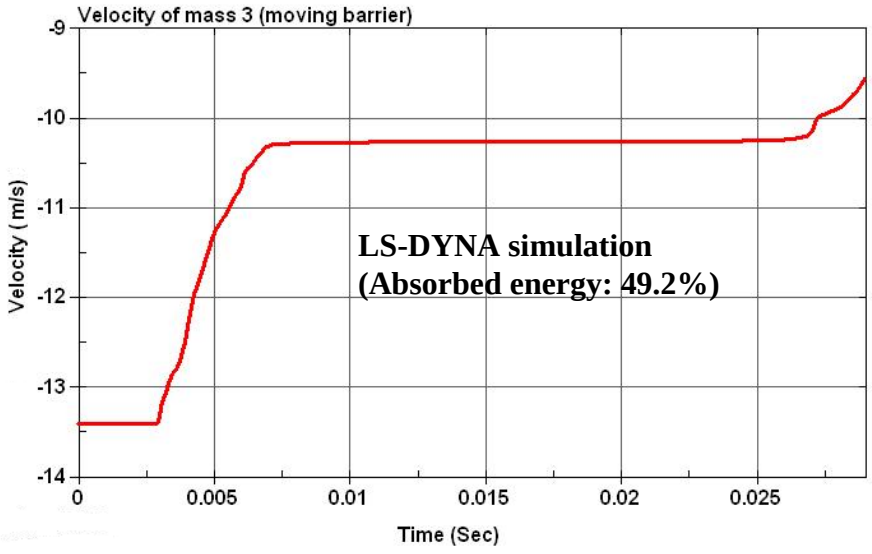

Figure 6.8 Velocity of Mass 3

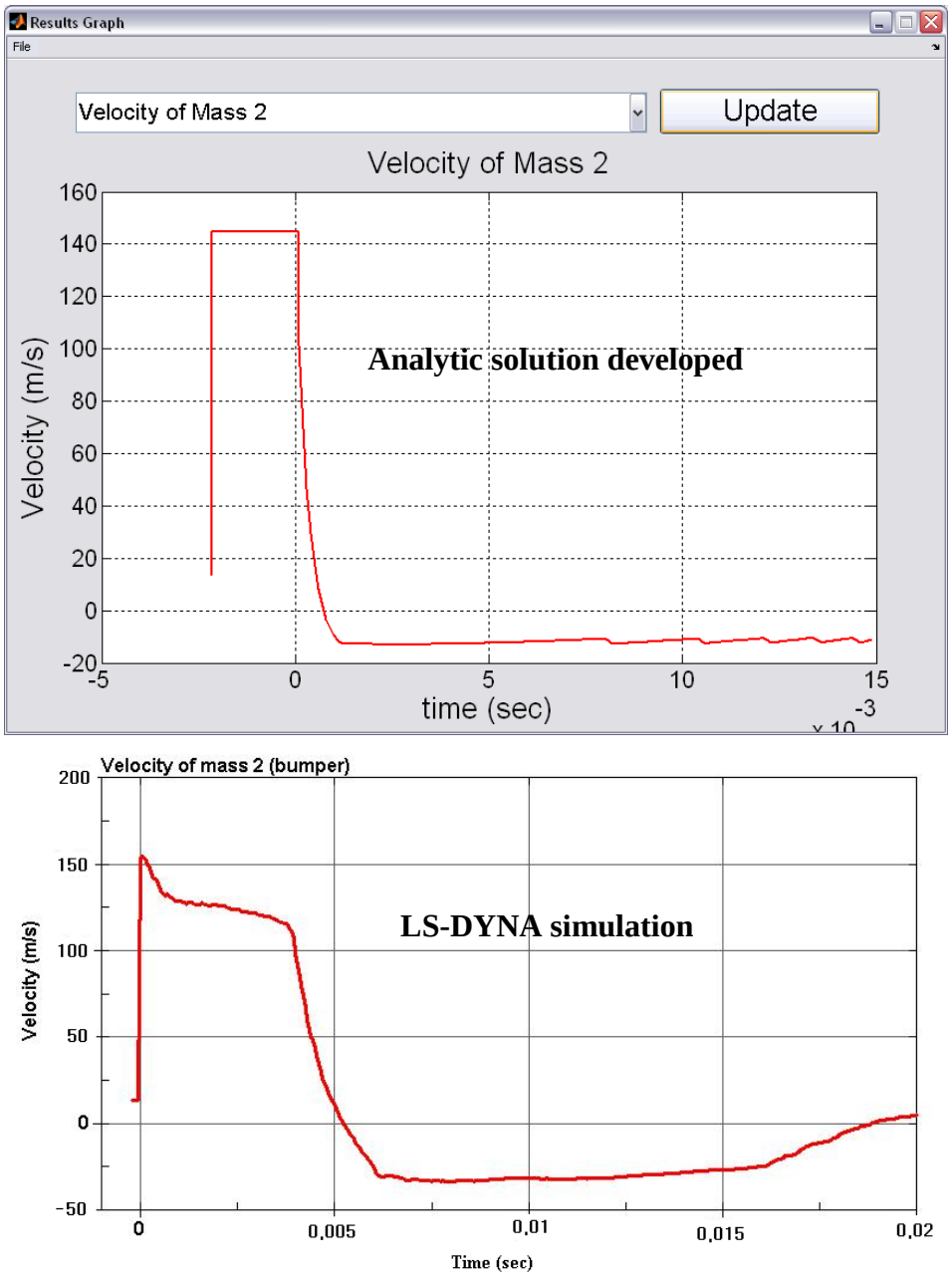

Figure 6.9 Velocity of Mass 2 (bumper)

To show the effectiveness and availability of an I-bumper, the acceleration values at the center of the compartment for the I-bumper car collision and a conventional car collision against a moving barrier are compared.

As shown in Fig. 6.10, the maximum acceleration of the car can be significantly reduced (by around 40%) during the collision with a system using an I-bumper along with a front post filled with granules.

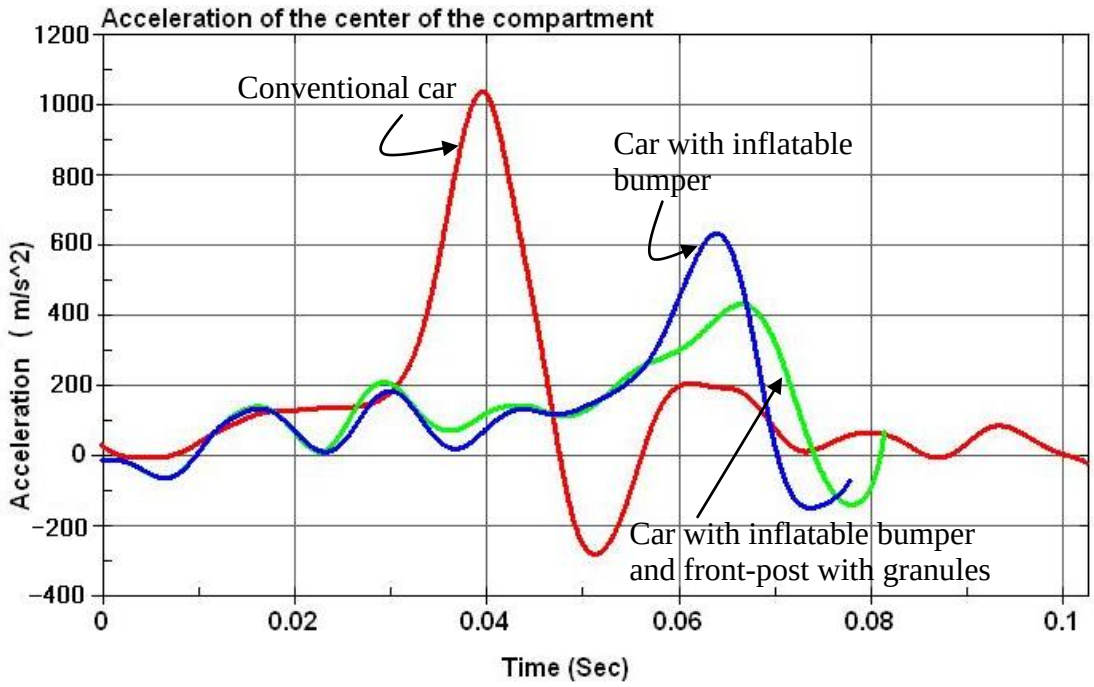

Figure 6.10 Accelerations of the center of the compartment

6.3 Software developed using MATLAB

Fig. 6.11 shows the snapshot of design software for the I-bumper system. This is the initial screen display of this software which features two buttons, one being for the optimization of the lattice structure (see Fig. 6.12), and the other one being for the analysis of the I-bumper (see Fig. 6.14). The optimization of the lattice structure should be performed before the analysis of I-bumper is started because the average stiffness of the lattice structure is one of the input parameters in the analysis of the I-bumper.

An optimization process has been implemented for the lattice structure (see Fig. 6.12). This optimization process can be used to predict the optimum shape of the plate as well as the average stiffness of the lattice structure and the energy absorbed by the lattice structure during the crash.

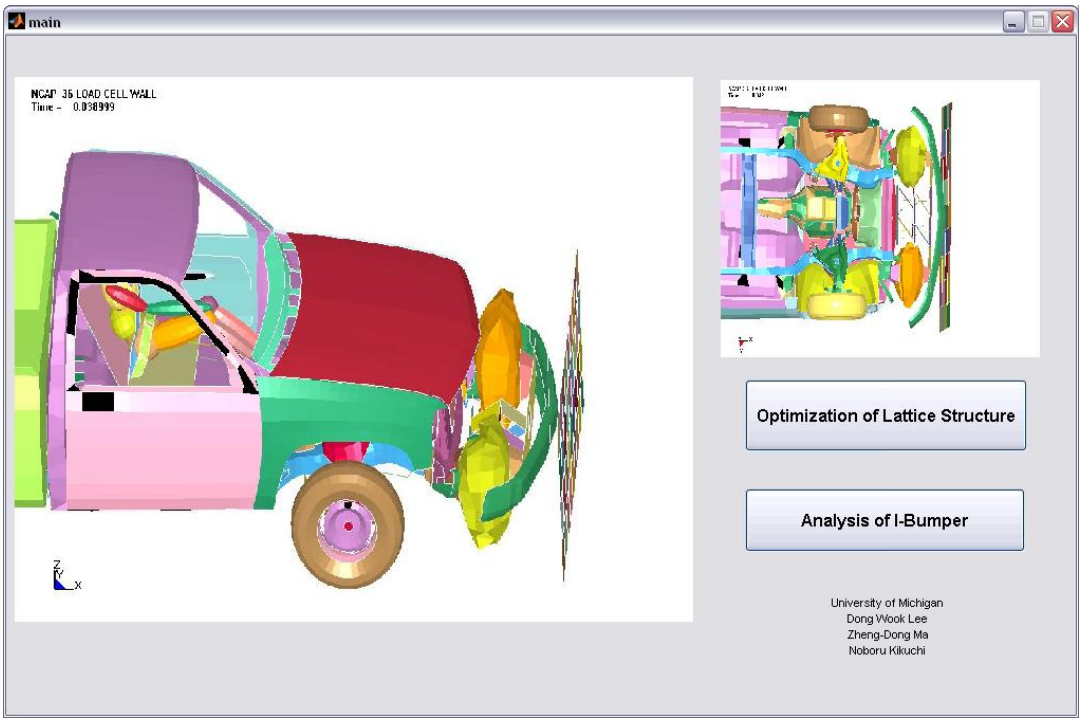

Figure 6.11 Snapshot of initial screen of analysis software

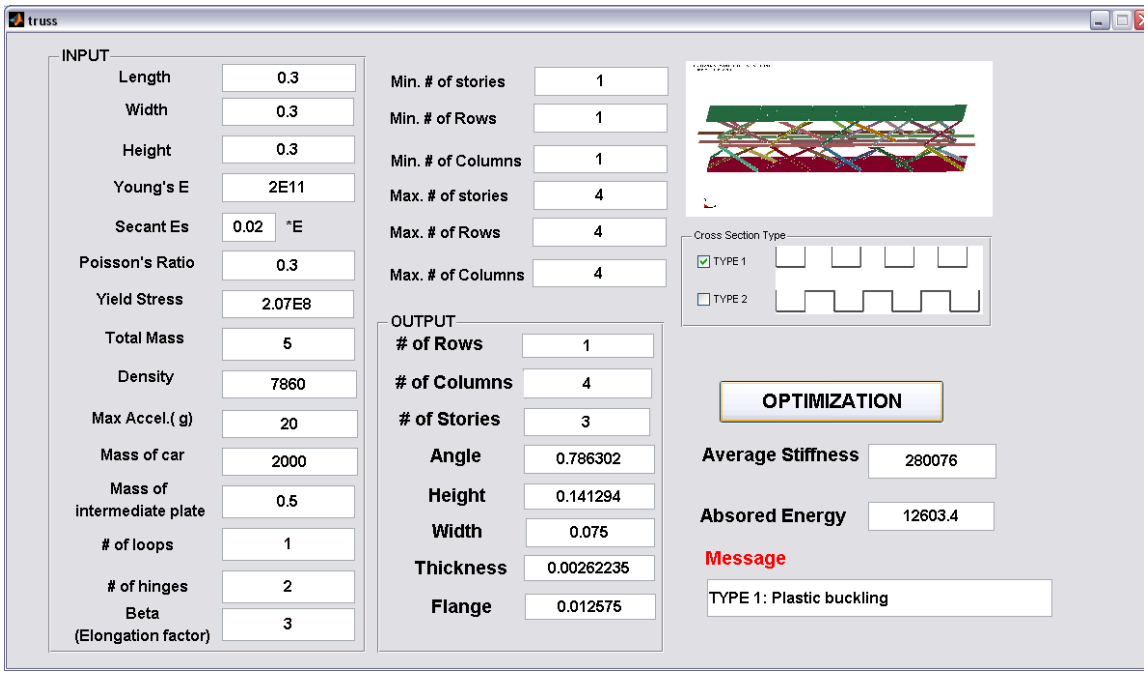

Figure 6.12 Optimization tool for lattice structure

Table 6.2 Input parameters for lattice structure

Input parameters	*Variables in this thesis*
1. Length (m)	*L*: in Fig. 4.18
2. Width (m)	*W*: in Fig. 4.18
3. Height (m)	*H*: in Fig. 4.18
4. Young's Modulus (E) (Pa)	E: Young's modulus of plate in eq.(4-3)
5. Secant Modulus (Es) (Pa)	Es: Secant modulus of plate in eq.(4-7)
6. Poisson's Ratio	μ: Poisson's ration of plate in eq.(4-3)
7. Yield Stress (Pa)	σ_y: Yield stress of plate in eq.(4-34)
8. Total Mass (Kg)	M: total mass of lattice structure in eq.(4-50)
9. Density (kg/m^3)	Density of plate
10. Maximum Acceleration (gravity)	Allowable maximum acceleration in unit g
11. Mass of the car (kg)	Mass of the car
12. Mass of intermediate plate (kg)	Mass of the intermediate plate and cover in the lattice structure in Fig. 4.3
13. Number of loops	Number of loops in Fig. 4.16
14. Number of hinges	Number of hinges in Fig. 4.16
14. Beta (elongation factor)	Elongation factor in eq. (4-36)
15. Minimum numbers of stories, rows, and columns	Available minimum number of stories, rows, and columns
16. Maximum numbers of stories, rows, and columns	Available maximum number of stories, rows, and columns

Table 6.3 Output values for lattice structure

Output Values	*Variables in this thesis*
1. Average stiffness (N/m)	
2. Absorbed energy (Nm)	
3. Optimized number of rows	See Fig. 4.3
4. Optimized number of columns	See Fig. 4.3
5. Optimized number of stories	See Fig. 4.3
6. Angle of lattice (Radian)	See Fig. 4.9
7. Height of element (m)	b in Fig. 4.5
8. Width of element (m)	a in Fig. 4.5
9. Thickness of element (m)	t in Fig. 4.5
10. Height of flange (m)	flange_h in Fig. 4.5

For a jagged member, "Optimized number of columns" means the number of jagged plates. The width, height, and length of each jagged member are shown in Fig. 6.13.

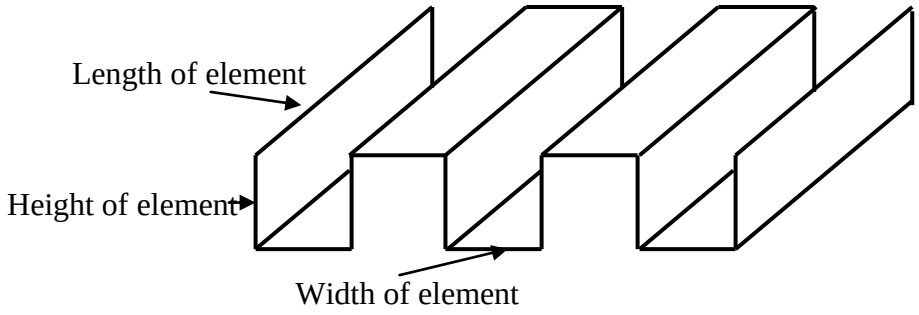

The number of jagged plates (the number of columns): 5

Figure 6.13 Jagged member element

This optimization tool will give the optimized size and shape and the average stiffness of the lattice structure. The average stiffness will be input in "Structure spring constant" for the analysis of the I-bumper (see Fig. 6.14).

Input parameters and output values for the lattice structure design are listed in Tables 6.2 and 6.3. When values are input and the optimization button is clicked, the software gives results including average stiffness, absorbed energy, and optimized values of element in lattice structure (width, length, and height of U-shape plate or jagged plate).

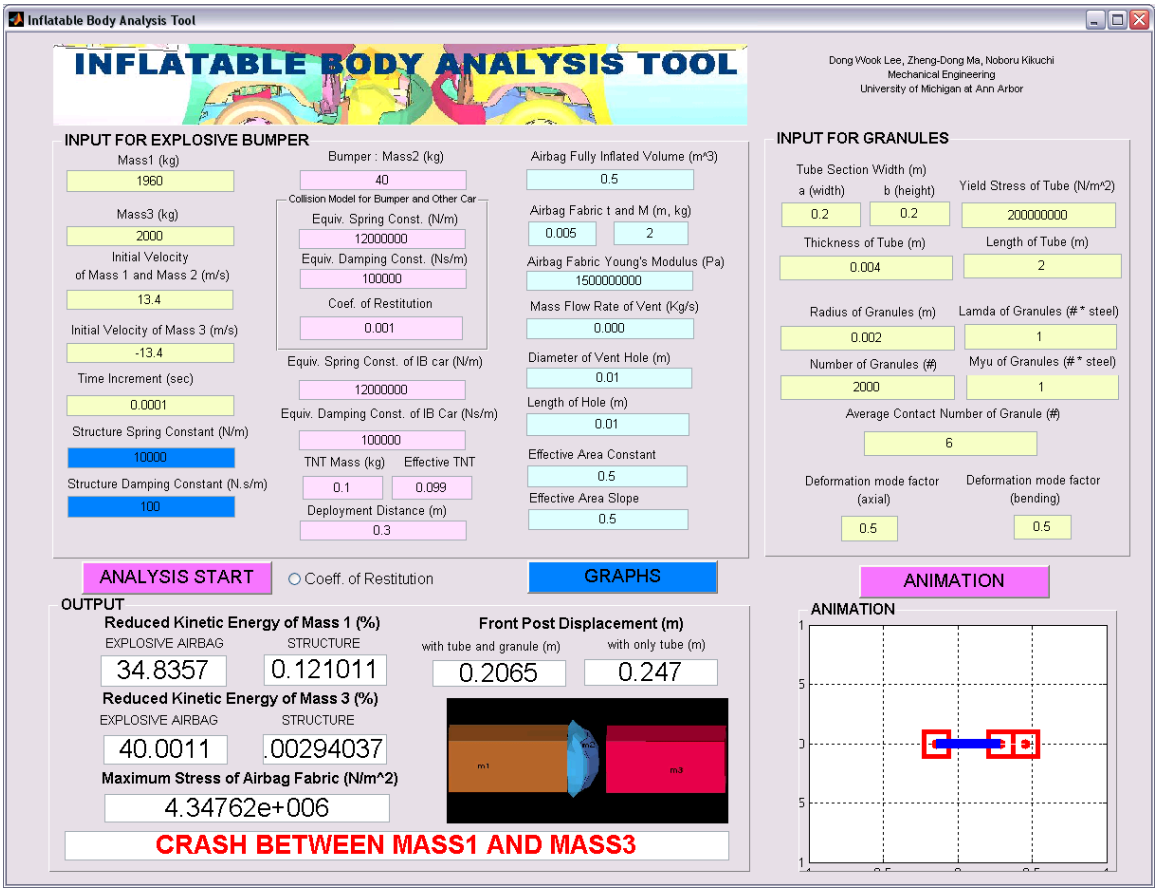

Figure 6.14 Snapshot of analysis software for the I-bumper

Figs. 6.14 and 6.15 are snapshots of the software developed for I-bumper analysis. Fig. 6.15 shows a screen that appears when the "GRAPHS" button in Fig. 6.14 is clicked. The screen for the I-bumper includes an input panel, output panel, and simple animation panel. After the entering all the parameter values into the input panel, the analysis results

will be shown in the output panel by clicking the “ANALYSIS START” button, as well as being shown in graphs by clicking the “GRAPHS” button. In the graph results window, an item can be displayed by selecting it from the drop-down menu (see Fig. 6.15). When the “ANIMATION” button is clicked, a simple animation will be shown in the animation panel.

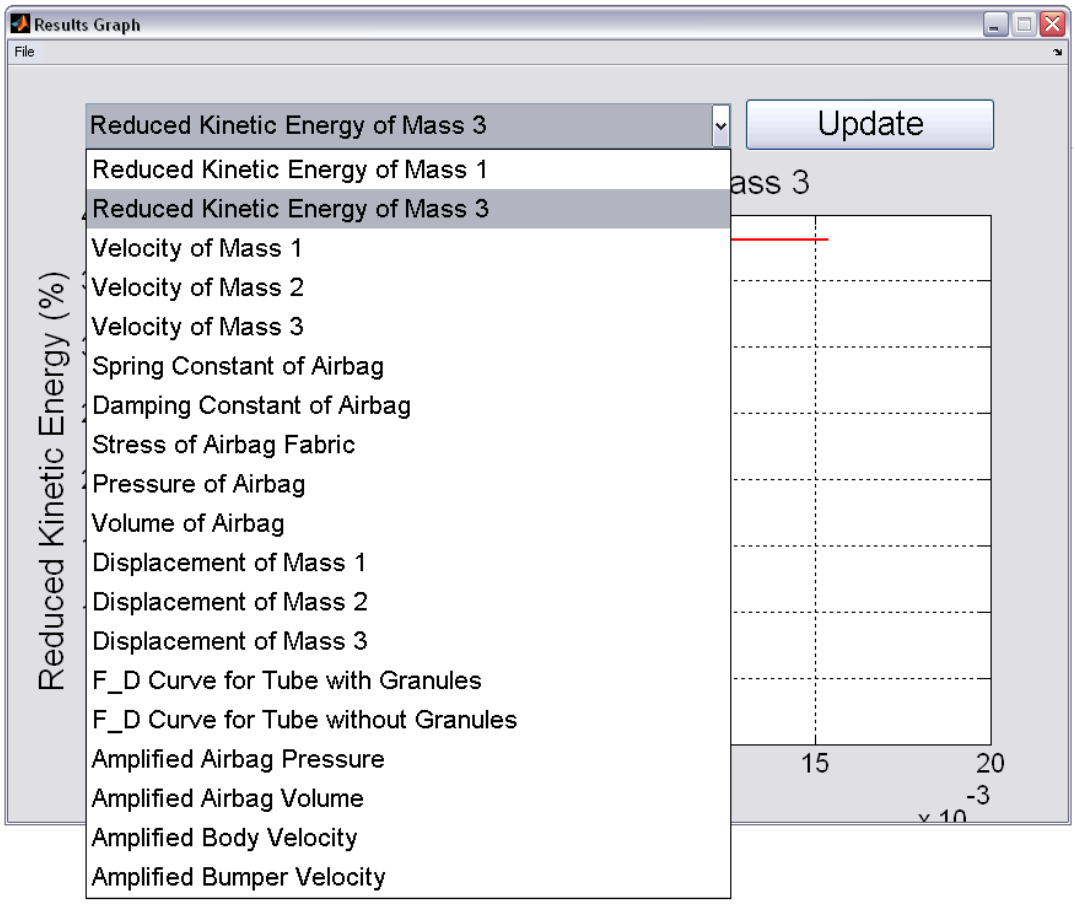

Figure 6.15 Snapshot of graphs shown by analysis software for the I-bumper

This software will estimate how much energy can be absorbed using the I-bumper. Input parameters are composed of the physical data from cars, explosive mass, airbag properties, front-post filled with granules, and lattice structure. The output results include the reduced kinetic energy of each mass, displacement, and velocity of each mass, as well as airbag state values such as pressure and volume.

Table 6.4 Input parameters for I-bumper

Input parameters	*Variables in this thesis*
1. Mass of m1 (kg)	Mass of car body in Fig. 6.1
2. Mass of m2 (kg)	Bumper mass in Fig. 6.1
3. Mass of m3 (kg)	Mass of moving barrier or colliding car in Fig. 6.1
4. Initial velocity of m1 and m2 (m/s)	Initial velocity of the car body and bumper
5. Initial velocity of m3 (m/s)	Initial velocity of the other colliding car
6. Time increment (sec)	Δt : time increment in eq.(6-3)
7. Structure spring constant (N/m)	Spring coefficient of lattice structure in eq.(4-42) and mechanical spring
8. Structure damping constant (Ns/m)	Adds mechanical damper
9. Equivalent spring constant between bumper and the other car (N/m)	See Fig. 6.1
10. Equivalent damping constant between bumper and the other car (Ns/m)	See Fig. 6.1
11. Equivalent spring constant car body (N/m)	Spring coefficient of I-bumper car body
12. Equivalent damping constant car body (Ns/m)	Damping coefficient of I-bumper car body
13. TNT mass (kg)	C: TNT mass in eq.(3-29)
14. Effective TNT mass (kg)	See Fig. 3.12
15. Deployment distance (kg)	H: in Fig. 4.18
16. Airbag fully inflated volume (m^3)	V_{20} in eq.(3-20)
17. Airbag fabric thickness (m)	t in eq.(3-17)
18. Airbag mass (kg)	
19. Airbag fabric Young's modulus (N/m^2)	E in eq.(3-18)
20. Mass flow rate of vent (kg/s)	$\dot{m}_{out}$: mass flow rate of vent in Fig. 3.5
21. Diameter of vent hole (m)	d : diameter of exit hole in Fig. 3.5
22. Length of hole (m)	L: length of exit hole in Fig. 3.5
23. Effective area constant	A_{e_cons} in eq.(3-25)
24. Effective area slope	A_{e_slope} in eq.(3-25)
25. Coefficient of restitution	See Fig. 6.2

Table 6.5 Output values and graphs for I-bumper

Output Values	*Output Graphs*
1. Reduced Kinetic Energy of Mass 1	1. Reduced Kinetic Energy of Mass 1
2. Reduced Kinetic Energy of Mass 3	2. Reduced Kinetic Energy of Mass 3
3. Maximum Stress of Airbag Fabric	3. Velocity of Mass 1
	4. Velocity of Mass 2
	5. Velocity of Mass 3
	6. Spring Constant of Airbag
	7. Damping Constant of Airbag
	8. Stress of Airbag Fabric
	9. Pressure of Airbag
	10. Volume of Airbag
	11. Displacement of Mass 1
	12. Displacement of Mass 2
	13. Displacement of Mass 3
	14. F_D curve for tube with granules
	15. F_D curve for tube without granules
	16. Amplified airbag pressure
	17. Amplified airbag volume
	18. Amplified body velocity
	19. Amplified bumper velocity

Mass1, mass2, and mass3 denote the mass of the car body to be designed, the bumper mass of the car to be designed, and the mass of the other car, respectively.

The impact between the bumper and the moving barrier will be modeled by the coefficient of restitution (COR) (input parameter 11 in Table 6.4) or spring and damping coefficients (input parameters 9 and 10 in Table 6.4). To use the coefficient of restitution, the combo button ("Coefficient of Restitution") next to the "ANALYSIS START" button should be checked and appropriate values should be inputted in parameter 11 in Table 6.4

Input parameters and output values for I-bumper and granule-filled tube are listed in Tables 6.4, 6.5, 6.6, and 6.7

Table 6.6 Input parameters for granules and front-post

Input parameters	*Variables in this thesis*
1. Width of tube (m)	a in the Fig. 5.3
2. Height of tube (m)	b in the Fig. 5.3
3. Thickness of tube (m)	Eq. (5.5)
4. Length of tube (m)	
5. Radius of granules (m)	R in eq. (5-20)
6. Number of granules	N in eq. (5-26)
7. Average contact number of granules	*n* in eq. (5-26)
8. Yield stress of tube (N/m^2)	σ_{t_y} In Fig. 5.3
9. Lambda of granules (N/m^2)	λ in eq. (5-24)
10. Mu of granules (N/m^2)	μ in eq. (5-24)
11. Axial deformation mode factor	α In eq. (5-11)
12. Bending deformation mode factor	β In eq. (5-11)

Table 6.7 Output values for front-post filled with granules

Output Values
1. Front-post length with granules (needed to absorb the remaining energy)
2. Front-post length without granules (needed to absorb the remaining energy)

6.4 Application of the I-bumper to a high-speed crash

Princess Diana died in a Paris car crash on Aug. 31, 1997. The princess' Mercedes-Benz car was apparently being pursued at a high rate of speed (80 mph) by photographers on motorbikes, when it hit a pillar and smashed into a wall. The problem was the high speed.

In this chapter, some applications of the I-bumper for high-speed crashes, and the mass incompatibility problem using the LS-DYNA FEA model, is considered. As shown in Fig. 6.16, the current automotive structure does not work well in high-speed crashes. Fig. 6.16 also illustrates that human injury from a high speed crash is much more serious and more probable than from low-velocity impacts.

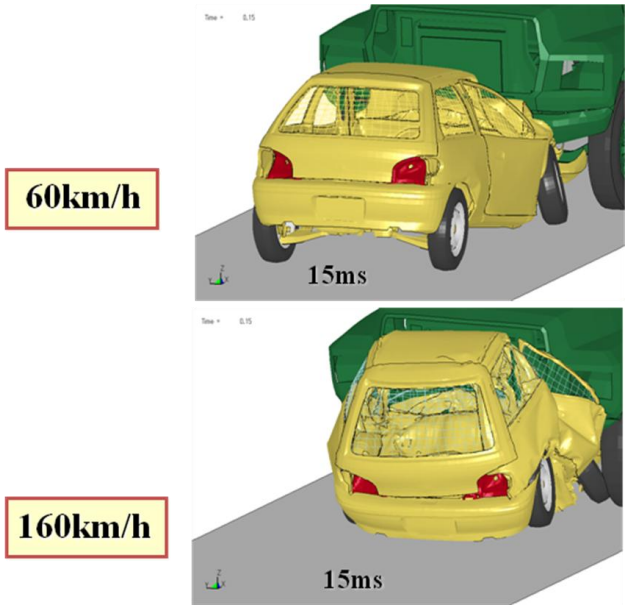

Figure 6.16 High speed crash and incompatibility problem (H. Nishigaki, Toyota Central R&D Lab.)

As mentioned in Chapter I, it was expected that the I-bumper system would work for high speed crashes and the mass incompatibility problem in crashes. The effectiveness and availability of the I-bumper for high speed crashes is shown in this chapter.

The crash test between a light truck and a heavy truck is considered (see Fig. 6.17) in two cases. In one case, both colliding vehicles have a velocity of 30 mph (13.4 m/s), and in the other case, both are traveling at 50 mph (22.35 m/s) before the collision. To compensate for the geometric incompatibility between the height of the trucks' bumpers, the position of the light truck was rearranged so that a bumper-to-bumper crash occurred.

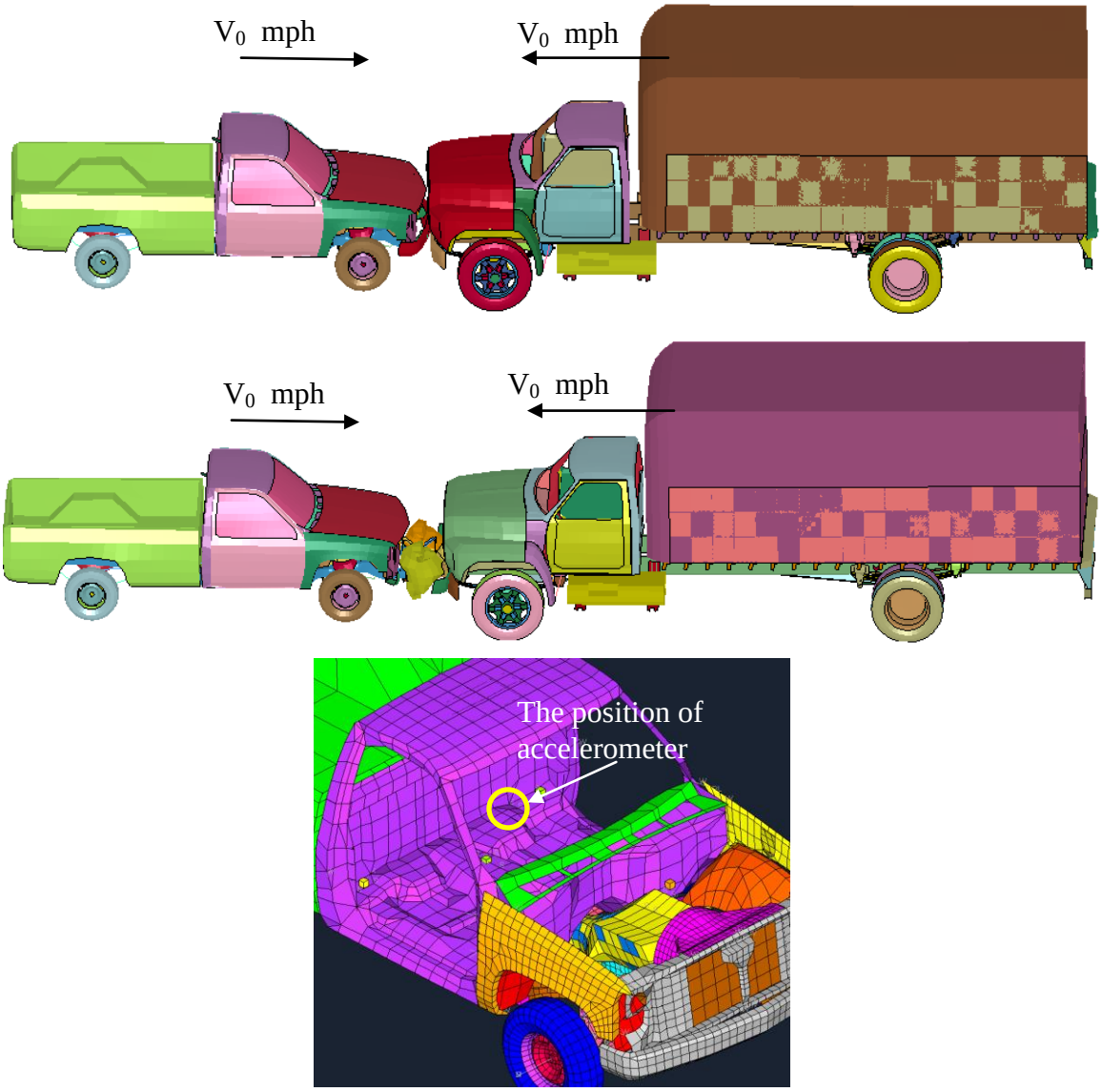

Figure 6.17 FEA model for a high speed crash

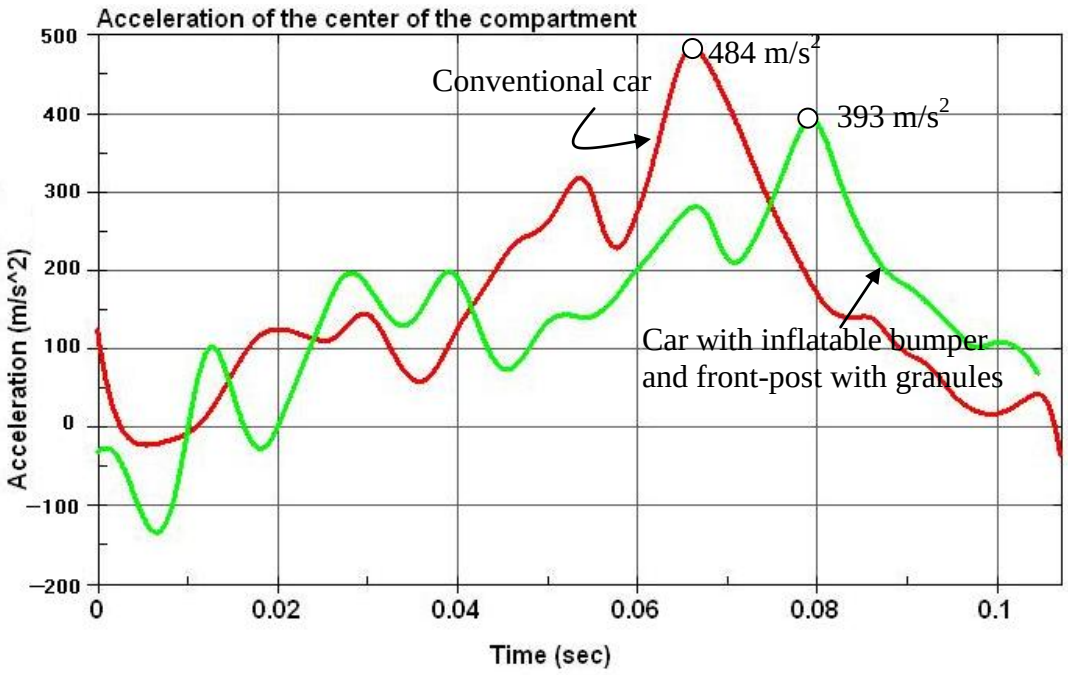

Figure 6.18 Accelerations of the center of the compartment (V_0=30 mph, TNT:100g)

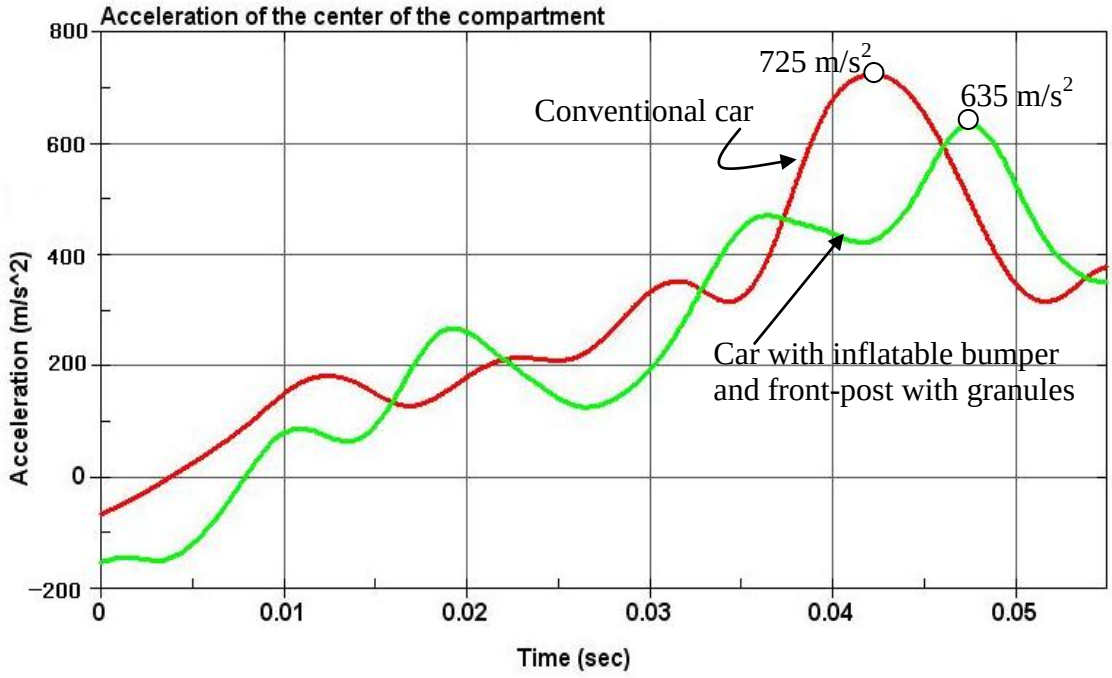

Figure 6.19 Accelerations of the center of the compartment (V_0=50mph, TNT:100g)

The results of the tests are shown in Fig. 6.18 and Fig. 6.19. These figures show the accelerations of the center of the compartment for each case (see Fig. 6.17 for the position of the accelerometer for these tests). As seen in these two figures, the acceleration of the center of the compartment of the car with the I-bumper is lower than the acceleration of the center of the conventional car. In this simulation, the I-bumper was charged with 100g of TNT. The acceleration of the center of the compartment was reduced by 18.8% (for the crash in which both cars were traveling at a speed of 30 mph) or 12.4% (for the crash in which both cars were traveling at a speed of 50 mph).

Fig. 6.20 shows the result of the car with the I-bumper when loaded with 500g of TNT. The maximum acceleration of the center of the compartment is 509 m/s^2. Compared to the result of the conventional car (Fig. 6.18), the acceleration of the car with the I-bumper is reduced by 29.8%.

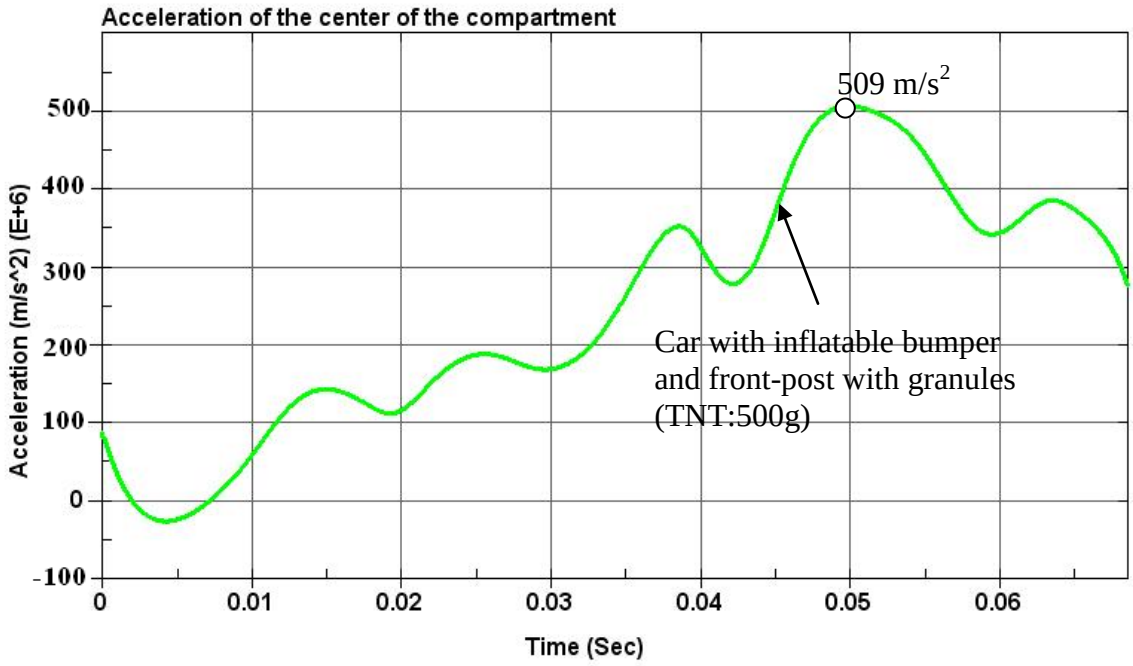

Figure 6.20 Accelerations of the center of the compartment (V_0=50mph, TNT:500g)

The maximum of allowable acceleration of the car during a crash in the industry is usually 20g's (where g means the acceleration of gravity: 9.81 m/s^2) and the result of Fig. 6.20 is about 50g's. More reduction of the maximum acceleration is needed for it to be within the acceptable limit of 20g's. Theoretically, changing design variables like using a

larger amount of TNT or a bigger bumper mass should reduce the acceleration of the compartment to a value closer to the 20g's threshold. It can be seen that the I-bumper system can reduce the acceleration of the compartment of the car and, correspondingly, the possibility of fatality or injury, and this performance will depend on design variables such as TNT mass and bumper mass.

CHAPTER VII

CONCLUSIONS AND FUTURE WORK

7.1 Conclusions

One of the main aims in automotive crashworthy design of automotive vehicles is to realize the maximum use of the front crumple zone in a frontal collision. Unfortunately, the current typical car front crumple zone is fixed and with a limited short distance of the crash. An innovative active safety device, called the "I-Bumper," has been therefore investigated in this research.

Analytical formulations for an explosive airbag have been developed and major design variables have been identified. These have been used to determine the required amount of explosive material and to predict airbag behavior, as well to predict their impact on the I-bumper system design. Related design guidelines and procedures have been introduced. This new explosive airbag model has been implemented in MATLAB, and has been validated with a high fidelity model using an LS-DYNA simulation.

The spring coefficients of an airbag have been expressed by volume and pressure changes. The Wang and Nefske airbag model has been used to find the value of pressure and volume changes. Airbag model spring coefficients have been computed using the iteration process and interaction with the FOA model. An analytic expression for C_β and $\Delta\dot{V}$ in the Wang and Nefske model have also been developed. The stress and radius of the airbag according to the pressure change has been obtained as well.

A modified version of Gurney's equation has been introduced for the velocity of moving mass with non-zero initial velocity after detonation based on the energy conservation equation and momentum conservation equation.

An analytic model for the absorbed energy of a lattice structure composed of plates during a crash has been developed. To quantify the absorbed energy, the deformation process is divided into pre-buckling and post-buckling stages. The buckling can be either plastic or elastic, according to when the buckling occurs. A method for predicting the total absorbed energy has been developed, and it accounts for the pre-elastic buckling, the pre-plastic buckling, and the post-buckling, based on strain energy theory or stiffness, and the plastic limit analysis. The analytic model developed for the absorbed energy of the lattice structure has been implemented in MATLAB. The validation has shown that the results of the developed analytic model are in good agreement with the results of the simulation based on LS-DYNA. It can be concluded that the analytic model developed in this research is useful for designing an expandable lattice structure for crashworthiness. Future research will combine a more detailed CEA (Crash Energy Absorption) structure with the strain rate effect. The main achievement of this work has been the development of a simplified analytic model of the expandable lattice structure for estimating the energy absorption during a crash.

An innovative post structure to be included in a vehicle body to enhance crashworthiness has been proposed. The design methodology for the tubes filled with granules has been developed and validated based on an effective thickness theory. The suitability of tubes filled with granules for crashworthiness has been demonstrated using simple analytic methods. In this research, the stress for granules can be assumed, obtained from Walton's simple equation, or determined by virtual tests. Future research will develop a general stress expression for the granules in a tube. This research may include multi-axial compression, general friction, non-identical spheres, composite materials, and non-spherical materials.

The analytic model has been then used to analyze alternative tubes filled with the selected granules in order to predict the effective (nonlinear) spring and damping coefficients of the crash energy absorption component. This has been further integrated with the other components in the inflatable morphing body structure to improve the crashworthiness of the design.

The above analysis models developed have been integrated into an active explosive bumper concept, called the "I-bumper," which is introduced as an example of innovative body designs for crashworthiness and improved safety for military and commercial vehicles. Major design variables and design guidelines and procedures have been introduced based on the integrated analytical design model, including the airbags with explosives described by a FOA (First-Order-Analysis) model. Design procedures and methods have been implemented using MATLAB. The approach developed for the I-bumper has been validated by the FEA model of LS-DYNA. The validation has shown that the results of the developed analytic model are in good agreement with the simulation results based on LS-DYNA.

7.2 Contributions

The major contributions of this research work are the introduction of the innovative I-bumper concepts for the crashworthy design of automotive vehicles as a solution to high speed crashes in which current automotive structure is inadequate.

We developed an advanced design methodology for novel active (inflatable, morphing, etc.) and passive (tubes with granules) body structures. We also developed innovative concepts for inflatable/morphing body structures that minimize crash damage and protect occupants, and finally we developed new standards and design guidelines for active and passive crash protection devices.

One of the major contributions of this research is the development of the analytic models for each of the I-bumper's components including explosive airbags, an expandable lattice structure, and tubes filled with granular materials. The development of these analytic models consists of innovations in several areas of design with the main contributions being in the following areas:

a. The development of the analytic model of external airbags using an explosive instead of a compressed gas. This development includes the modification of Gurney's equation, which is significant for its simplicity and versatility with

calculations involving a non-zero initial velocity. The spring coefficients and damping coefficient for the airbag has been developed.

b. The development of the analytic model of an expandable lattice structure for crashworthy design. This development includes the derivation of absorbed crash energy in this lattice structure and the equivalent spring coefficient of the lattice structure, which is foldable and expandable.

c. The development of the analytic model of a tube filled with granular materials for crashworthy design. This development includes the effective thickness theory for crash energy absorbed in the granule-filled tubes and the equivalent spring coefficient of the tubes.

d. The development of an integration method of I-bumper components, incorporating an explosive external airbag, a lattice structure, and a granule-filled tube. The availability and effectiveness of the I-bumper concept for the crashworthy design of automotive vehicles has been verified.

The innovative structure concepts that are developed can be used for designing better and safer vehicles and for improving the crashworthiness of military and civilian vehicles. The advanced body design methodologies developed can be used for innovative structural concepts for manned, unmanned, and alternative vehicles, including application to vehicle configuration, body shape, and morphing structures.

7.3 Future work

There are several directions for potential future work that arise from this research.

In this research, a simplified FOA model of an I-bumper was developed. It needs to be extended to include, for example, body flexibility, human and restrained systems in order to estimate the probability of human injury (i.e. HIC indices) more accurately. Mathematical models of the human body, together with an FOA model of the vehicle

structure can offer economical and useful methods for analyses of the crash response (see Fig. 7.1). Lobdell (1973) developed a one-dimensional model of the human thorax. This model simulates the thorax response in case of loading by an impacting mass. The first example of a multi-body model was presented by McHenry (1963). This model is two-dimensional and offers multiple-degrees of freedom, and the human body part of the model was characterized by rigid bodies representing the thorax/head, upper arms, upper legs, and lower legs. A more recent example of a multi-body model, specifically, a three-dimensional MADYMO model, was presented by the European Community and NHTSA (2000). Shugar (1977) developed an FEA model that was three-dimensional and that included a representation of the skull and brain.

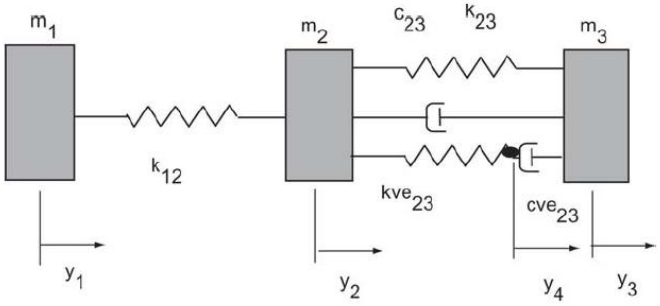

Lumped mass model (Lobdell, 1973)

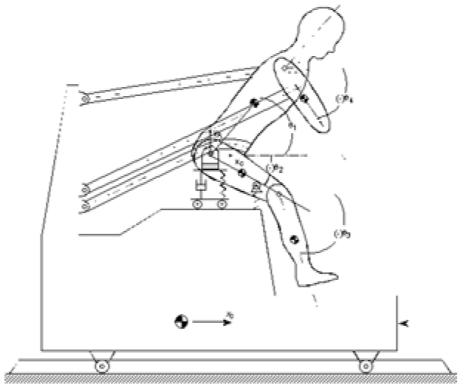

Multi-body model (McHenry, 1963)

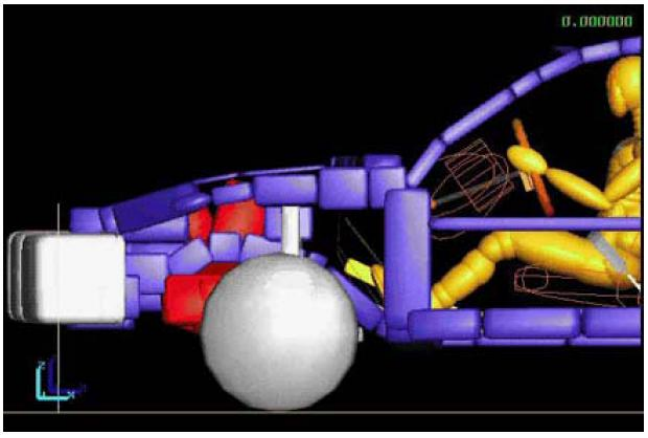

Multi-body model (European Community and NHTSA)

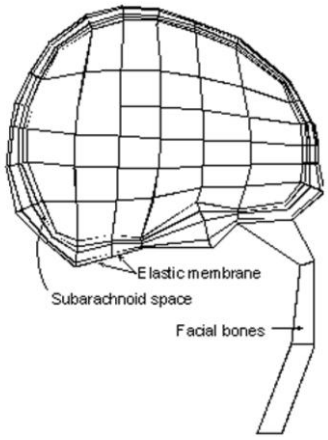

FEA model (Shugar, 1977)

Figure 7.1 Human body models

The extension of the I-bumper to other applications (for example, side impacts, rear impacts, roll-over, and collisions with pedestrians) can be performed. In the United States, side and rear collisions are the second and third most common type of vehicle crashes, after frontal impacts. Side impacts constitute approximately 30 percent of motor vehicle crash injuries and 26 percent of motor vehicle crash fatalities. Rear impacts constitute approximately five percent of motor vehicle crash fatalities. Usually, the side and rear structures of automobiles are less crashworthy than the front structure, so the application of the I-bumper to side and rear impacts will be challenging but likely to increase the energy absorbed in the side and rear structure of the automobile. Road accident statistics indicate that a considerable proportion of casualties involve cyclists and pedestrians who are injured as a result of contact with a moving vehicle. Extension of the I-bumper to protect pedestrians offers a promising possibility of saving more lives.

It is also necessary to consider the triggering conditions and mechanism of the I-bumper. The I-bumper should be designed to deploy immediately prior to a car crash, so the car needs to be equipped with a sophisticated sensor and radar system to detect an impending collision. Airbag sensors usually contain a MEMS accelerometer, which is a microscopic mechanical element that moves in response to sudden deceleration. This motion causes a change in capacitance, which then sends a signal to fire the airbag. For the I-bumper, the algorithms and the mechanism that trigger the explosive airbag must be much more complex. To protect pedestrians, inappropriate deployment of the I-bumper must be prevented, because a sudden deployment of the I-bumper during driving or parking could injure pedestrians. Many crash avoidance systems and other safety systems rely on high-tech sensors like radar or laser sensors to tell when a car ahead slows down, so either the driver can be alerted to slow down or the car can reduce its own speed. These sensors are good candidates for indicating when the I-bumper should be deployed. Sensing methodology will be a key field to be investigated in the future for the I-bumper system.

The I-bumper system has potential applications beyond the civilian automotive industry; it may also contribute to military needs. All-around protection with passive

armor for military vehicles is becoming too heavy for even the most powerful tanks, and even the best passive protection cannot stop all threats from all directions. In military vehicles, the Active Protection Systems commonly consist of an array of soft-kill and hard-kill techniques. Soft-kill methods, similar to Electronic Counter-Measures (ECM) in aircraft, confuse an incoming missile, by using decoys, smoke, and electro-optical signals, as well as infrared or laser jamming. Other concepts, which include "hard-kill" methods, are designed to intercept and destroy the incoming projectile or missile before it hits its target. The I-bumper could be implemented as an innovative hard-kill means for military vehicles. The Inflatable Air Bag System (IABS, see Fig. 7.2) is a good example of use of external active device for blast-worthiness. IABS combines an inexpensive radar sensor and airbag systems which are inflated before the Rocket Propelled Grenade (RPG – an anti-tank infantry weapon) hits the protected vehicle. The airbag disrupts the shaped charge fuse, as the projectile collapses upon itself, jamming the time-out fuse, thus defusing the shaped charge before it hits the vehicle's skin. During tests, the system was installed on up-armored Humvee doors, and demonstrated effective protection of the crew compartment.

IABS was also effective in protecting the transparent armor (windows). The considerations and criteria of blast-worthiness are different from those of crashworthiness. More details about blast-worthiness will be described in appendix II.

Source: www.defense-update.com

Figure 7.2 IABS

APPENDICES

APPENDIX I

COEFFICIENT OF RESTITUTION (COR) AND COEFFICIENT OF CRASH (COC)

In this study, two schemes are used for a collision between an inflated bumper and an oncoming car's body (see Fig A1.1). These are the spring-damping coefficients approach, and the COC or COR approach. In this appendix, a clear explanation of the COR and COC is given. Usually, the COC can be called "minus COR". The new terminology COC (minus COR) is introduced and discussed in this appendix.

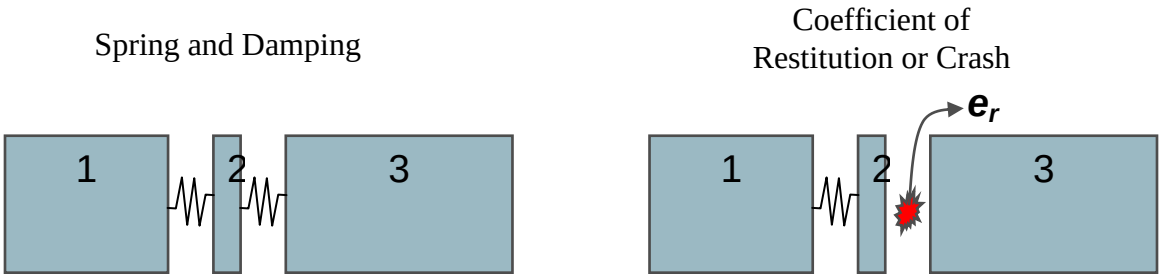

$$v_2' = \frac{m_2 - e_r m_3}{m_2 + m_3} v_2 + \frac{(1+e_r)m_3}{m_2+m_3} v_3$$

$$v_3' = \frac{(1+e_r)m_2}{m_2 + m_3} v_2 + \frac{m_3 - e_r m_2}{m_2+m_3} v_3$$

Figure A1.1 Two schemes for collision model between inflated bumper and oncoming car's body

A1.1 Coefficient of Restitution (COR) [Meriam and Kraige, 1993; Greenwood, 1988]

The coefficient of restitution (COR) of two objects is a fractional value representing the ratio of relative velocities before and after an impact. The coefficient itself is given by:

$$e_r = \frac{v_2' - v_1'}{v_1 - v_2} \tag{A1-1}$$

for two colliding objects, where

v_1 : the scalar initial velocity of the first object before impact
v_1' : the scalar final velocity of the first object after impact
v_2 : the scalar initial velocity of the second object before impact
v_2' : the scalar final velocity of the second object after impact

The constant e_r is a number between 0 and 1. A coefficient near 1 indicates a nearly perfectly elastic collision (the relative velocities before and after impact are equal and the capacity of the two particles to recover equals their tendency to deform), while a coefficient near 0 indicates a perfectly inelastic collision (objects remain in contact after the collision).

The constant e_r can be expressed by the ratio of the magnitude of restoration impulse to the magnitude of the deformation impulse. If F_r and F_d represent the magnitudes of the contact forces during the restoration and deformation periods, respectively, as shown in Fig. A1.2, for mass 1 the definition of e_r together with the impulse momentum equation gives us

$$e_r = \frac{\int_{t_0}^{t} F_r dt}{\int_{0}^{t_0} F_d dt} = \frac{m_1(-v_1' - (-v_0))}{m_1(-v_0 - (-v_1))} = \frac{v_0 - v_1'}{v_1 - v_0} \tag{A1-2}$$

Similarly, for mass 2 it is

$$e_r = \frac{\int_{t_0}^{t} F_r dt}{\int_{0}^{t_0} F_d dt} = \frac{m_2(-v_2' - (-v_0))}{m_2(-v_0 - (-v_2))} = \frac{v_2' - v_0}{v_0 - v_2} \tag{A1-3}$$

Eliminating v_0 between the two expressions for e_r gives us

$$e_r = \frac{v_2' - v_1'}{v_1 - v_2} \tag{A1-4}$$

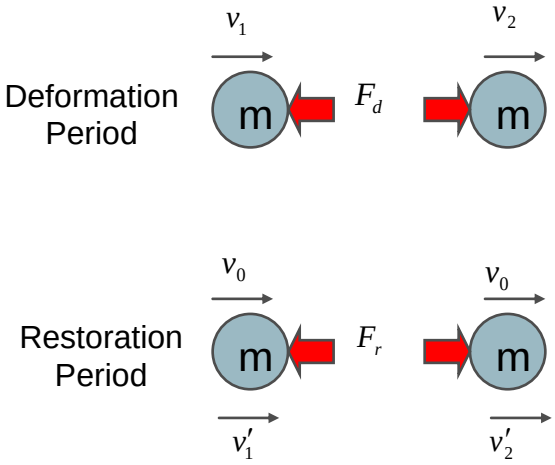

Figure A1.2 Collision between two masses

Usually, the deformation impulse is bigger than the restoration impulse (see Fig. A1.3), so e_r is less than 1. The deformation force and restoration force are going in the same direction. The variable e_r is equal to 1 when these two forces are equal. A COR greater than one is theoretically possible, representing a collision that generates kinetic energy, such as land mines being thrown together and exploding. A COR less than zero is also theoretically possible, representing a collision that pulls two objects closer together instead of bouncing them apart. For the case of a COR less than zero, more explanation is given in the next chapter.

An equation to address COR was obtained. One more equation is still needed in order to solve the final velocities after impact. This is a momentum equation given by:

$$m_1 v_1 + m_2 v_2 = m_1 v_1' + m_2 v_2' \qquad \text{(A1-5)}$$

For a collision occurring between mass 1 and mass 2 in an isolated system, the total momentum of the two masses before the collision is equal to the total momentum of the two masses after the collision. That is, the momentum lost by mass 1 is equal to the momentum gained by mass 2. The above statement tells us that the total momentum of a collection of masses (a *system*) is "conserved" - that is, the total amount of momentum is a constant or unchanging value.

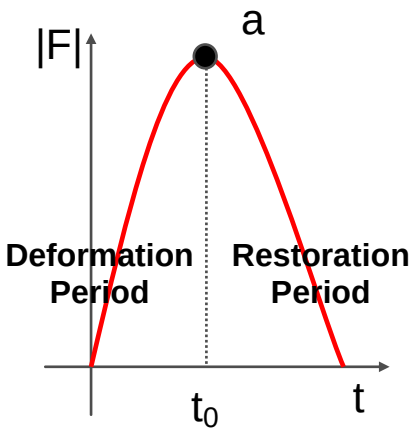

Figure A1.3 Deformation period and restoration period

To understand the basis of momentum conservation, a short logical proof may be helpful. Consider a collision between two masses, mass 1 and mass 2. In such a collision, the forces acting between the two masses are equal in magnitude and opposite in direction (Newton's third law). This statement can be expressed in equation form as follows.

$$F_{d1}(\textit{deformation force for mass}1) = -F_{d2}(\textit{deformation force for mass}2)$$
$$F_{r1}(\textit{retoration force for mass}1) = -F_{r2}(\textit{retoration force for mass}2)$$

The forces are equal in magnitude and opposite in direction

Finally, the equation for final velocity after impact is obtained from the momentum equation and the COR equation.

$$v_2' = \frac{m_2 - e_r m_3}{m_2 + m_3} v_2 + \frac{(1+e_r)m_3}{m_2+m_3} v_3$$
$$v_3' = \frac{(1+e_r)m_2}{m_2 + m_3} v_2 + \frac{m_3 - e_r m_2}{m_2+m_3} v_3 \qquad \text{(A1-6)}$$

If e_r is equal to 1, the energy equation will be expressed as

$$\frac{1}{2} m_1 v_1^2 + \frac{1}{2} m_2 v_2^2 = \frac{1}{2} m_1 v_1'^2 + \frac{1}{2} m_2 v_2'^2 \qquad \text{(A1-7)}$$

Fig. A1.4 shows the result of an experimental test for the coefficient of restitution of a vehicle with various closing velocities.

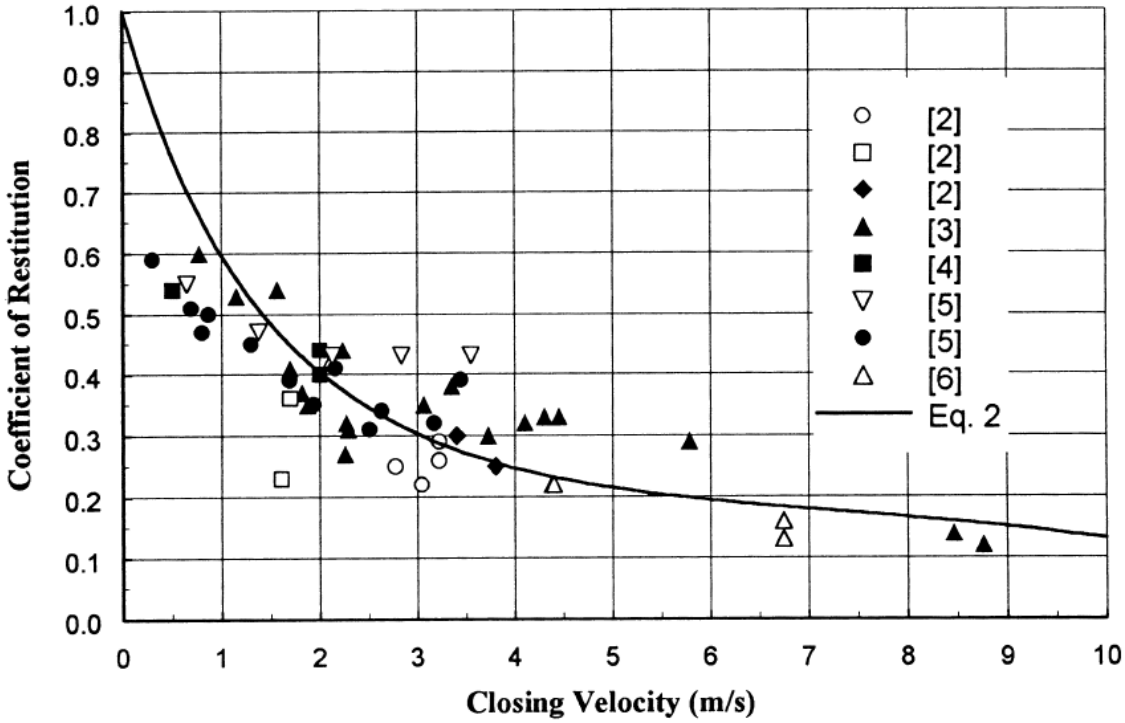

Figure A1.4 Experimental tests for COR with various closing velocities (Antonetti, 1998)

A1.2 Coefficient of Crash (COC) – Minus COR

In the previous chapter, the COR was discussed. In this chapter, the new terminology for automotive collision, defined as the Coefficient of Crash (COC), is introduced. In automotive collisions, COC should be considered because the bodies of two cars remain each other close together instead of bouncing apart during impact. There are many components in the front of an automobile that play an important role during a collision, including the bumper, rail, and hood. After a collision, they will have moved closer to the second car, rather than bouncing further away. So, the COC would be a good measure for automotive collision. The constant e_c (COC) is a number between -1 and 0. A coefficient near -1 signifies that there was no collision, while a coefficient near 0 indicates a perfectly inelastic collision (the two objects remain in contact after the collision).

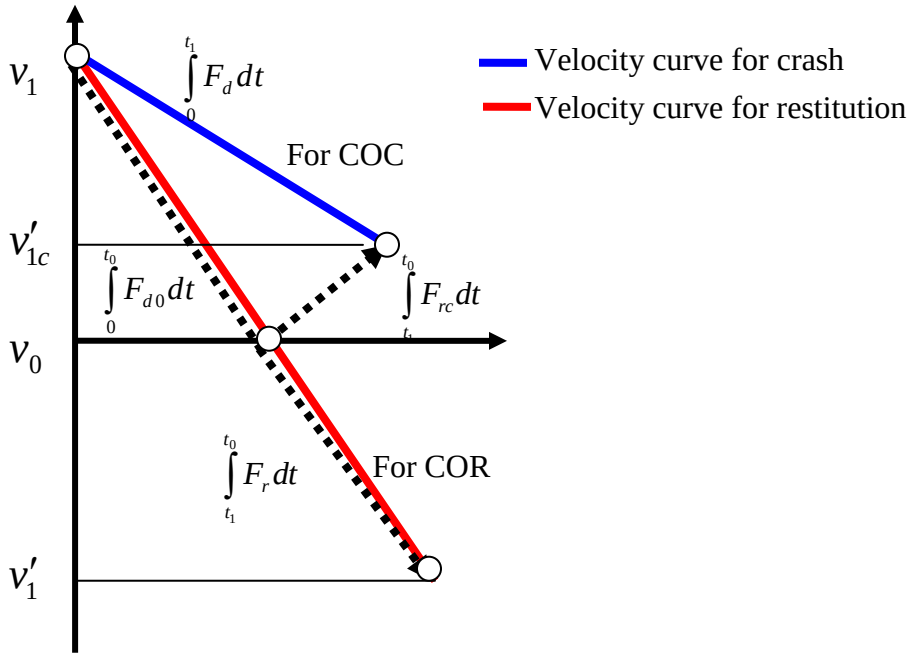

Figure A1.5 Velocity curve of mass for COC and COR

Figs. A1.5 and A1.6 show the velocity curve for COC and COR, and the momentum equation for the velocity change. For a crash, the momentum equation can be expressed by

$$\int_0^{t_1} F_d dt = \int_0^{t_0} F_{d0} dt - \int_{t_1}^{t_0} F_{rc} dt \qquad \text{(A1-8)}$$

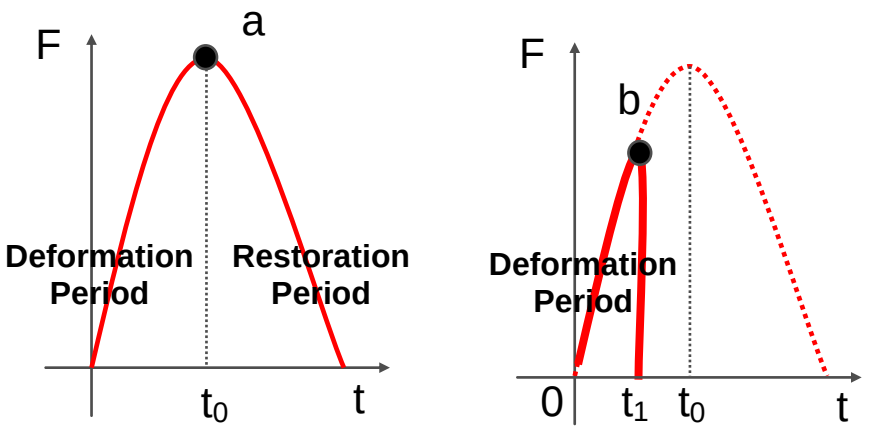

Figure A1.6 Momentum curve for COC and COR

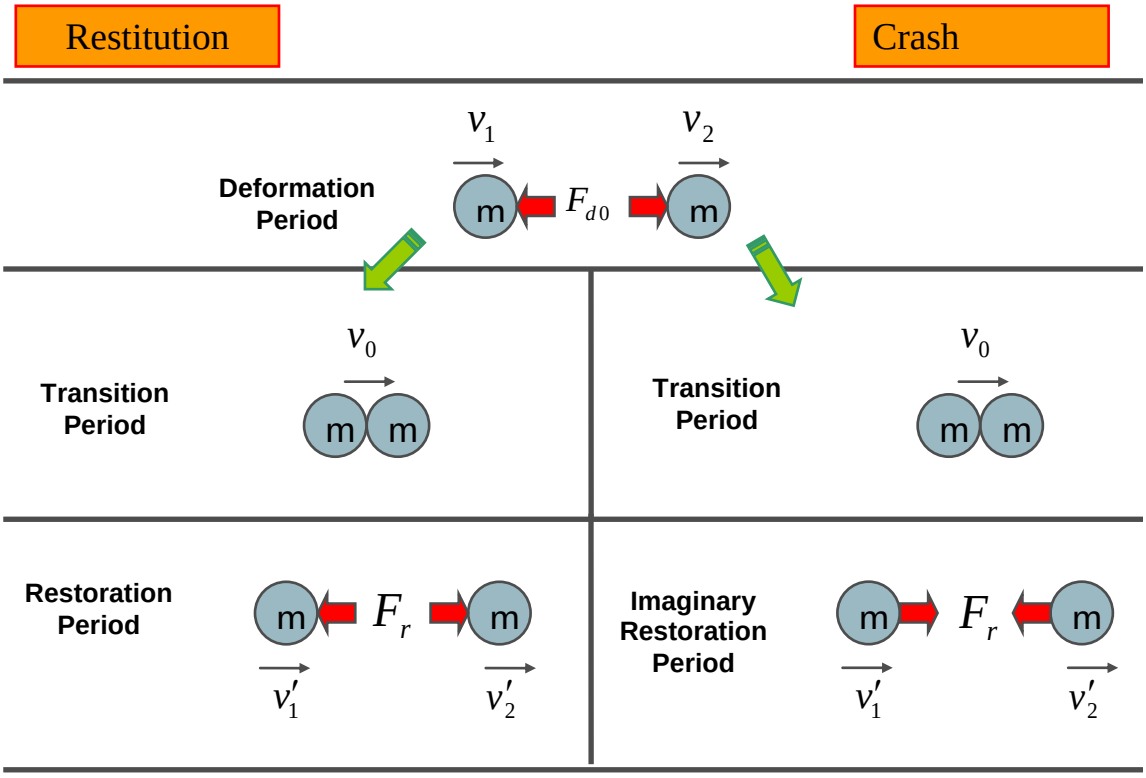

Figure A1.7 Deformation and restoration period for COC and COR

The e_c can be defined together with the impulse momentum equation for mass 1 like

$$e_c = \frac{\int_{t_1}^{t_0} -F_{rc}\,dt}{\int_{0}^{t_0} F_{d0}\,dt} = \frac{m_1(-v_1' - (-v_0))}{m_1(-v_0 - (-v_1))} = \frac{v_0 - v_1'}{v_1 - v_0} \tag{A1-9}$$

Similarly, for mass 2 it is

$$e_c = \frac{\int_{t_1}^{t_0} -F_{rc}\,dt}{\int_{0}^{t_0} F_{d0}\,dt} = \frac{m_2(-v_2' - (-v_0))}{m_2(-v_0 - (-v_2))} = \frac{v_2' - v_0}{v_0 - v_2} \tag{A1-10}$$

Eliminating v_0 between the two expressions for e_c gives us

$$e_c = \frac{v_2' - v_1'}{v_1 - v_2} \tag{A1-11}$$

An equation of COC, identical to COR, can be obtained as.

$$e_c = \frac{v_2' - v_1'}{v_1 - v_2} \tag{A1-12}$$

One more equation is still needed to solve the final velocities after impact. This is a momentum equation given by:

$$m_1 v_1 + m_2 v_2 = m_1 v_1' + m_2 v_2' \tag{A1-13}$$

Using the equation of COC and the equation of momentum conservation gives

$$v_2' = \frac{m_2 - e_c m_3}{m_2 + m_3} v_2 + \frac{(1+e_c)m_3}{m_2+m_3} v_3$$
$$v_3' = \frac{(1+e_c)m_2}{m_2 + m_3} v_2 + \frac{m_3 - e_c m_2}{m_2+m_3} v_3 \qquad \text{(A1-14)}$$

A1.3 Application of Coefficient of Crash (COC) in tennis balls (Cross, 2002) and rigid bodies with stacking (Geundelman et al., 2003)

The collision of a tennis ball with a firm surface can be described in terms of the vertical and horizontal values of the COR by Cross (2002). The COR for the vertical collision can be expressed by

$$e_y = -\frac{v_{y2}}{v_{y1}} \qquad \text{(A1-15)}$$

where subscripts 1 and 2 denote conditions before and after the collision, respectively, and where e_y is between 0 and 1. Similarly, e_x can be defined by the relation.

$$e_x = -\frac{v_{x2} - R\omega_2}{v_{x1} - R\omega_1} \qquad \text{(A1-16)}$$

where $v_x - R\omega$ is the net horizontal speed of a point at the bottom of the ball. Unlike e_y, e_x can be positive or negative. If a ball is incident at a sufficiently small angle and without spin, then it can slide through the impact without rolling and will bounce with $R\omega_2 < v_{x2}$, in which case $e_x < 0$. A value $e_x = -1$ corresponds to a bounce on a frictionless surface, where $v_{x2} = v_{x1}$ and $\omega_2 = \omega_1$ (See Fig. A1.8).

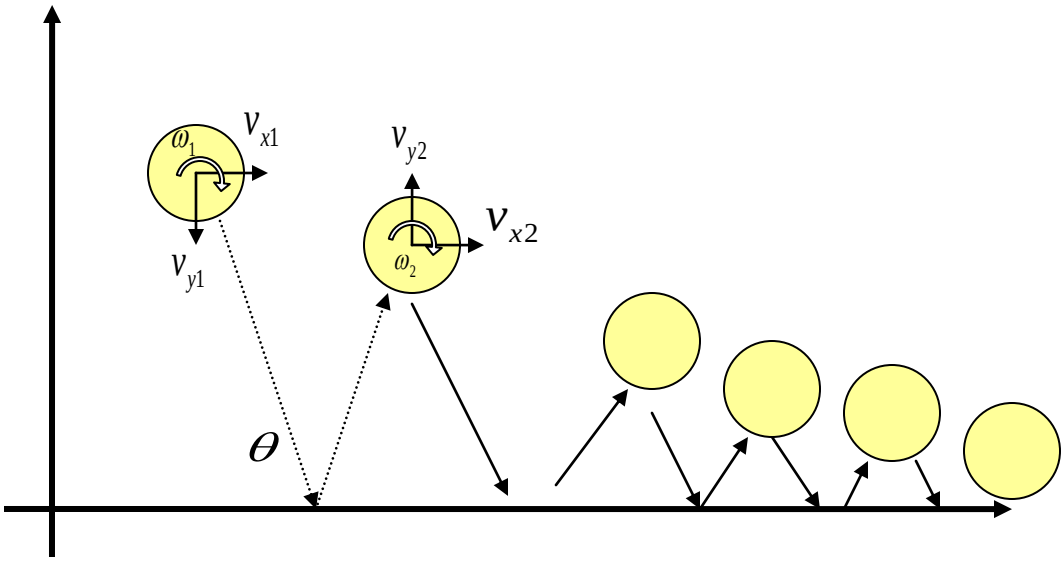

Figure A1.8 Typical bounce of tennis ball on a hard surface

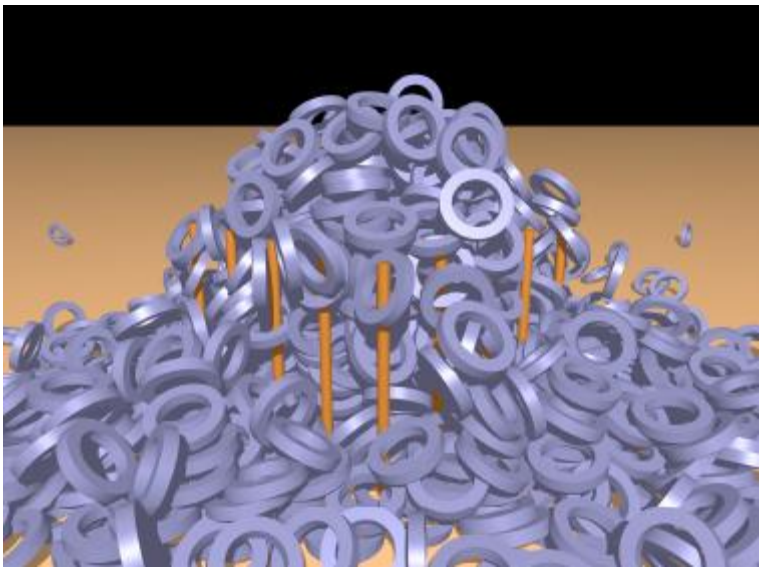

Figure A1.9 Stacking of 1000 non-convex rings (Guendelman et al., 2003)

Guendelman et al. (2003) simulated the non-convex rigid bodies focusing on interactions using the following procedure. Rather than applying a fully inelastic impulse of $e_c = 0$ at each point of contact, they gradually stopped the object from approaching.

For example, on the first iteration of contact processing, they applied impulses using $e_c = -0.9$, on the next iteration they used $e_c = -0.8$, and so on, until they finally used $e_c = 0$ on the last iteration. A negative coefficient of restitution simply indicates that rather than stopping or reversing an approaching object, they only slow it down.

A1.4 Application of Coefficient of Restitution (COR) and Coefficient of Crash (COC) in automotive collision

Infinite serial slow-downs are equal to perfectly plastic collisions (e_c=0). Automotive collisions cannot be expressed by using only multiple serial slow-down or COC. It is more useful to express the automotive collision with a combination of COR and COC.

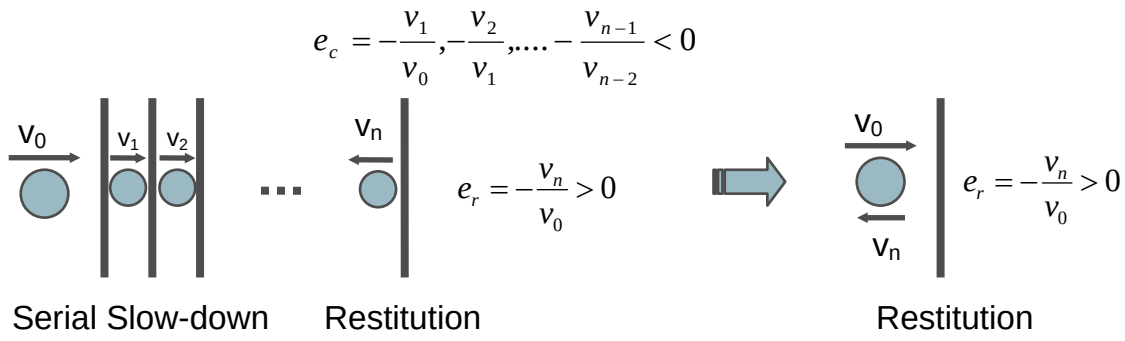

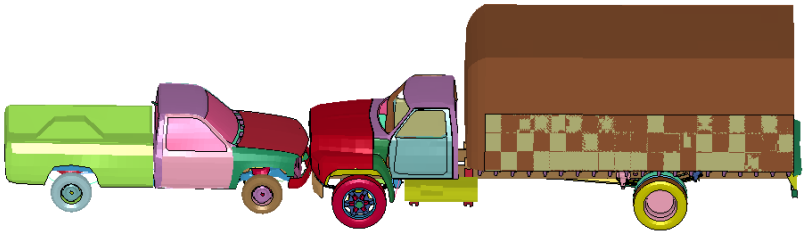

Figure A1.10 Relationship between COC and COR

COC can be used for the bumper and crush zone rail, the upper structure, and the hood. After that, COR can be used for a final collision in which the velocity is reversed. The combination of COR and COC can be represented by only one COR, where the combination of COR and COC shows us a trace of velocity during collision, and only one

COR shows a terminal velocity after collision. Fig. A1.10 shows a case in which the mass penetrates through several stationary walls. COC is appropriate for each penetration or slow-down. After penetrating many walls, it will lose so much momentum that it can no longer penetrate the wall, at which point COR is appropriate for the collision. The same concept can be used for automotive collision. The real rigid wall frontal collision was repeated in Fig. A1.12 and Fig A1.13.

COR or COC	Velocity of mass before collision	Velocity of mass after collision	
-1	V_0	V_0	No crash
-0.5	V_0	$1/2*V_0$	Crash
0	V_0	0	Perfectly plastic
0.5	V_0	$-1/2*V_0$	
1	V_0	$-V_0$	Perfectly elastic

Figure A1.11 Example of COC and COR

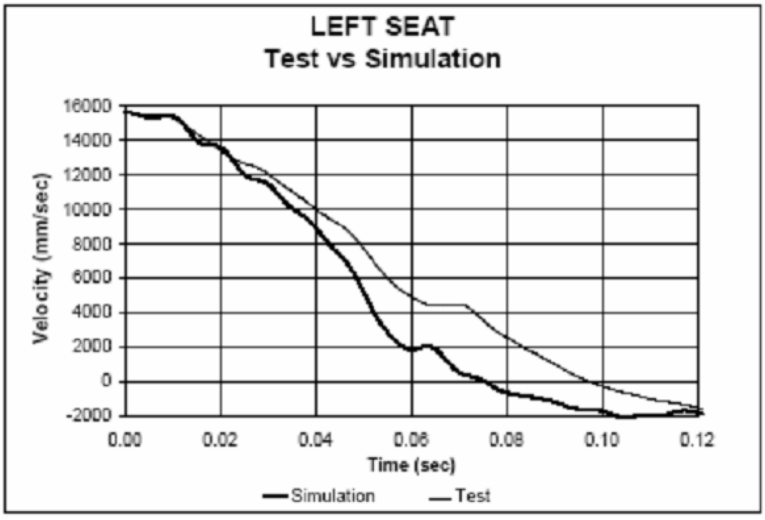

Figure A1.12 Test velocity curve for a car (Zaouk, et al., 1996)

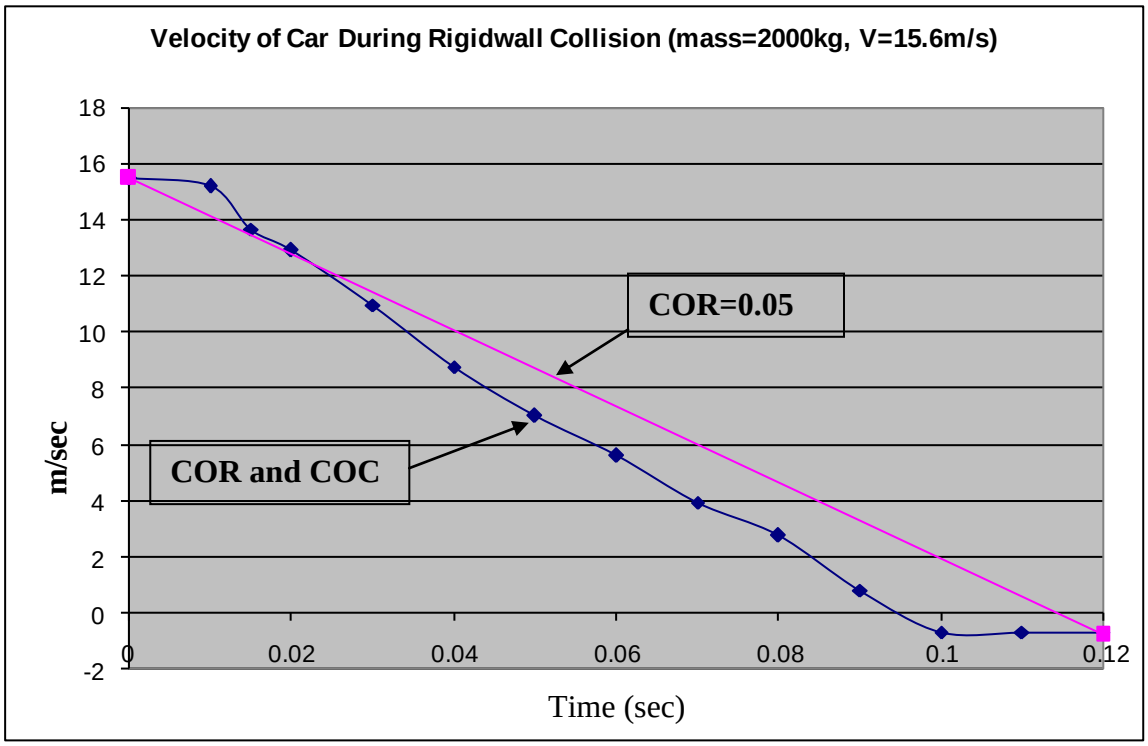

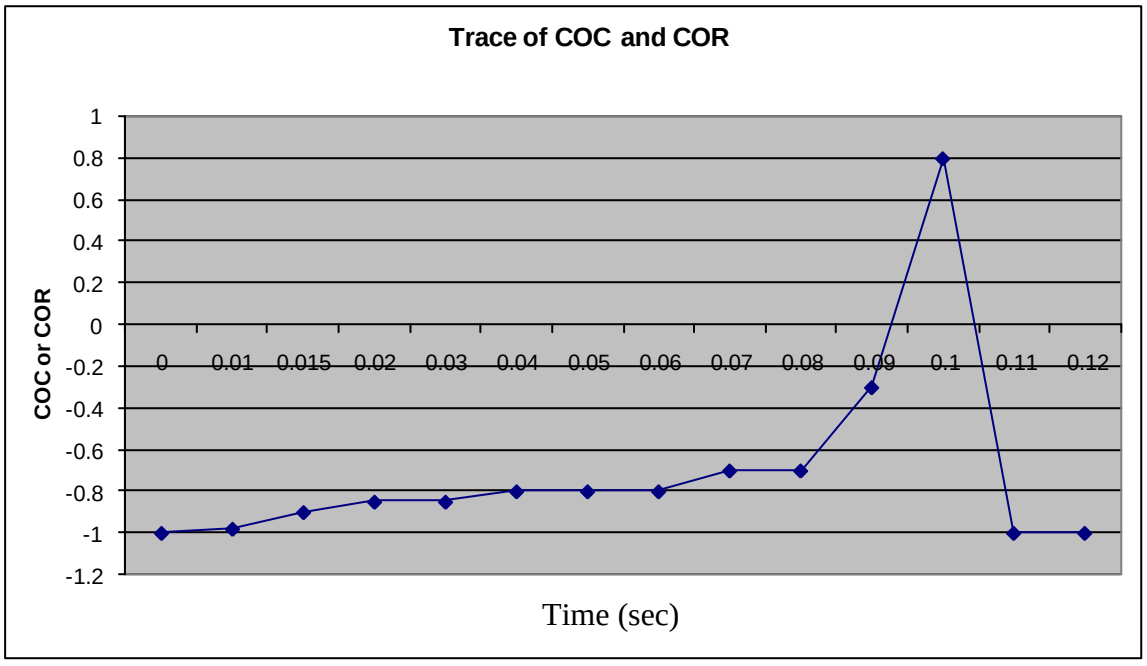

Figure A1.13 Repeat of Fig. A1.12 with COC and COR

Fig. A1.11 shows some examples of COR and COC for a case in which the mass collides with a stationary wall. Values of -1, 0, and 1 indicate no collision, a perfectly plastic collision, and perfectly elastic collision, respectively.

The rigid wall front collision test of Fig. A1.12 was repeated with COC and COR in Fig. A1.13. As can be seen from the comparison between Fig. A1.12 (experimental and simulation results by Zaouk, et al., 1996) and Fig. A1.13, reconfiguration from the COC and COR is more realistic and useful than the case with only COR. COC and COR can be determined by experimental testing.

APPENDIX II

CONSIDERATIONS OF BLAST-WORTHINESS OF VEHICLES

In this chapter, basic considerations and criteria for blast-worthiness design are addressed. High explosives produce shock waves and create underwater pressure pulses or an air blast, depending on where they are detonated, meaning that they can burst, shatter, lift, drive, or penetrate structures or materials, when detonated.

An explosion is a very rapid release of stored energy. Part of the energy is released as thermal radiation, and part is released into the air (air-blast) and soil (ground-shock) as radically expanding shock waves. Air-blast is the principle damage mechanism.

When the shock waves encounter vehicle surfaces, they are reflected, amplifying the overpressure so that it is higher than the initial peak pressure. A secondary effect of the air-blast is dynamic pressure or drag loading, which is a very high velocity movement of air. It accelerates the debris generated by the air-blast, creating secondary projectiles. In this chapter, the blast-worthiness focuses mainly on the air-blast or shock wave.

The following principles can be incorporated into the design of vehicles to render protection against the blast effect of mines:

1. Absorption of energy
2. Deflection and mitigation of blast effect away from the hull
3. Prevention of entrapment of the blast wave
4. Distance from detonation point
5. Protection against the fragmentation (penetration) effect of mines

A2.1 Absorption of energy

In the case of crash, some of the crash energy is absorbed, while the remaining energy is transferred to other components. It can be described as

$$Total\ Energy = absorbed\ energy + transferred\ energy$$

In the case of a blast, some of the blast energy is absorbed and the remaining energy is transferred to other components or deflected. The total energy can be expressed as

$$Total\ Energy = absorbed\ energy + transferred\ energy + deflected\ energy$$

where the quantity of energy transferred or absorbed energy depends on the inside structure (of an inflatable body). The amount of energy deflected depends on the shape of the structure (inflatable body) and the stand-off distance.

A2.2 Deflection of blast away from the hull

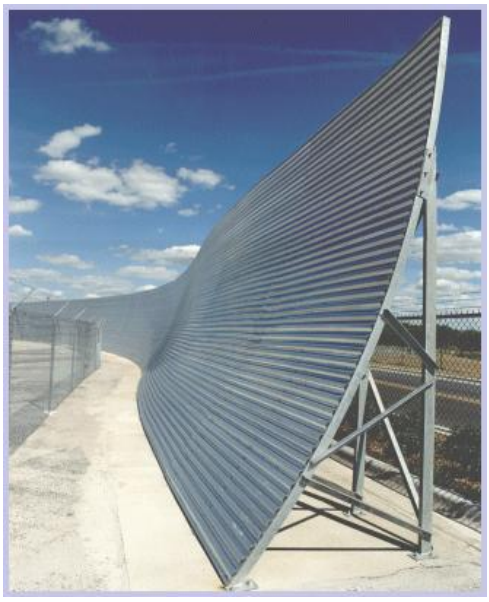

Figure A2.1 Blast deflection system (RKT Constructors Inc.)

The effect of a blast against the vehicle hull can be alleviated considerably by using steel plates placed at an angle to the direction of the blast wave. Face-on pressures are developed when the plate is at a 90 degree angle to the blast direction. Side-on pressures are developed if the plate angle is at a 0 degree angle to the blast direction (see Fig. A2.1 and Fig. A2.2). Therefore, it can be said that the effect of a blast will be reduced to a value between the face-on pressure and the side-on pressure, if the plate is angled between 0 degree and 90 degree. This approach has lead to the introduction of V-hulls.

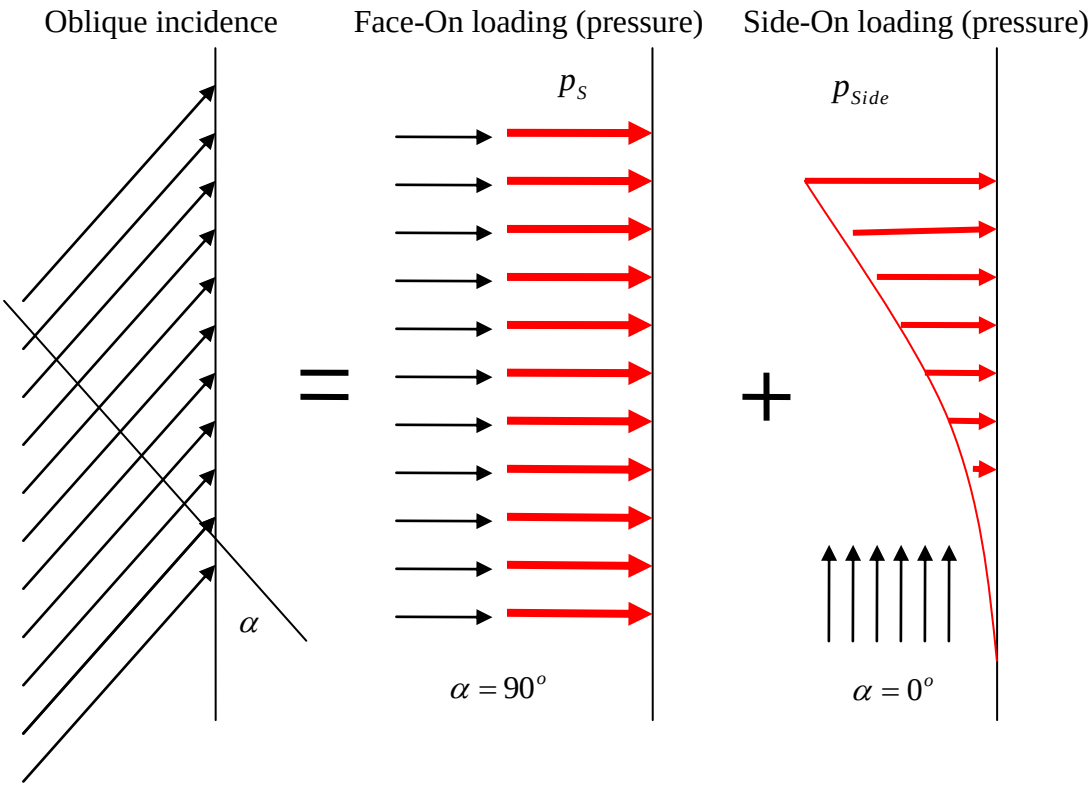

Figure A2.2 Face-on loading and side-on loading of explosive wave

A2.3 Prevention of entrapment of the blast wave

It is also important to prevent the "entrapment" of the blast wave. The U.S. Army found that unexpectedly, flat foam and honeycomb-faced panels transmitted more energy

to the pendulum (that is, target) than a flat rigid panel without energy absorbing material on the blast face. This phenomenon may be due to the non-uniform deformation (dishing) of the front face, which may increase the overall pressure loaded on the panel from the blast. Therefore, the effect of dishing during the deformation of a structure due to an explosion should be avoided.

A2.4 Distance from the detonation point

The effect of a blast is mitigated significantly with the distance from the detonation point. Thus, by increasing the distance from the ground and by spacing the wheels further apart, the maximum distance can be realized from the detonation point. There is a limitation in addressing this factor in the automotive structure for the blast-worthiness design.

A2.5 Protection against the fragmentation (penetration) effect of mines

Protection against the fragmentation (penetration) effect of mines is accomplished by using reinforced structure or armored glass and steel plating of sufficient thickness. Normal ballistic protection levels such as those required in military armored vehicles are used effectively for protection against fragmentation.

The distance out to which debris from an explosion may be propelled is given as

$$r = 45W^{1/3} \tag{A2-1}$$

where yield W is in kilograms of TNT and r is a radial horizontal distance in meters
The penetration depth would be given by the equation

$$p = \frac{W_P}{A} K \log_{10}\left[1 + \frac{V^2}{215000}\right] \tag{A2-2}$$

where

p = depth of vertical penetration in feet

W_P = total projectile weight in lb

A = cross-sectional area of the projectile in in^2

K = constant depending on target material

V = striking velocity in feet/sec

A roll prevention, heat transfer, ductile material, and wave arrival time should also be considered.

A2.6 Blast-worthiness design strategies and criteria

Fig. A2.3 shows the general considerations and corresponding criteria for the blast-worthiness design of vehicles based on the factors discussed above. Fig. A2.4 shows some considerations and corresponding design parts and corresponding criteria for the blast-worthiness design of vehicle in terms of vehicle structure.

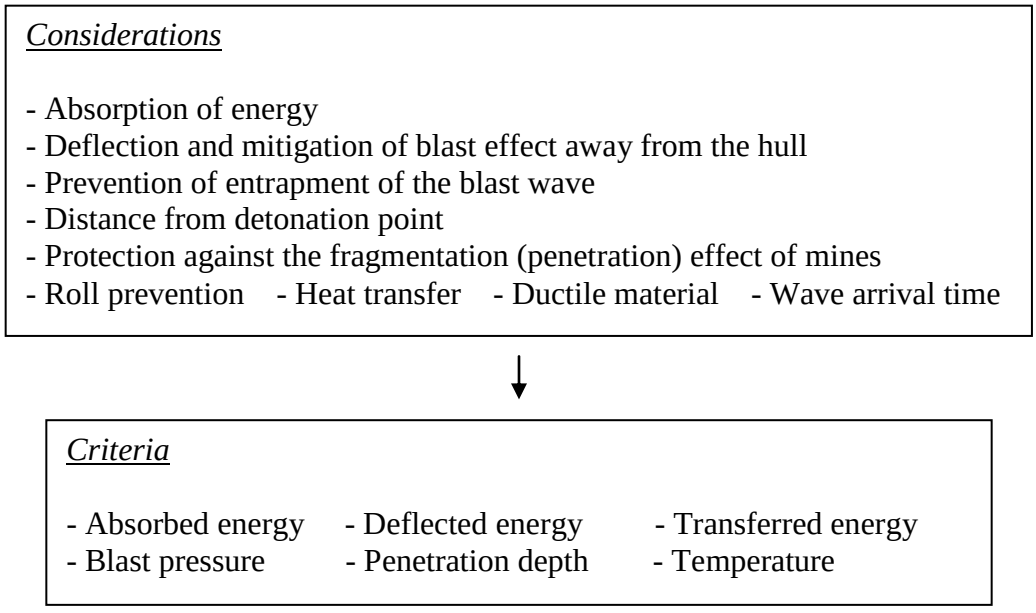

Figure A2.3 General considerations and criteria for blast-worthiness design

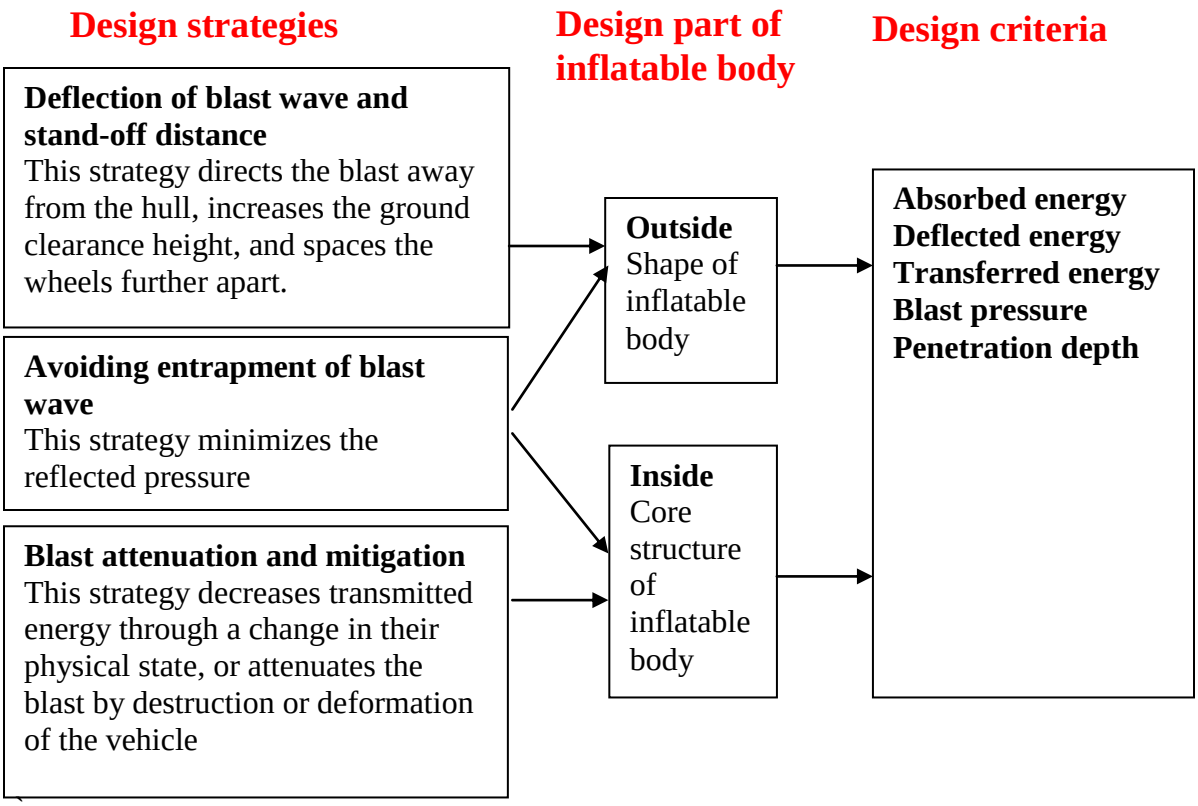

Figure A2.4 Design strategies and criteria

BIBLIOGRAPHY

BIBLIOGRAPHY

Abramowicz, W., Wierzbicki T., "Axial Crushing of Foam-Filled Columns," International Journal of Mechanical Science, Vol. 30, No. 3-4, pp. 263-271, 1988

Aktay, L., Johnson, A.F., Holzapfel, M., "Prediction of Impact Damage on Sandwich Composite Panels," Computational Materials Science, Vol. 32, No. 3-4, pp. 252-260, 2005

Alghamdi, A., "Collapsible Impact Energy Absorbers: an Overview," Thin-Walled Structures, Vol. 39, No. 2, pp. 189-213, 2001

Andersson, R., Schedin, E., et al. "The Applicability of Stainless Steel for Crash Absorbing Components," SAE Technical Paper Number 2002-01-2020

Andrews, K.R., England, G.L., Ghani, E., "Classification of The Axial Collapse of Cylindrical Tubes under Quasi-static Loading," International Journal of Mechanical Science, Vol. 25, No. 9-10, pp. 687-696, 1983

Antonetti, V.W., "Estimating The Coefficient of Restitution of Vehicle-to-Vehicle Bumper Impacts," SAE Technical Paper Number 980552

Avalle, M., Chiandussi, G., Belingardi, G., "Design Optimization by Response Surface Methodology: Application to Crashworthiness Design of Vehicle Structures," Structural and Multidisciplinary Optimization, Vol. 24, No. 4, pp. 325-332, 2002

Avriel, M., "Nonlinear Programming: Methods and Analysis," Prentice-Hall, Inc., Englewood Cliffs, New Jersey, 1976

Beer, F.P., Dewolf, J.T, Johnston, E.R., "Mechanics of Materials," McGraw-Hill, pp. 464, 2002

Bloom, F., Coffin, D., "Handbook of Thin Plate Buckling and Postbuckling," Chapman & Hall/CRC, 2001

Butler, M., Wycech, J., et al., "Using Terocore Brand Structural Foam to Improve Bumper Beam Design," SAE Technical Paper Number 2002-01-2018

Carley, M.E., Mallela, V., Sharma A.K., "Advancements in Expanded Polypropylene Foam Energy Management for Bumper Systems," SAE Technical Paper Number 2002-01-2018

Chen, X., et al., "Aluminum Subframe Design for Crash Energy Management," SAE Technical Paper Number 2004-01-1775

Cheon, S.S., Choi, J.H., Lee, D.G., "Development of The Composite Bumper Beam for Passenger Cars," Composite Structures, Vol. 32, pp. 491-499, 1995

Clark, C.C., Young, W.A., "Car Crash Theory and Tests of Airbag Bumper System," SAE Technical Paper Number 951056, 1995

Clark, C.C., Young, W.A., "Airbag Bumper Just Inflated Before The Crash," SAE Technical Paper Number 941051, 1994

Crandall, S.H., Dahl, N.C., Lardner, T.J., "An Introduction to The Mechanics of Solids," McGraw-Hill, pp. 452-461, 1978

Cross, R., "Measurements of the Horizontal Coefficient of Restitution for a Superball and a Tennis ball," Am. J. Phys. Vol. 70, No. 5, pp. 482-489, May 2002

Deb, A., Mahendrakumar, M.S., Chavan, C., et al., "Design of an Aluminium-Based Vehicle Platform for Front Impact Safety," International Journal of Impact Engineering, Vol. 30, No. 8-9, pp.1055-1079, 2004

Delaney, A., Newstead, S., "The Effectiveness of Anti-Lock Brake Systems: a Statistical Analysis of Australian Data," Proceedings 2004 Road Safety Research, Policing and Education Conference, 14-16 November, Perth, Western Australia, Vol. 1, 2004

Escrig, F., Valcarcel, J.P., Sanchez, J., "Roofing Geometry of Deployable X-frames," International Journal of Space Structures, Vol. 13, No. 1, pp. 1-12, 1998

European Community and NHTSA, Final report for publication, "EU Compatibility Project," European Commission, Brussel, 2000

Evans, D., Morgan, T., "Engineering Thermoplastic Energy Absorbers for Bumpers," SAE Technical Paper Number 1999-01-1011

Fletcher, R., "Practical Methods of Optimization, Vol. I, Unconstrained Optimization," John Wiley and Sons, Inc., New York, 1981

Fletcher, R., "Practical Methods of Optimization, Vol. II, Constrained Optimization," John Wiley and Sons, Inc., New York, 1981

Fredricson, H., "Structural Topology Optimisation: an Application Review," International Journal of Vehicle Design, Vol. 37, No. 1, 2000

Gill, P. E., Murray, E., and Wright, M.H., "Practical Optimization," Academic Press, New York, 1981

Glass R.J., Segui-Gomez M., Graham J.D., "Child Passenger Safety: Decisions about Seating Location, Airbag Exposure, and Restraint Use," Risk Analysis, Vol. 20, No. 4, pp.521-527, 2000

Greene, J.E., "Computer Simulation of Car-to-Car Collisions," SAE Technical Paper Number 770015

Greenwood, D.T., "Principles of Dynamics (Second Edition)," Prentice Hall, 1988

Guendelman E., Bridson R., Fedkiw R, "Nonconvex Rigid Bodies with Stacking," Proceedings of ACM SIGGRAPH, 2003

Han, J., Yamazaki, K., "Crashworthiness Optimization of S-Shape Square Tubes," International Journal of Vehicle Design, Vol. 31, No.1, pp. 72-85, 2003

Hibbeler, R.C., "Mechanics of Materials," Pearson /Prentice Hall, pp. 727-728, 2005

Himmelblau, D.M., "Applied Nonlinear Programming," McGraw-Hill Book Company, New York, 1972

Huelke, D.F., Moore, J.L., Ostrom, M., "Air Bag Injuries and Occupant Protection," Journal of Trauma-Injury Infection and Critical Care, Vol. 33, No. 6, pp. 894-898, 1992

Huston R.L., "A Review of The Effectiveness of Seat Belt Systems: Design and Safety Considerations," International Journal of Crashworthiness, Vol. 6, No. 2, pp. 243-252, 2001

Jones, G.E., Kennedy, J.E., Bertholf, L.D., "Ballistics Calculations of R. W. Gurney," American Journal of Physics, Vol. 48, No. 4, 1980

Kamal, M.M., "Analysis and Simulation of Vehicle to Barrier Impact," SAE Technical Paper Number 700414

Kassabian, P.E., You, Z., Pellegrino, S., "Retractable Roof Structure," Proceedings of Institution of Civil Engineers, Structures and Buildings, Vol. 134, No. 2, pp. 45-56, 1999

Kawamura, H., Ohmori H., Kito, N., "Truss Topology Optimization by a Modified Genetic Algorithm," Structural and Multidisciplinary Optimization, Vol. 23, pp. 467-472, 2002

Kennedy, J.E., Cherry, C.R., Warnes, R.H., Fischer, S.H., "Momentum Transfer in Indirect Explosive Drive," International Pyrotechnics Seminar, Fort Collins, CO

(United States), 15-19 Jul 1996 (Report No.: LA-UR--96-1837; SAND--96-1606C;CONF-9607122—2)

Kikuchi, N., "Creative Approaches to Vehicle Safety," Mechanical Engineering 2005-2006 Annual Report, University of Michigan, Ann Arbor, 2007

Kim, C.H., Mijar, A.R., Arora, J.S., "Development of Simplified Models for Design and Optimization of Automotive Structures for Crashworthiness," Structural and Multidisciplinary Optimization, Vol. 22, pp. 307-321, 2001

Kim, H.S., Wierzbicki, T.(a), "Effect of The Cross-Sectional Shape on Crash Behaviour of a Three Dimensional Space Frame," International Journal of Vehicle Design, Vol. 25, No.4, pp. 295-316, 2001

Kim, H.S., Wierzbicki, T.(b), "Effect of The Cross-Sectional Shape of Hat-Type Cross-Sections on Crash Resistance of an S-Frame," Thin-Walled Structures, Vol. 39, No. 7, pp. 535-554, 2001

Kim, H.S., Wierzbicki, T.(c), "Crush Behavior of Thin-Walled Prismatic Columns under Combined Bending and Compression," Computers and Structures, Vol. 79, pp. 1417-1432, 2001

Kinney, G.F., Graham, K.J., "Explosive Shocks in Air," Springer, 1985

Lee, D.W., Ma, Z.D., Kikuchi, N., "Analytic Model of a Crash Energy Absorption Structure for Crashworthy Design of an Inflatable Morphing Body," Proc. of ASME IMECE., Nov. 2007, Seattle

Lee, D.W., Ma, Z.D., Kikuchi, N., "Application of Tubes Filled with Granules for Crashworthiness Design of Automobiles," Proc. of ASME IMECE., Nov. 2007, Seattle

Lee, D.W., Ma, Z.D., Kikuchi, N., "An External Explosive Airbag Model for an Innovative Inflatable Bumper (I-Bumper) Concept," SAE 2008 World Congress, SAE Technical Paper Number 2008-01-0508

Lee, D.W., Ma, Z.D., Kikuchi, N., "An Innovative I-Bumper Concept for Improved Crashworthiness of Military and Commercial Vehicles," SAE 2008 World Congress, SAE Technical Paper Number 2008-01-0512

Lin, K.H., Kamal, M.M., Justusson, J.W., "Effect of Vehicle Mix on Two-Car Head-On Impact," SAE Technical Paper Number 750117

Lingyun W., Mei Z., et al., "Truss Optimization on Shape and Sizing with Frequency Constraints Based on Genetic Algorithm," Comput. Mech., Vol. 35, pp. 361-368, 2005

Lobdell, T.E., Kroell, C.K., Schneider, D.C., Hering, W.E. and Nahum, A.M., "Impact Response of the Human Thorax," Human Impact Response Measurement and Simulation, W.F. King, H.J. Mertz, eds., Plenum Press, London, pp.201-245, 1973.

Mahmood, H.F., Paluszny, A., "Design of Thin Walled Columns for Crash Energy Management: Their Strength and Mode of Collapse," SAE paper No. 811302

Malen, D., Kikuchi, N., "Course Pack of ME513: Auto Body Structure," University of Michigan, 2006

Manche, E.E., Goldberg, R.A., Mondino, B.J., "Air Bag-Related Ocular Injuries," Ophthalmic Surgery and Lasers, Vol. 28, No. 3, pp. 246-250, 1997

Marshall, K.W., Koch, B.L., Egelhoff, J.C., "Air Bag-Related Deaths and Serious Injuries in Children: Injury Patterns and Imaging Findings," American Journal of Neuroradiology, Vol. 19, No. 9, pp. 1599-1607, 1998

McCormick, G.P., "Nonlinear Programming: Theory, Algorithms and Applications," John Wiley and Sons, Inc., New York, 1983

McHenry, R.R., "Analysis of The Dynamics of Automobile Passenger Restraint Systems," Proc. 7th Stapp Car Crash Conference, pp. 207-249, 1963

Meriam, J.L., Kraige, L.G., "Engineering Mechanics (Volume Two); Dynamics (Third Edition)," John Wiley and Sons, Inc., 1993

Mooi, H.G., Huibers, J.H.A.M., "Simple and Effective Lumped Mass Models for Determining Kinetics and Dynamics of Car-to-Car Crashes," IJCRASH '98, Conference Proceedings, Dearborn, Michigan, September 9-11, 1998

Nefske, D.J., "A Basic Airbag Model," SAE Technical Paper Number 720426

Paz, Mario, "Structural Dynamics: Theory and Computation Fourth Edition," Kluwer Academic Publishers 1997

Pedersen, N.L., Nielsen A.K., "Optimization of Practical Trusses with Constraints on Eigenfrequencies, Displacement, Stresses, and Buckling," Structural and Multidisciplinary Optimization, Vol. 25, pp. 436-445, 2003

Pedersen, C.B.W., "Crashworthiness Design of Transient Frame Structures Using Topology Optimization," Computer Methods in Applied Mechanics and Engineering, Vol. 193, pp. 653-678, 2004

Pellegrino, S., "New Concepts for Spacecraft Antennas and Radar Structures Based on Ultra-Thin Composites," 46th Israel Annual Conference on Aerospace Sciences, Tel Aviv and Haifa, 2006

Pipkorn, B., Fredriksson, R., and Olsson, J., "Bumper Bag for SUV to Passenger Vehicle Compatibility and Pedestrian Protection," International Technical Conference on the Enhanced Safety of Vehicles (ESV), Paper Number 07-0056, 2007

Presthus, M., "Derivation of Air Spring Model Parameters for Train Simulation," Master Dissertation, Lulea University of Technology, Sweden, 2002

Pride, R.A., Heimerl, G.J., "Plastic Buckling of Simply Supported Compressed Plates," NACA TN No. 1817, 1949

Reid, S.R., Reddy, T.Y., Gray, M.D., "Static and Dynamic Axial Crushing of Foam-Filled Sheet-Metal Tubes," International Journal of Mechanical Sciences, Vol. 28, No. 5, 1986

Reklaitis, G.V., Ravindranl, A., and Ragsdell, K.M, "Engineering Optimization, Methods and Applications," John Wiley and Sons, Inc., New York, 1983

Santosa, S., Wierzbicki, T., "Crash Behavior of Box Columns Filled with Aluminum Honeycomb or Foam," Computer & Structures, Vol. 68, No. 4, pp. 343-367, 1998

Schafer, B.W., "Local, Distortional, and Euler Buckling of Thin-Walled Columns," Journal of Structural Engineering, pp. 289-299, March 2002

Schulenburg, J.O., Kramer A., "Structural Adhesives-Improvements in Vehicle Crash Performance," SAE Technical Paper Number 2004-01-0244

Sedaghati, R., Suleman A., et al., "Optimum Design of Adaptive Truss Structures Using The Integrated Force Method," CMES, Vol. 2, No. 2, pp. 259-271, 2001

Sefrin P., Kuhnigk H., Koburg R., "Injuries to Car Passengers Protected by Air Bags," Anasthesiologie Intensivmedizin Notfallmedizin Schmerztherapie, Vol. 39, No. 11, pp. 662-667, 2004

Shanley, F.R., "Inelastic Column Theory," J. Aeronaut. Sci, 14, pp. 261-267, 1947

Shaout A., Mallon C.A., "Automotive Airbag Technology Past, Present and Future," International Journal of Computer Applications in Technology, Vol. 13, No. 3-5, pp. 159-171, 2000

Singace, A.A., "Axial Crushing Analysis of Tubes Deforming in The Multi-lobe Mode," International Journal of Mechanical Sciences, Vol. 41, pp. 865-890, 1999

Singace, A.A., "Collapse Behaviour of Plastic Tubes Filled with Wood Sawdust," Thin-Walled Structures, Vol. 37, No. 2, pp.163-187, 2000

Singace, A.A., "Characteristics of Wood Sawdust and Chips as Energy Absorption Filling Mediums," JSME International Journal Series A-Solid Mechanics and Material Engineering, Vol. 46, No. 4, pp. 642-651, 2003

Skutek, M., Mekhaiel, M., Wanielik, G., "A Precrash System Based on Radar for Automotive Applications," Intelligent Vehicles Symposium 2003, Proceedings of IEEE, pp. 37-41, June 2003.

Soto, C.A., "Structural Topology Optimization: from Minimizing Compliance to Maximizing Energy Absorption," International Journal of Vehicle Design, Vol. 25, No. 1-2, pp. 142-163, 2001

Soykasap, O., Pellegrino, S., Howard, P., and Notter, M., "Tape Spring Large Deployable Antenna," 47th AIAA/ASME/ASCE/AHS/ASC Structures, Structural Dynamics and Materials Conference, 1-4 May 2006, Newport, RI, AIAA-2006-1601, 2006

Stowell, E.Z., "A Unified Theory of Plastic Buckling of Columns and Plates," NACA TN No. 1556, 1948

Shugar, T.A., "A Finite Element Head Injury Model," Final Report Vol. 1, Contract DOT HS 289-3-550-IA, NHTSA, Washington DC, July 1977.

Suh, M.W., Lee, J.H., Cho, K.Y., et al., "Section Property Method and Section Shape Method for The Optimum Design of Vehicle Body Structures," International Journal of Vehicle Design, Vol. 30, No. 1-2, pp. 115-134, 2002

Vaziri, A., Hutchinson, J.W., "Metallic Sandwich Plates Subject to Intense Air Shocks," Int. J. Solid and Structures , Vol. 44, No. 1, pp. 2021-2035, 2007

von Karman, T., "Discussion of Inelastic Column Theory," J. Aeronaut. Sci, 14, pp. 267-268, 1947

Walton, K., "The Oblique Compression of Two Elastic Spheres," Journal of Mechanical Physics and Solids, Vol. 26, No.3, pp.139-150, 1978

Walton, K., "The Effective Elastic Moduli of a Random Packing of Spheres," Journal of the Mechanics and Physics of Solids, Vol. 35, No. 2, pp. 213-226, 1987

Wang, J.T., Nefske, D.J., "A New CAL3D Airbag Inflation Model," SAE Technical Paper Number 880654

White, F.M., "Fluid Mechanics," McGraw-Hill, pp. 307-311, 1994

White, M.D., Jones, N., "A Theoretical Analysis for The Dynamic Axial Crushing of Top-Hat and Double-Hat Thin-Walled Sections," Proc. Instn. Mech. Engrs., Vol. 213, Part D, pp. 307-325, 1999

Wilde, D.J., "Optimum Seeking Methods," Prentice Hall Inc., Englewood Cliffs, New Jersey, 1964

Yasui, Y., "Dynamic Axial Crushing of Multi-Layer Honeycomb Panels and Impact Tensile Behavior of The Component Members," International Journal of Impact Engineering, Vol. 24, No. 6-7, pp. 659-671, 2000

Yang, R.J., Rui, Y., Mohammed, A. and Singh, G., "Spot weld/Adhesive Pattern Optimization," Proceedings of ASME Design Engineering Technical Conference, Irvine, 1996

Yu, W.W., "Cold-Formed Steel Design," John Wiley and Sons, pp. 71-145, 2000

Zaouk, A.K., et al., "Validation of a Non-Linear Finite Element Vehicle Model Using Multiple Impact Data," Proc. of ASME IMECE., Nov. 1996, Atlanta.

Zukas, J.A., Walters, W.P., "Explosive Effects and Applications," Springer, pp.224-254, 1998